A Thesis

Entitled

Developing an Active Ankle Foot Orthosis Based On Shape Memory Alloys

By

Ehsan Tarkesh Esfahani

Submitted as a partial fulfillment of the requirement for

The Master of Science in Mechanical Engineering

_____

Advisor: Dr. Mohammad H Elahinia

_____

Graduate School

The University of Toledo

December 2007

The University of Toledo

College of Engineering

I HEREBY RECOMMEND THAT THE THESES PREPARED UNDER MY

SUPERVISON BY Ehsan Tarkesh Esfahani

ENTITLED Developing an Active Ankle Foot Orthosis

Based on Shape Memory Alloys

BE ACCEPTED IN PARTIAL FULFILMENT OF THE REQUIREMENT FOR THE

DEGREE OF Master of Science in Mechanical Engineering

_____

Thesis Advisor: Dr. Mohammad H Elahinia

Recommendation Concurred by

_____ _____

Dr. Mohamed S Hefzy Dr. Medi Pourazadi

Committee on
Final Examination

_____

Dr. Charles Armstrong

_____

Dean, College of Engineering

An Abstract of

Developing an Active Ankle Foot Orthosis

Based On Shape Memory Alloys

Ehsan Tarkesh Esfahani

Submitted as partial fulfillment of the requirements for

The Master of Science in Mechanical Engineering

University of Toledo

December 2007

This thesis is aimed toward the development and evaluation of a novel active ankle foot orthosis (AAFO) based on shape memory alloy (SMA) actuators. This device intends to fill the gap in the existing research aimed at helping patients with drop foot muscle deficiencies as well as rehabilitation activities. To examine the feasibility of this idea, the current study focuses on the dynamic behavior of the ankle joint. A SMA manipulator with a similar dynamic behavior is experimentally evaluated.

Nonlinear behavior of SMA wires requires nonlinear control techniques such as Sliding Mode Controller (SMC) for tracking the desired ankle angle. Simulation results of several different techniques are compared (PID, SMC, SMC-PID and Adaptive PID) and

finally the experimental result of an Adaptive PID is used to check the stability of walking. This results shows that an Adaptive PID controller as a robust and precision control can be used to track the desired position of the ankle. However for frequencies more than 0.25 Hz (time cycle less than 4 seconds), the walking conditions will be unstable due to slow cooling process.

To all whom I love;

those who are far from me but close to my heart.

Acknowledgment

I would like to thank my advisor, Dr. Mohammad Elahinia, for his help and support throughout my studies at University of Toledo. This research would not have been possible without his suggestions and guidance. In addition, I would like to thank my co-advisor Dr. Moamed S Hefzy and my committee members Dr. Charles Armstrong and Dr. Mehdy Pourazadi.

I should mention that this research was supported by deArce Memorial Endowment Fund in Support of Medical Research and Development at University of Toledo.

Also I want to thank all my lab mates at the Dynamic and Smart System Lab especially Christopher Schroeder for reviewing my thesis and my dearest friend Amin Mohaghegh to be always not only a friend but also an older brother for me.

Finally I can not find any word to express my feelings to all whom I love, those who are far from me but close to my heart.

I can just say that I love you all for ever.

Ehsan Tarkesh Esfahani

December 2007

Table of Contents

List of Figures

List of Tables

Chapter 1

1. Introduction

Locomotion, a characteristic of animals, is the process by which the animal moves itself from one location to another [Rose and Gamble, 94]. In nature, locomotion takes on many different forms, walking is a very interesting and complex form of locomotion that is mainly restricted to human beings. It is a common observation that individuals walk uniquely and one can usually recognize someone by one's gait. Short and slim people walk differently as compared to tall or thick individuals. Human emotions also have clear effects on walking patterns. As a result, walking can be called a learned activity that defines a certain characteristic of human life. There are however millions of individuals who cannot experience the pleasures of walking. These 'individuals' require either rehabilitation or permanent assistance in the form of assistive devices (orthosis or prosthesis) to restore some of their walking abilities. In the past, the majority of prosthetic patients lost limbs in combat, but this appears to be changing. National trends indicate that typical patients are middle-aged who have suffered an amputation due to vascular disease [Kirkup, 07].

The amputee population in the U.S. is approximately 1.2 million [Harman 04]. About 9 out of 10 amputations involve the leg, from the foot to above the knee. Three-quarters of

all amputations are the result of disease, often cancer or peripheral vascular disease. The latter is a narrowing of the arteries in the extremities that is often associated with diabetes. Most other amputations are the result of workplace or automobile accidents. A small fraction, approximately 3 percent, is due to birth defects that constrict bone growth [Kirkup, 07]. Walking problems, however, are not limited to the amputee population; there are a large number of patients who have lost muscular force control due to a disruption of major neural pathways at some point along the spinal column. Similar disabilities can be due to aging.

An orthosis is a device that is applied externally to a part of the body. The main function of an orthosis is to correct orthopedic maladjustment. These functions are performed by the device through supporting or through assisting the musculo-neuro-skeletal system. Only in the US, approximately 866,000 people use an orthosis on a lower extremity [US DOC, 94] and 8 million people are in immediate need for new technologies that will help them walk.

A common need of orthosis devices exist for drop foot patients. These patients are unable to lift their foot because of reduced or no muscle activity around the ankle. The major causes of drop foot include severing of the nerve, stroke, cerebral palsy and multiple sclerosis [Perry, 92]. There are two common complications caused by drop foot. First, the patient cannot control the falling of their foot after heel strike. As a result, the foot slaps the ground on every step. The second complication is the inability of the patients to clear their toe during swing. This causes the patients to drag their toe on the ground throughout the swing. The objective of this thesis is to develop a nonlinear controller for an Active Ankle Foot Orthosis (AAFO). The force and motion in this active orthosis is provided by

shape memory alloy (SMA) actuators. This orthosis device will fill the gap in the existing research aimed at helping patients with drop foot muscle deficiencies as well as rehabilitation activities.

1.1. Powered Assistive Locomotion Technologies

Leonardo DaVinci, Galileo, Lagrange and Bernoli were among the first scientists who had primary interest in the application of mechanics to the study of human locomotion. The first efforts in building a powered assistive device go back to the mid-1970s [Hughes, 72, Vukobratovic et al., 74, Townsend and Lepofsky, 76]. In 1974 a Yugoslavian researcher, Miomir Vukobratovic, invented one of the most advanced models of the time period (Figure 1.1-A). His device used pneumatic actuators at the hip, knee and ankle to provide assistance in the frontal and sagittal planes [Vukobratovic et al. 74, 90]. In 1978 Ali Seireg at the University of Wisconsin developed a hydraulic orthosis with a dual axis hip, dual axis ankles and single axis knees [Seireg, 81]. (Figure 1.1-B)

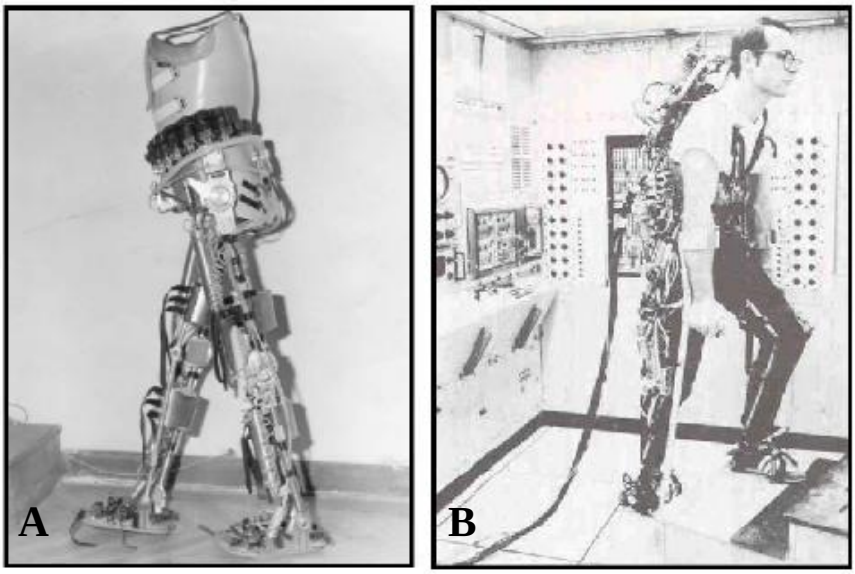

Figure 1-1 A-The exoskeleton developed by Vukobratovic in Yugoslavia in the 1970s [Vukobratovic, 74]. B- A computer controlled hydraulic exoskeleton in University of Wisconsin in 1978 [Seierg, 81].

More recently, new versions of powered orthoses have been developed at Michigan Technological University [Ruthenberg et al. 97] and in Italy [Belforte et al. 01]. All of these devices underwent testing on human subjects, but they did not achieve sufficient utility to be produced on a broad scale. Achieving better and smaller actuators, sensors, and computer processors will help powered orthoses become a reality in the clinical community. Perhaps the most advanced academic laboratory focusing on integrating new technology into orthotics and prosthetics is the Biomechatronics Laboratory at the MIT Media Laboratory. Researchers at this lab have developed a computer-controlled above-knee prosthesis to rival the Otto Bock C-Leg which is currently being sold commercially by Ossur [Herr, 03]. Blaya, in the same lab, also developed a powered ankle-foot orthosis based on Series Elastic Actuators [Blaya and Herr, 04] (Figure 1.2-A). The basic idea of this AAFO is to change the orthosis impedance (stiffness) actively, which eliminates the slap foot. As a result, the AAFO minimizes the kinematic walking difference from normal people. The MIT group developed a Series Elastic Actuator (SEA) for the AAFO to realize variable stiffness. This actuator is comprised of a DC motor, mechanical links and torsional springs. A control algorithm was developed to create proper stiffness for each part of the walking (gait) cycle. Although this AAFO shows promising results in a lab environment, the actuator weighs 2.6 kg and requires bulky batteries and electronics for operation. In addition, the patient may not be able to sit while wearing this AAFO.

Another magnificent work done on developing AAFOs is a pneumatically powered lower limb exoskeleton which is developed in the Human Neuromechanics Lab at the University of Michigan [Ferris et. al 05]. This AAFO is actuated by McKibben Muscles which are pneumatic actuators. One pneumatic actuator provides plantar flexion torque

and a second actuator provides dorsiflexion torque. A control algorithm adjusts air pressure in each actuator independently. The study has shown promising results in gait rehabilitation, Human motor adaptation and muscle activations [Ferris et. al 05; Cain et al, 07] (Figure 1.2-B). However, the size and weight of the pneumatic auxiliary components such as the compressor is prohibitive for outdoor walking and activities.

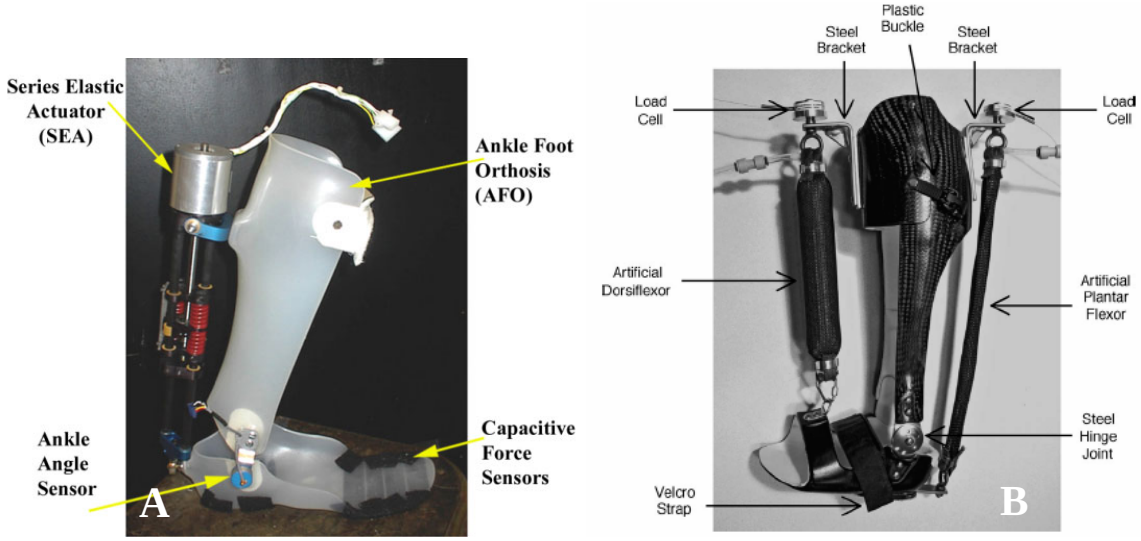

Figure 1-2 A-Powered ankle-foot orthosis for drop foot correction in MIT media lab. [Blaya and Herr, 04]B- McKibben muscle actuators in AAFOs. [Ferris, 05]

Mechanical system laboratory at the University of Delaware is another research group working on walking assistive devices. Researchers at this lab designed a gravity balancing leg orthosis to assist persons with hemiparesis to walk through elimination of the effects of gravity. The proposed device is designed to be passive (Figure 1.3). This device is intended to be used as a rehabilitation device for patients to train their muscles and in order to regain their former control and strength. This device has the following features: (i) it can fully or partially gravity-balance the human leg over the range of its motion; (ii) it is tunable to the geometry and inertia of a specific human subject to achieve the desired level of gravity balancing [Fattah and Agrawal, 05; 06].

The same group also designed an active leg exoskeleton for gait rehabilitation of patients with walking disabilities. They proposed a force-field controller which can apply suitable forces on the leg to help it move along a desired trajectory. The interaction forces between the subject and the orthosis were designed to be 'assist-as-needed' for safe and effective gait training [Banala and Agrawal, 05].

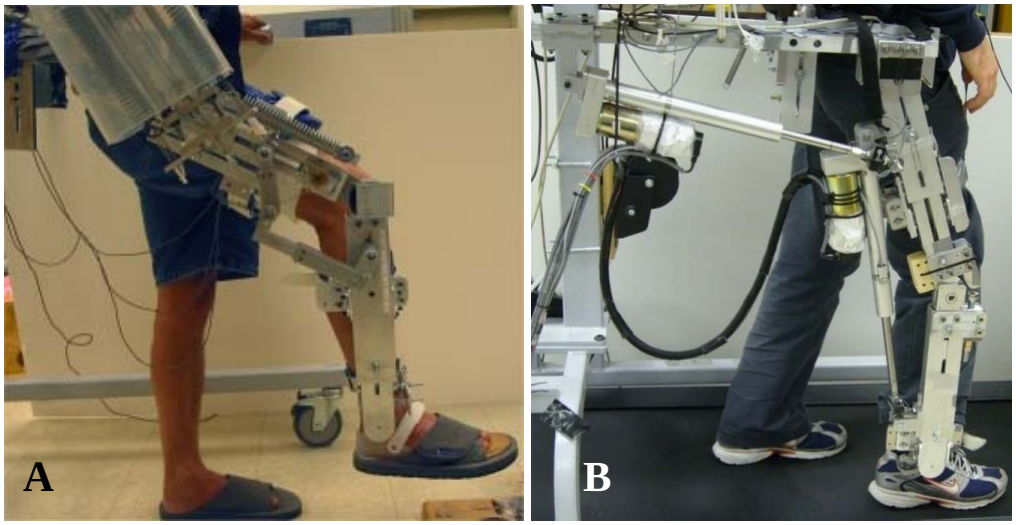

Figure 1-3 A-Gravity balance leg orthosis designed at University of Delaware [Fattah, 05, 06] B-Active leg exoskeleton [Banala and Agrawal, 05]

Applications of a powered orthosis are not limited to assisting people with walking disabilities. There is another class of powered orthoses (robotic exoskeletons) which are used to increase human motor abilities over and above normal levels. These human performance augmentation devices provide superhuman motor function to neurologically intact individuals. The Defense Advanced Research Projects Agency (DARPA) in the United States hopes to yield devices that can increase the speed, strength, and endurance of soldiers in combat environments [Ferris et. al, 05]. Berkeley Robotics lab at UC Berkeley and Sarcos Inc. are two groups currently developing working exoskeletons financed by DARPA. Sarcos protptype is shown in Figure 1.4-B and the other prototype called BLEEX (Berkeley Lower Extremity Exoskeleton) is shown in Figure 1.4-C

[Kazerooni, 96]. While the exact devices created by these research groups may not be readily used as assistive technology, it is likely that their research will result in spin-off technology that can later be incorporated into powered orthoses for neurologically impaired humans.

Another academic laboratory that is leading the way in developing powered orthoses for assistive technology and also super humans is the Cybernics Laboratory at the University of Tsukuba in Japan. They have developed an electromechanical powered orthosis called Hybrid Assistive Limb (HAL) (Figure 1.4-A). It includes four rotational motors that assist knee and hip joints on both lower limbs based on feedback from force sensors and muscle activation amplitudes [Kasaoka and Sankai, 01; Kawamoto and Sankai 04].

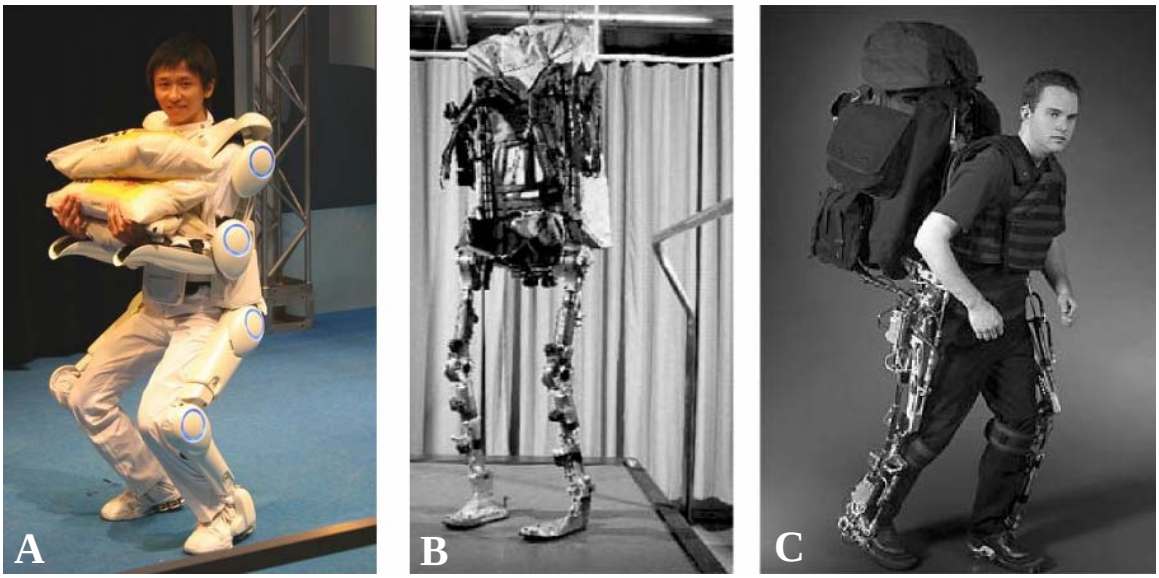

Figure 1-4 Powered orthosis for power augmentation. A-HAL (TesKoba University, Japan) [http://sanlab.kz.tsukuba.ac.jp/english/r_hal.php] B-The Sarcos prototype [MIT Technology review, 04] C-BLEEX, the Berkeley Lower Extremity Exoskeleton [bleex.me.berkeley.edu/bleex.htm]

1.2. Other Locomotion Assistive Technologies

There are some other locomotion assistive technologies which use non-conventional actuators. These techniques include Functional Electric Stimulation, Weight Bearing

Control or simply a passive orthosis. These alternative mechanisms are explained in the following sections.

1.2.1. Functional Electrical Stimulation (FES)

Functional electrical stimulation (FES) is a technique that uses electrical currents to activate nerves innervating extremities affected by paralysis resulting from spinal cord injury (SCI), head injury, stroke or other neurological disorders in an attempt to restore function in people with disabilities. FES consists of electrically stimulating a muscle using electrodes [Bajd et al., 99; Guyton, 96]. In this methodology shorts bursts of electrical pulses are used to generate muscle contraction. If muscles are stimulated in the right order, a walking-like motion can be attained by paraplegic subjects.

The first electrical stimulator for drop foot problems was created in 1961 by Liberson. He used a heel switch in the affected leg. As soon as the patient raise the heel, the heel switch triggered the stimulation electrodes positioned in the fossa popliteal area and above the peroneal nerve. This in turn causes a dorsal flexion at ankle joint [Liberson et al., 61]. Walking pattern, based on flexion response triggering, was also applied by Graupe et al [Graupe et al. 83; 84]. In the investigation conducted by Bajd et al. a simple hand switch, built into the handle of a walker or crutches, was used to initiate a step [Bajd et al. 83]. The advantage of Graupe's approach was the control of stimulation sequences based on a patient's electromyogram (EMG) signal.

Current hybrid systems use a combination of electrical stimulation and walkers to allow paraplegic subjects to walk. The latest system was developed by Case Western Reserve University as shown in Figure 1.5 [Kobetic et al 03].

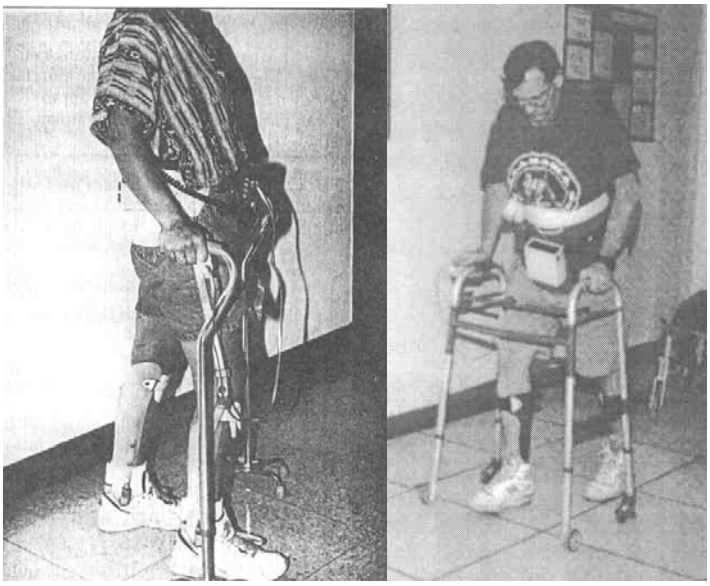

Figure 1-5 CWRU hybrid gait orthosis [Kobetic, 03]

It should be mentioned that a work by Mizrahi et al. [Mirzahi et al., 85; Isakov et al., 86] shows a 20% heart rate increase during FES exercise while the subject was in a sitting position. The heart rate was then increased to 100% and 150% during standing and FES induced walking, respectively. Similarly, the oxygen uptake was doubled during exercise, tripled during standing and about five times higher during walking as compared to the resting values. These results demonstrate the high level of effort during FES-restored walking, which also requires an anaerobic source of energy [Kralj and Bajd, 89].

1.2.2. Weight Bearing Control (WBC) Orthosis

The weight bearing control (WBC) orthosis (Figure 1.6) consists of a rigid frame that supports the user's body weight, a special hip joint device that reciprocally propels each leg forward, a gas powered foot device for foot/floor clearance and a control system for the orthosis [Kaneoko et al 97]. The patient uses special crutches with two buttons to signal the WBC orthosis when to begin each step. The sequence of each step is retraction

of the sole of the swinging leg, forward swing powered by the subject and extension of the sole for foot contact.

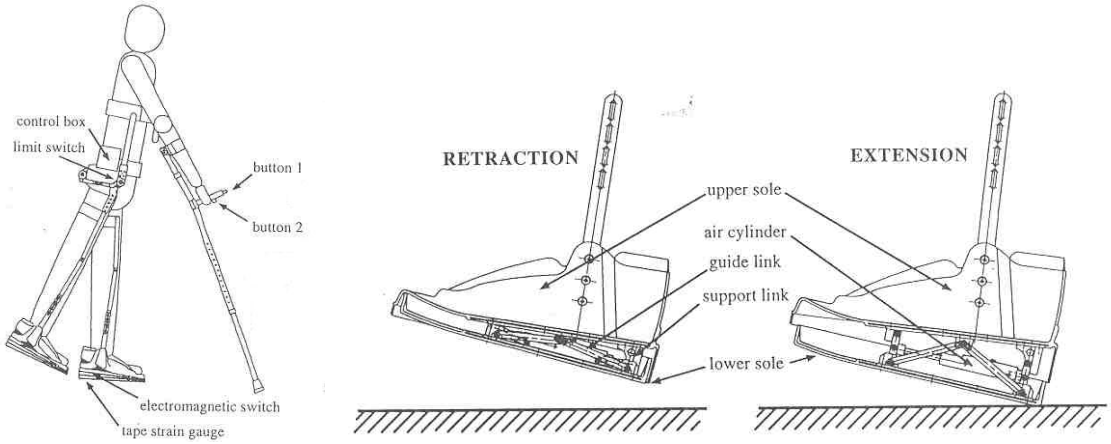

Figure 1-6 The weight bearing control (WBC) orthosis

1.2.3. Passive Ankle Foot Orthosis

An ankle foot orthosis (AFO) is defined as a medical mechanical device to support and align the ankle and foot, to suppress spastic and overpowering ankle and foot muscles, to assist weak and paralyzed muscles of the ankle and foot, to prevent or correct ankle and foot deformities and to improve the functions of the ankle and foot [Wu, 90].

Currently, clinicians must choose between metal alloy-based devices (Traditional AFOs), plastic-based devices and a hybrid assembly incorporating both materials. In most cases, this choice is left to the orthotist and patient. Traditional AFOs are widely being replaced by plastic or polypropylene. The major advantages of polypropylene AFOs are that they distribute pressure over a larger surface area of the limb resulting in less discomfort, are lighter than metal braces, more cosmetically appealing and they can be worn with a variety of shoe types [Good and Supan, 89]. (Figure 1.7)

Polypropylene AFOs are fabricated by making a cast of the patient's leg below the knee, then molding the polypropylene over it. This ensures a close fit for improved pressure distribution. The AFOs are divided into rigid and flexible types.

Figure 1-7 Polypropylene Ankle Foot Orthosis

1.2.4. Dynamic Ankle Foot Orthoses

The family of dynamic AFOs include thermoplastic and conventional double upright orthotic designs. The feature that distinguishes dynamic from static AFOs is that they allow, or have the potential to allow, sagital plane motion at the ankle. This is accomplished by incorporation of a mechanical ankle joint or, in the case of a posterior leaf spring orthosis (PLS), strategically minimized thermoplastic trimlines [Lusardi and Nielsen, 2000]. Figure 1.8 shows different views of a dynamic AFO form.

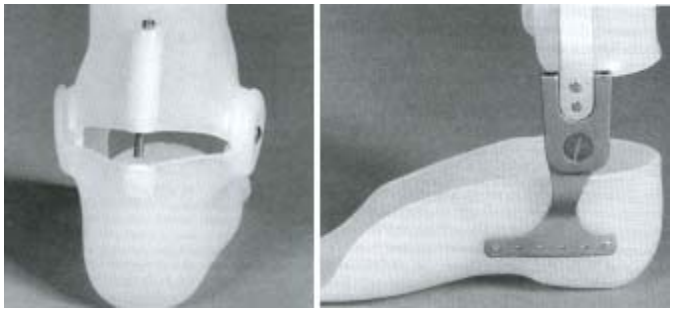

Figure 1-8Different views of a dynamic ankle foot orthosis [Lusardi and Nielsen, 2000]

1.3. Shape Memory Alloy actuators

Shape memory alloys have been used in a variety of actuation, energy absorbing, and sensing applications. The key feature of this material is its ability to undergo seemingly large seemingly plastic strains and subsequently recover these strains when a load is removed or the material is heated. This unique ability occurs due to a reversible thermoelastic material phase transformation. This key feature allows SMAs to serve as very compact actuators. Few other materials or devices can generate significant tensile force over a large displacement while occupying such a small volume. A secondary useful feature of many SMAs is their ability to change resistivity with a change in strain. The change in resistivity as an SMA undergoes strain has enabled investigators to use them as coarse position sensors. The coarseness is due to a complex relationship between resistivity and the material state and its coupling with mechanical load and temperature.

For miniature/micro actuators (10gm or lighter) almost no actuator of any conventional type is useful in practice. SMA actuators have several advantages for miniaturization as described below:

- Experiments have shown that the power to mass ratio of SMA wire is 4 watts/gm which is much higher than servomotors, oil and air cylinders. The efficiency is lower than that of conventional actuators [Hashimoto et al., 85].
- SMA actuators have no frictional parts as seen in electrical and hydraulic devices. The so called solid state actuator does not generate noise in operation and is dust free so that it is suitable for operation in a clean room. Its mechanical simplicity results in excellent maintainability and reliability.

- Simplicity of mechanism, since the SMA actuator is a direct drive linear actuator, using phase transformation of the alloy, a reduction gear system is not required.
- Silent actuation.
- Sensing ability, the electric resistance change of SMA due to progress in phase transformation can be utilized as a monitor variable of phase transformation.
- Low driving voltage, compared to piezoelectric and electro static actuators, applied voltage for joule heating is much smaller (such as 5-12V).

Among smart materials suitable for actuator development, SMAs are known for their capabilities in applying both large forces (stress of 600 MPa) and large displacements (strain of 10%). This property is due to the solid phase martensite to austenite transformation in SMAs, which can be achieved simply by electrical (resistive) heating. SMAs have very high force to weight ratio: an SMA wire can lift close to 80,000 times its own weight. Simplicity of the actuation, high actuation force, and large actuation displacement of SMA wires can be combined with proper control algorithms to develop an effective active AFO. The SMA actuated AAFO can provide the deficit muscle force and enable the drop foot patients to walk normally. The mechanical (stress-strain) behavior of SMA material is very similar to that of muscle tissues. This biocompatibility is the main reason a SMA AAFO will be surpassing the existing solutions. In addition, since SMA actuators are flexible, they will allow the patients to sit while wearing the AAFO.

1.4. Objectives

The objective of this thesis is to develop a lightweight AAFO for drop foot patients based on SMA actuators. The main steps of this research are as follow:

- Determine the torque requirements and necessary angular rotation of the orthosis during walking motions,
- Develop an analytical model of the SMA actuator and experimentally verify the model
- Design a control algorithm for the active orthosis device to achieve the time varying torque while undergoing complex thermo-mechanical loading,
- Develop a method to test the performance of the SMA AAFO
- Test a control method both in a simulation environment and a prototype of an AAFO

1.5. Approach

In this study, based on ankle behavior, a foot orthosis activated with shape memory alloy is designed. Like any other actuator SMA needs to be controlled during a walking cycle to perform the desired task. To avoid running an experimental test on a real subject, a trajectory generation method and stability criterion is being used to check the functionality of the AAFO. SMA modeling is another part of this research which is necessary to model the actuator behavior and its response to the input task. The accuracy of SMA modeling is proved by running experiments.

The most important part of this research is to design a control algorithm for AAFO during the entire walking cycle. This algorithm is tested over the entire cycle in a simulation environment. Then it will be experimentally tested on a SMA prototype with a similar dynamic to swing cycle in human walking.

To investigate the control algorithms for mimicking the normal walking gait, a dSPACE control system will be used. This system will use the angle measurement feedback

provided by an encoder and adjusts the voltage to SMA wire to create the required level of force and torque at each stage of the walking cycle.

1.6. Contribution

The following list shows all the accomplishments in this thesis:

1. Designing a trajectory generation method for different walking speeds and step lengths. (The walking of a healthy human at a constant speed is captured first and then by picking some key points the whole trajectory for different speeds is predicted.)
2. Introducing an experimental setup with similar dynamics to the ankle to check the feasibility of using SMA actuators in AFO.
3. Modeling the SMA actuation mechanism
4. Designing a nonlinear adaptive control technique to track the desired trajectory at the ankle joint
5. Experimentally check the robustness of the control technique.
6. Find the limitation of using SMA in AAFO through using the control method in the simulation environment.

1.7. Outline

Chapter 1 concludes with the outlines of the intended contributions of this study. An introduction to human walking is given in Chapter 2. Section 2.1 talks about the basic definition in human walking and different events of gait cycle are studied in Section 2.2. Section 2.3 covers the drop foot problem and its main reasons while ground reaction force and ankle behavior are the topics of Section 2.4 and 2.5, respectively.

Modeling the human walking is discussed in Chapter 3. Different techniques to capture the kinematics of the movement and simulate the walking are presented in Section 3.1 and 3.2. In Section 3.3 an approach based on the trajectory generation and stability of the walking is introduced to check the functionality of the SMA AAFO.

Chapter 4 is about modeling the AAFO. Since the SMA is the actuation techniques, Section 4.1 present a background on Shape Memory Alloys. In Section a conceptual design of an AAFO based on SMA wires is considered, at the end of this section an SMA arm with a similar dynamic model is selected as an experimental setup. In Section 4.3 the SMA-actuated robotic arm is modeled in order for investigating different control methods. In the last section simulation results will be used to evaluate the SMA arm model. Chapter 5 presents a few control designs for the SMA-actuated robotic arm. What makes this system interesting is that the stress of the SMA wire changes due to actuation. This makes the control of this system challenging, since the phase transformation as the basis of the SMA actuation depends on stress (Section 5.1). Several control algorithms are presented for position control of this system in sections 5.2-5.3.

Chapter 6 contains all the simulation and experimental results and finally Chapter 7 will summarize the main steps of the thesis.

Chapter 2

2. Human Walking

There is not an exact definition for ‘walking’. In simple words, it can be described as a cyclic pattern of body movements which is repeated over and over, step after step to advance an individuals position. Assuming that all walking cycles are about the same, study of the walking process can be simplified by investigating one walking cycle. Although this assumption is not always true, it is a reasonable approximation that will be used in this work. This chapter deals with investigating the mechanism of biped walking in order to make a solid foundation for the following chapters in developing an assistive active device for walking.

In general, human walking consists of several sequential steps. Each of these steps is composed of two phases: the single support phase and the double support phase. During the single support phase, one leg is on the ground and the other leg is undergoing a swinging motion. The double support phase starts as soon as the swinging leg meets the ground and ends when the support leg leaves the ground.

There are two basic elements which are necessary for any form of biped walking regardless of the existence and the level of possible physical disabilities.

1. Periodic movement of each foot from one position of support to the other in the direction of progression.
2. Continuing ground reaction forces (GRF) that support the body

As stated by Rose and Gamble, "these two requisites of walking are equally necessary when prosthetic or orthotic devices are used" [Rose and Gamble 1994]. Therefore the first step to design an assistive device is to understand these two aspects. Section 2.1 of this chapter will start by providing some basic terms and definitions used frequently in this work. Following in section 2.2 will be a study of the periodic motion of each segment in as "Gait Cycle". Section 2.3 will provide some information on ground reaction force (GRF), which is the only external force applied to the body during walking. In the last section (2.5) a combination of GRF and the periodic motion of a foot will be studied with a stiffness plot of an ankle joints. This plot will show the relationship between ankle moments versus ankle angle and will be used to design the AAFO.

2.1. Basic Definitions

There are usually three anatomical planes, which are used to describe and to analyze the human movement. These three reference planes are shown in Figure 2.1.

Dorsiflexion and Plantar Flexion are defined as the rotation of the ankle in the sagittal plane towards or away from the body, respectively.

The period of time between two successive occurrences of one of the repetitive events of walking is called stride cycle. It is usually measured from an initial heel contact (HC) of one foot to the subsequent HC of the same foot. In order to compare the stride characteristics of different strides within the same subject or across different subjects, the

stride cycle is usually normalized and expressed as a percentage (0% to 100%) [Winter, 1996].

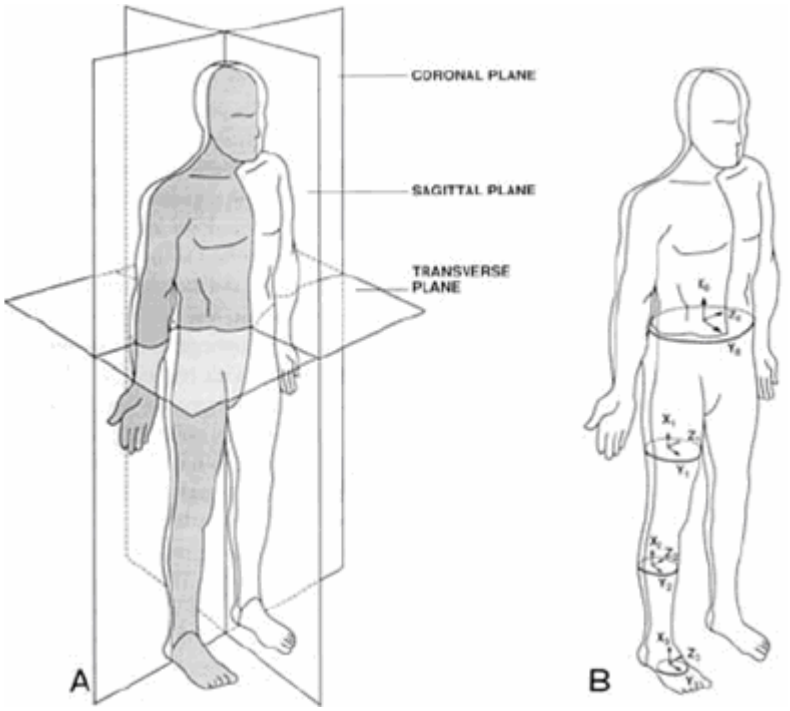

Figure 2-1 A-Reference planes of body B-Coordinates system for lower limb [Rose and Gamble, 94]

2.2. Gait Cycle

Gait has been defined in different ways by different researchers. Smidt introduces it as "manner of moving the body from one place to another by alternately and repetitively changing the location of the feet" [Smidt, 90]. Norkin defines gait as "a translatory progression of the body, which is produced by coordinated rotary movements of body segments. Normal gait is rhythmic and characterized by alternating propulsive and restraining motions of the lower extremities." [Norkin and Levangie, 83]. The gait cycle is the time interval between two successive occurrences of one of the repetitive events of locomotion [Novacheck, 98]. Based on all these definitions we can safely say that, a gait cycle is defined as an interval of time during which one sequence of regularly recurring

walking event is completed. The beginning of the gait cycle is represented as initial contact of one foot with the ground, usually termed heel strike (HS) [Bowker and Hall, 75; Gage, 91; Perry, 92; Smidt, 90; Whittle, 91] or foot strike [Rose and Gamble, 94]. Although there are many types of gait including walking, running [Novacheck, 98], skipping [Minetti, 98], and many pathological gaits, the focus of this thesis is on walking.

2.2.1. Gait Phases

During any self selected walking, a cycle of repeated events is consistently observed. These events can be listed as 'Foot Strike' and 'Toe Off '. Since there are two extremities involved in biped walking, there are four consecutive events, foot strike (FS), opposite toe-off, opposite foot strike and toe off. The entire cycle then repeats itself with the second foot strike starting the following cycle. The two phases (stance and swing) and most of the periods of the basic gait cycle can be described in reference to these basic repeated events [Sutherland, 81, 84]. Events of a gait cycle remarkably occur in similar sequences and are independent of time. That is why the cycle is commonly described in terms of percentage, rather than the time elapsed. Therefore initial foot strike is designated as 0% and the second foot strike as 100% (0-100%). Furthermore, in normal subjects, the opposite limb repeats the same sequence of events, while 180^{o} out of phase. This way, the opposite foot strike is equivalent to 50% and the second opposite foot strike occurs at 150% of the gait cycle. The phases of the basic walking cycle are as follows.

The gait cycle consists of two repeated events, which are the stance and swing periods. Swing is the period of time that the foot is in the air for limb advancement. Swing phase occurs between the toe off (62%) and the second heel strike (100%). Stance phase

comprise the period between the heel strike (0%) and the toe off (62%). As shown in Figure 2.2, Stance is the period where the foot is in contact with the ground.

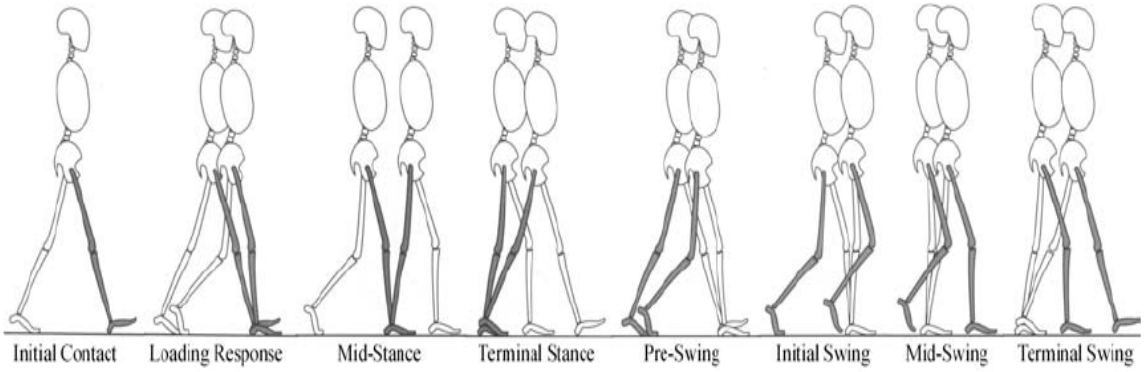

Figure 2-2 Typical normal walking cycle illustrating the phases of gait [Perry, 92]

The Stance phase is commonly divided into three periods:

1. Initial double limb support (foot strike to opposite toe off)
2. Single limb support (opposite toe to opposite heel strike)
3. Second double limb support (opposite foot strike to toe off)

Each of these periods consists of some gait events, and is completely shown in Table 2.1.

Table 2-1Events, periods and phases [Rose and Gamble, 94]

Event	% Gait Cycle	Period	Phase
Foot Strike	0	Initial double limb support	Stance 62% of Cycle
Opposite Toe Off	12	Single limb support	
Opposite foot strike	50	Second double limb support	
Toe-Off	62	Initial swing	Swing 38% of Cycle
Foot Clearance	75	Mid swing	
Tibia Vertical	85	Terminal swing	
Second Foot Strike	100		

Initial double limb support is characterized by a very rapid loading onto the forward limb with shock absorption and slowing of the body's forward momentum.

After opposite toe off, the opposite leg is in swinging. As the body passes over the fixed foot, the center of mass rises to its pick while both forward and vertical velocities decrease. Forward shear then reverses to after shear, the center of mass falls, and forward and vertical velocities increase.

Second double limb support is also defined as preswing. The preparation for swing/limb acceleration actually occurs during this period of time. At this time the leg must be flexed at the knee and hip with the plantar flexed at the ankle to prepare for lift off.

Swing phase can be functionally subdivided to into tree periods: Initial swing (toe off to foot clearance), mid swing (foot clearance to vertical tibia) and late swing (vertical tibia to foot strike).

The critical event of foot clearance occurs around 75% of the cycle when the swinging limb passes the standing limb. Vertical tibia occurs when the tibia becomes perpendicular to the floor, heralding the beginning of limb deceleration [Rose and Gamble, 94]. (All this information are summarized in Table 2.2)

Table 2-2 Gait cycle: Period and Functions [Rose and Gamble, 94]

Period	%Cycle	Function
Initial double limb support	0-12	Loading, weight transfer
Single limb support	12-50	Support of entire body weight, center of mass moving forward
Second double limb support	50-62	Unloading and preparing for swing (pre-swing)
Initial swing	62-75	Foot clearance
Mid swing	75-85	Limb advance in front of body
Terminal swing	85-100	Limb deceleration, preparation for weight transfer

2.2.2. Physiology of Gait

Success in developing orthotic devices is dependent on a clear understanding of the functions of each assisted joint. In this research, analyzing each of the joints involved in

walking individually in the sagittal plane has been chosen as one of the easiest way of investigating the gait.

2.2.2.1. Hip

During a normal stride, hip movement can be categorized into two basic motions.

1. Extension, which happens during stance and has the primary role of stabilization of the trunk.
2. Flexion in swing which in this motion, the hip's basic role is controlling the limb [Perry, 92].

Figure 2.3 shows the muscle activation pattern during a normal gait, the active muscles are darkened. In the first three frames it can be seen that all five hip extensors (biceps femoris, semimembranosis, semitendinosis, adductor magnus, gluteus maximus) contract to resist the flexor moment created by the vertical ground reaction force (GRF). This results in keeping thigh position relatively stable [Inman, 81].

The abductor muscle group stabilizes the pelvis, which loses its contra lateral support with the transfer of body weight to the forward limb [Perry, 97].

In mid and terminal stance, the hip progressively extends, reaching neutral position at 38% of the gait cycle. In terminal stance the erect pelvis and trunk roll forward over the forefoot rocker causing the body weight to move posterior to the hip joint and the thigh to be pulled into hyperextension. The anterior portion of the tensor fascia lata responds to restrain passive hip extension and to provide a low level of abduction force [Perry, 92].

Hip flexion to the neutral position during pre and initial swing results form two events. The first event is the contraction of the iliopsoas aided by gravity, the rectus femoris and the adductors [Gage, 91]. This is shown in the fifth frame of Figure 2.3 (b).

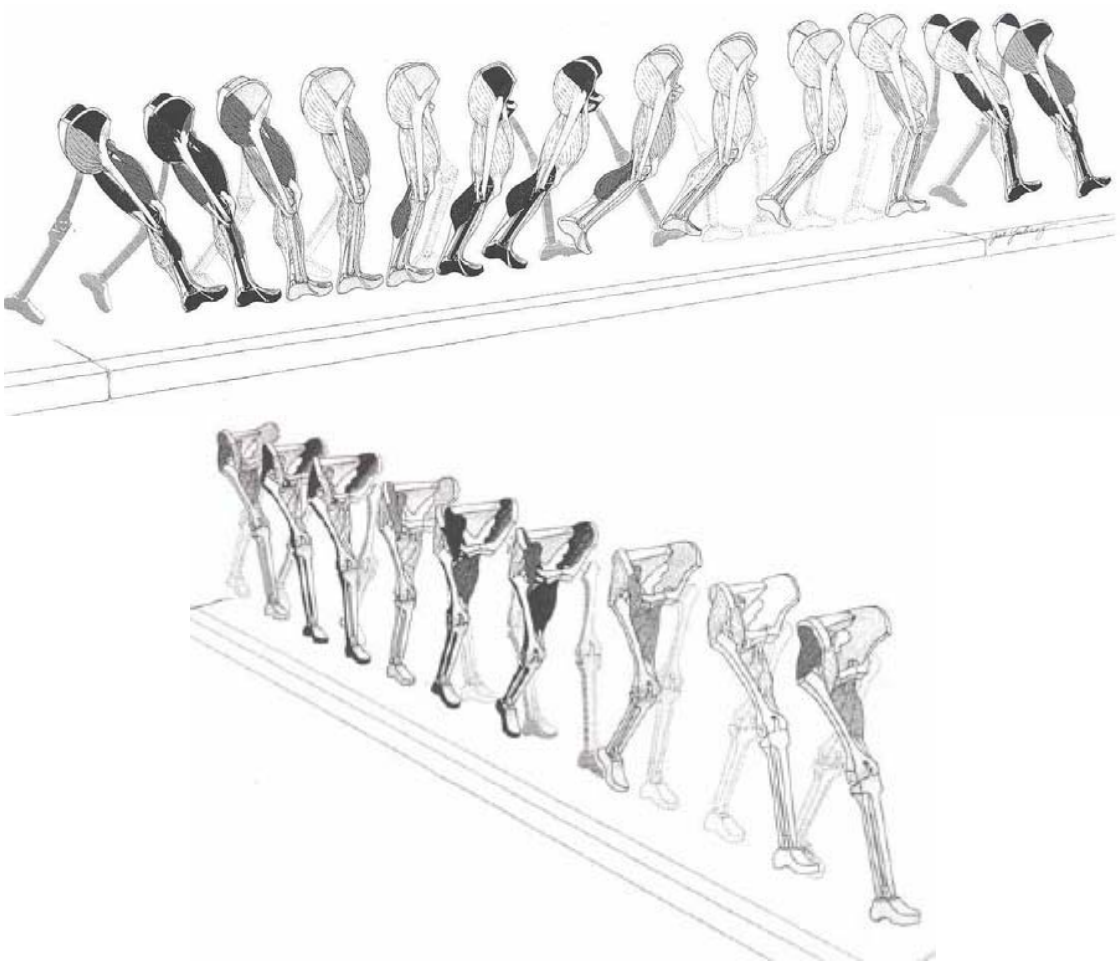

Figure 2-3 Muscle activation pattern of gait [Inman, 81]

The second event is the ankle mechanics that advance the tibia, induce knee flexion and carry the thigh forward. The contraction of the gastrocnemius is a major part of this event, as can be seen in Figure 2.3(a).

When tibial inertia causes excessive knee flexion, the rectus femoris preserves accelerated hip flexion while correcting knee motion. Minimal hip flexion and partial knee extension continue to advance the limb during mid swing. During terminal swing, strong action by the hamstring muscles prepares the limb for stance by stopping further flexion. The reduction of hamstring activity and accompanying onset of the gluteus maximus and adductor magnus provide hip extension. Because of these actions, the limb

is positioned for initial contact [Perry, 92]. The entire range of motion of the hip for normal gait can be seen in Figure 2.4.

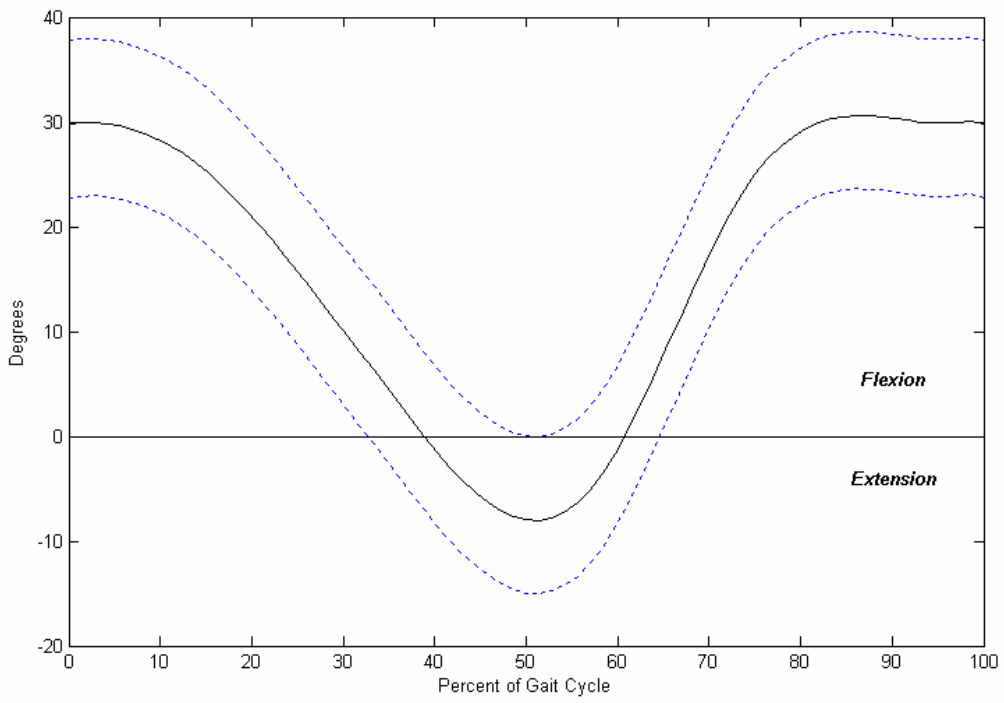

Figure 2-4 Hip range of motion

2.2.2.2. Knee

During stance, the knee is the basic determinant of limb stability. In swing, knee flexibility is the primary factor in the limb's freedom to advance [Perry, 92].

At initial contact, the knee is extended approximately two to five degrees in flexion, as can be seen in Figure 2.5. During loading, body weight is accepted with the knee flexed and the GRF falls behind the knee to produce an external flexion moment. This moment is counteracted by contraction of the quadriceps, including the vastus laterialis, medialis, and intermedius, to prevent the knee from buckling and places the knee under maximum weight-bearing load [Gage, 91]. The activation of these muscles can be seen in the first four phases of Figure 2.3.

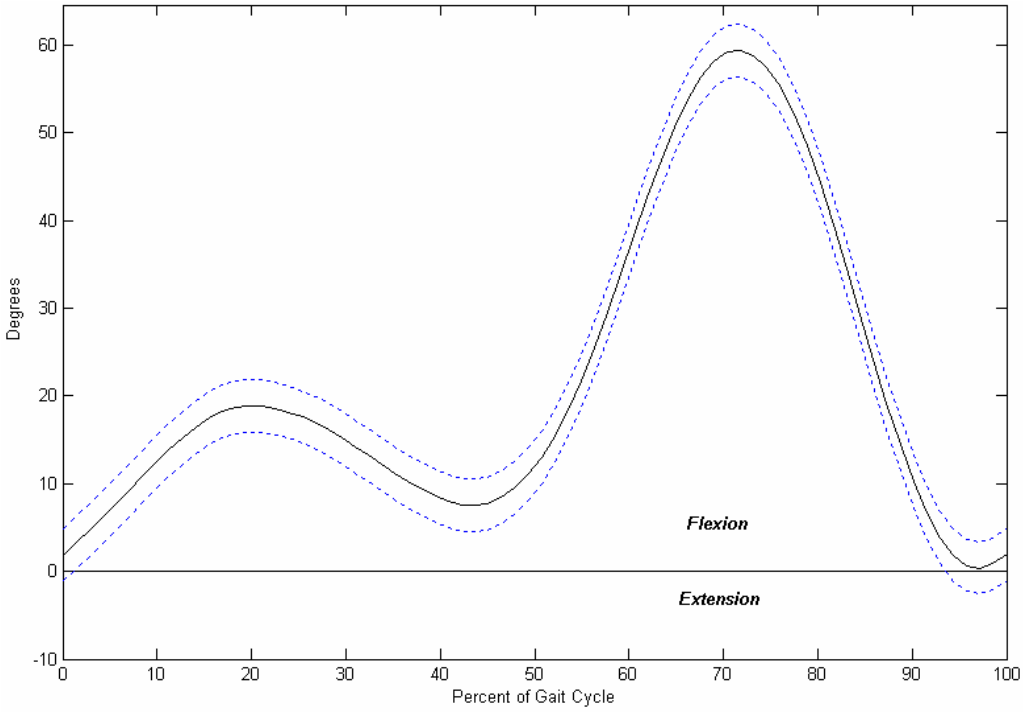

Figure 2-5 Knee range of motion

At mid stance, total body weight is transferred onto the flexed knee, resulting in an additional five degrees of flexion. The quadriceps reacts to inhibit further flexion and is then assisted by tibial stability gained through the combined action of the soleus and the forward motion of the body weight. Three mechanisms contribute to knee extension stability during terminal stance. The first is strong plantar flexion that provides a stable tibia over which the femur advances. Limb momentum and the forefoot rocker that facilitates the forward fall of the body weight over the leg also assist in stabilizing the knee. To avoid knee hyperextension, the popliteus and gastrocnemius provide a flexor action posteriorly. The knee begins to flex at the end of terminal stance from the rolling of the leg. Tibial stability is then lost and the posterior muscles become free to initiate knee flexion.

Body weight is transferred to the opposite limb and as the trailing limb reduces its floor contact, the lower leg is free to roll forward. This is accelerated by the release of the

tension stored in the stretched soleus, gastrocnemius and hip flexors. This force coupled with the force from the adductor longus initiate early hip flexion and assist knee flexion. The critical event for initial swing is sufficient knee flexion for the toe clearance as the thigh advances [Perry, 97].

Attainment of full knee flexion largely depends on the imbalance between the forward momentum of the femur generated by hip flexion, inertia of the tibia and the active knee flexion by the biceps femoris, as can be seen on the last drawings of Figure 2.3. Only gravitation forces and the momentum generated by hip flexion are required during mid swing. All four vasti are involved in terminal knee extension to lift the weight of the lower leg. These are counteracted by the hamstrings, which prevent knee hyperextension and decelerate the hip [Perry, 92].

2.2.2.3. Ankle

The arcs of motion of the ankle are not large, but they are critical for progression and shock absorption during stance. Momentum is preserved by the creation of a pivotal system in the heel, ankle and forefoot that allow the body to advance while the knee maintains an extended posture, as shown in Figure 2.6 [Perry, 92]. In swing, ankle motion contributes to limb advancement. The range of motion for the ankle can be seen in Figure 2.7.

Initial contact occurs as the heel contacts the floor with the ankle in neutral position pulled by the tibialis anterior. To keep the body moving forward without interruption, a heel rocker is used. Rapid loading of the limb generates a plantar flexion moment that drives the foot toward the floor. The external plantar flexion moment is resisted by the internal dorsiflexion moment of the pretibial muscles (tibialis anterior, extensor

digitorum longus, and peroneus tertius) as they provide a controlled, eccentric contraction [Gage, 91]. This extends the heel support period, draws the tibia forward, and rolls the body weight forward on the heel. This also provides shock absorption for the brief period when the body weight free falls before heel strike.

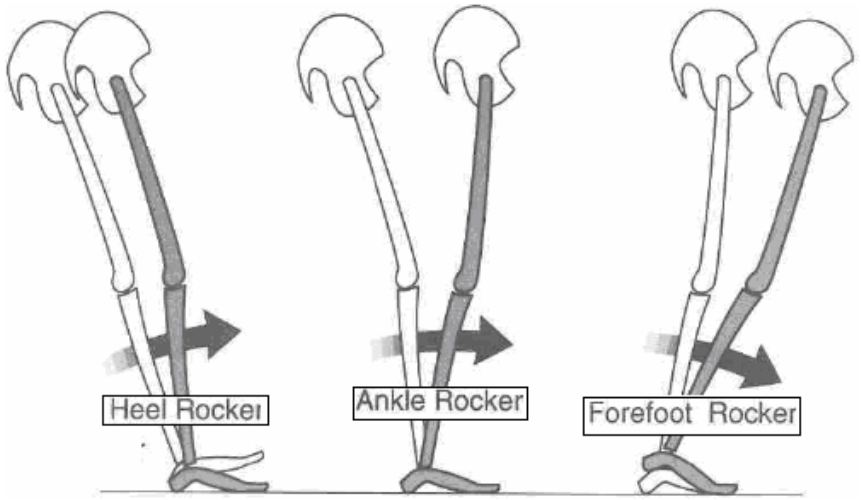

Figure 2-6 Heel, ankle and forefoot rockers used for body advancement [Perry, 92]

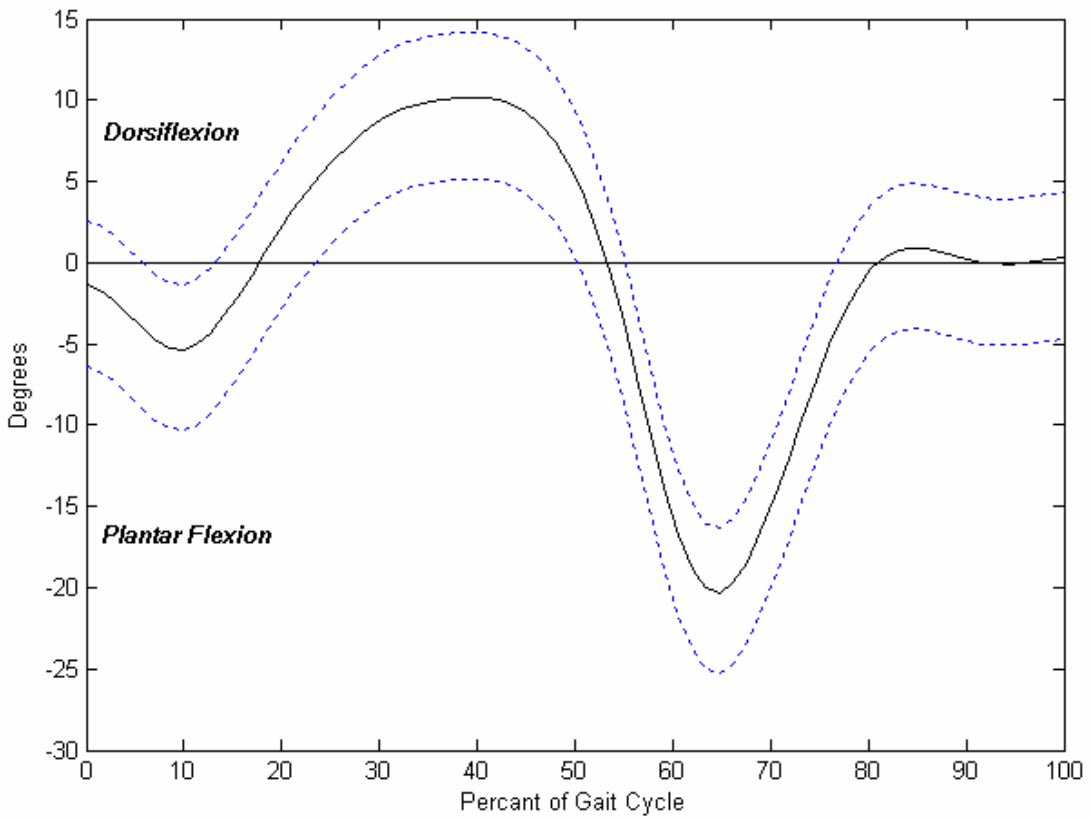

Figure 2-7 Ankle range of motion

Ankle motion during mid stance serves as an ankle rocker to continue progression. The displacement of the body over the foot creates an increasing dorsiflexion moment that rolls the tibia forward from an initial eight degrees of plantar flexion to five degrees dorsiflexion, while the foot remains in contact with the floor [Perry, 92]. The gastrocnemius and soleus muscles slow the rate of tibial advancement until the end of mid stance to restrain the forward movement of the tibia on the foot [Whittle, 91]. Soleus activity is the dominant decelerating force because of its larger size and its direct attachment between the tibia and calcaneus, as shown in Figure 2.3.

By the end of mid stance, the ankle is locked by the gastrocnemius and soleus, and the heel rises due to continued tibial advancement. This makes the forefoot the sole source of foot support and creates a forefoot rocker to allow for forward progression. During terminal stance, a combination of limited ankle dorsiflexion and heel rise places the ground reaction force (GRF) anterior to the source of foot support. As the GRF moves more anterior to the metatarsal head axis, the foot rolls with the body, leading to a greater heel rise and an increasing dorsiflexion moment. This creates a free forward fall situation that passively generates the major progression force used in gait. The ground reaction force created is greater than body weight and varies with gait velocity. By the end of terminal stance, there is no stabilizing force within the foot, so it is free to plantar flex in response to the triceps surae muscle, commonly called push off [Perry, 92].

Following the onset of double limb support, the body weight is transferred to the other limb in preparation for pre-swing. Peak soleus and gastrocnemius activity only support a heel rise and accelerate advancement of the unloaded limb. The tibia moves forward as the toe is stabilized by floor contact and the knee flexes in preparation for swing.

During toe off, the ankle is plantar flexed approximately 20 degrees. The pretibial muscles increase intensity in initial swing to dorsiflex the foot to neutral by the time the swing foot is opposite the stance limb. The dorsiflexion moment decreases in mid swing since only an isometric force to support the foot at neutral or slightly plantar flexed is required. During terminal swing, pretibial muscle activity increases to assure the ankle is at neutral position for optimal heel contact and in preparation for the increased force requirement of initial contact [Gage, 91].

2.3. Drop Foot

Drop foot is the inability of an individual to lift one's foot because of reduced or no muscle activity around one's ankle. When a person with drop foot walks, the foot slaps down onto the floor. To compensate for the toe drop, the patient must raise the thigh excessively, as if walking upstairs. Major causes of drop foot include: severing of the nerve, stroke, cerebral palsy and multiple sclerosis. There are two common complications from drop foot. First, the patients cannot control the falling of their foot after heel strike, and the foot slaps the ground on every step. This condition is referred to as slap foot. The second complication is the inability of drop foot patients to clear their toe during swing. A conventional approach to the treatment of drop-foot gait is a mechanical brace called an ankle foot orthosis (AFO).

An ankle–foot orthosis can be prescribed for patients with musculoskeletal or neuromuscular dysfunction to accomplish a variety of goals. For patients with an unstable ankle, whether from injury or muscular imbalance, an AFO can be used to support the foot and ankle to maintain optimal functional alignment during activity or to limit motion to protect healing structures. For patient with neuromotor dysfunction, the AFO can also

be a substitute for inadequate muscle function during key point in the gait cycle. The AFO can optimize alignment and help to manage abnormal tone, or can minimize the risk of deformity associated with long-term hypertonicity [Lusardi and Nielsen, 2000].

The simplest passive AFO is a rigid polypropylene structure that prevents any ankle motion and the foot will always be leveled with the ground. This passive AFO is a mechanical device that provides the additional stiffness needed to hold the foot. Although a passive constant stiffness AFO is able to provide safe toe clearance in drop-foot patients, the device does not reduce the occurrence of slap foot. The other method is placing a dorsiflexion assist spring on a more flexible AFO to help lift the foot. This AFO provides a moment to lift the ankle slightly above neutral position, while allowing the patient to have more ankle motion. This passive AFO helps patients during normal walking by lifting their toe during initial swing. However, it does not remedy slap foot because the ankle moment required for controlled plantar flexion is too large for the spring. Passive AFOs cannot account for different walking speeds and as patients speed up, slap foot becomes more prominent as the foot needs to be raised faster for ground clearance. Lastly, the passive AFOs cannot compensate for other factors such as inclines or muscles fatigue.

2.4. Ground Reaction Force

To be able to find the required power at each joint during walking, an inverse dynamic analysis must be performed. Kinetic data and external forces should be known for this purpose. The kinetic data was explained in the previous sections.

Ground reaction force is the main force acting on the body during different human movements. It is a three dimensional force which consists of a vertical component plus

two shear components acting along the contact area. These shear forces are usually resolved into anterior-posterior and medial-lateral directions [Winter, 04].

The two shear forces are small compared to the vertical GRF and result from any non-perpendicular components of the GRF [Wu, 99]. Herein, only the vertical GRF is investigated, therefore, the two shear components are not discussed. Figure2.8 shows a typical GRF profile of a single walking step.

The GRF has two peaks separated by a valley. Figure 2.8 shows a rapid rise to a value exceeding the body weight at the heel contact. This peak is due to accelerated body motion at heel contact and increases with higher speeds. Then by knee flexion during midstance, the body rolls forward over the stationary foot and GRF drops below the body weight level. During the push off phase, because of the ankle plantar flexion, a second peak is occurred.

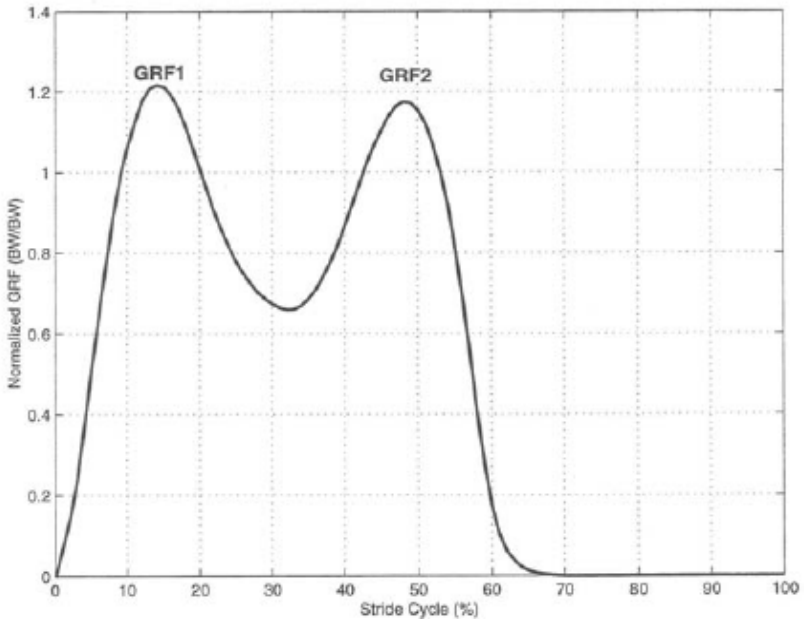

Figure 2-8 Typical ground reaction forces profile for one walking step

The second peak is greater than the body weight, indicating a downward acceleration and a lowering of the center of mass as the body falls forward over the forefoot. In simple

words, the ground reaction force can be related to the acceleration of the center of mass as shown in Equation 2.1

$$GRF = M(g + a) \tag{2.1}$$

Where, 'M' is mass of the body and 'a' is acceleration of the center of mass.

2.5. Ankle Behavior

Complex active and passive components are involved within the human foot–ankle system to create the kinematics and kinetics which were introduced in the last two sections. In order to design effective prosthetics and orthosis devices, the information gathered about the overall system should be carefully examined.

In 2004 Hansel et al. ran a series of experiments to check the effect of walking speed on ankle stiffness and the results are shown in Figure 2.9.

The ankle moment versus angle curves show clockwise hysteresis loops at slow walking speeds, a behavior that can be exhibited by either active or passive mechanical systems. In the human ankle–foot system, active musculo-skeletal components are likely utilized with passive components at all walking speeds. However, an ankle prosthesis consisting of a rotational spring–damper system could be used to mimic the behavior at slow walking speeds. As the walking speeds approach normal self-selected levels, the quasi-stiffness of the ankle changes such that the hysteresis loop essentially disappears. This behavior could be mimicked by a highly efficient rotational spring system. Lastly at fast walking speeds the hysteresis loop of the ankle moment versus ankle angle curve changes to a counterclockwise loop [Hansel et al., 04]

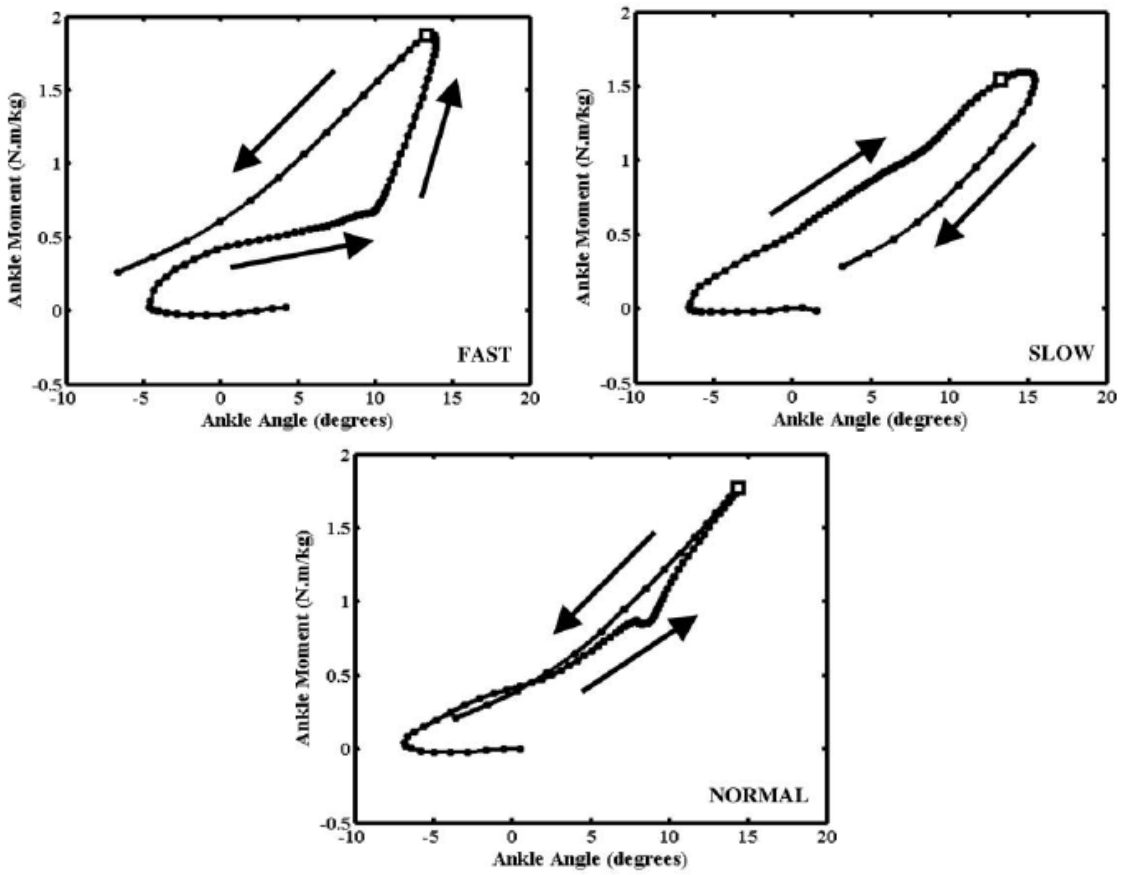

Figure 2-9 Ankle moment versus ankle angle plots for a typical subject walking at three speeds. 1.2 m/s (slow), 1.5m/s (normal) and 1.9m/s (fast) [Hansel et al., 04]

To mimic the behavior of the ankle at fast speed, an augmented system (i.e. a system with active components) would be necessary. A theoretical passive ankle prosthesis designed to mimic the external mechanical characteristics of the human ankle could utilize a spring-damper system with a quasi-stiffness loading characteristic similar to the unloading curves in Figure 2.10. Additionally, the device reduces damping to nearly zero as the walking speed is increased to normal ranges. The behavior of the unloading ankle moment versus ankle angle curves (Figure 2.10) could be mimicked using the same rotational spring with a changing equilibrium angle (angle at which the torque would go to zero). This behavior can be explained by Feldman's [Feldman, 86] equilibrium point

theory [Mesplay, 93], and may be harder to replicate in a prosthetic device without the use of active components.

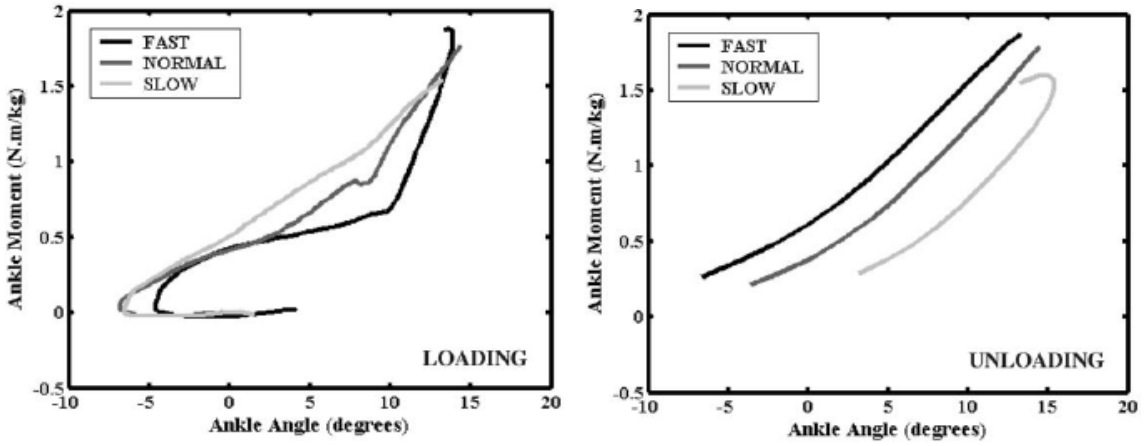

Figure 2-10 Loading and unlading portions of the ankle moment versus ankle angle plots from a typical subject walking at three different speeds[Hansel et al., 04]

Chapter 3

3. Modeling Human Walking

It is essential to study human movement in order to effectively design assistive devices. However, it is not always possible to use human subjects. This is due to the fact that research involving human subjects may be associated with discomfort or even injuries. Therefore, as an alternative method, modeling can be use to obtain joint loading information through computer simulation.

In this research, a mathematical model is developed to investigate the effectiveness of the SMA actuated AAFO. To this end, human walking has been modeled as well as the behavior of the AAFO. This chapter covers the modeling and simulation of human motion while the next chapter focuses on modeling of the shape memory alloy actuator for the active orthosis. The first part of this chapter talks about recording the kinetic data. In the second section, a method is proposed to design a trajectory for any given walking speed. In the last sections, a new approach is provided to simulate human walking.

3.1. Kinematics

To understand the kinematics of human walking, it is necessary to track the human movement. There are different types of human movement tracking systems including

non-vision based tracking systems and vision based tracking systems with and without markers [Zhou and Hu, 04]. The following sections each of these methods.

3.1.1. Non-Vision Based Tracking System

In non-vision based systems, sensors are attached to the human body to collect movement information. These sensors are commonly classified as mechanical, inertia, acoustic, radio or microwave and magnetic sensing. Some of these devices have a small enough sensing footprint to monitor small amplitudes such as finger or toe movements. Each one of these sensors has certain advantages and limitations. Limitations include modality specific, measurement-specific and circumstance specific limitations that accordingly affect the use of the sensor in different environments [Welch and Foxlin, 02].

3.1.2. Vision Based Tracking System

This is a technique that uses optical sensors, e.g. cameras, to track human movements, which are captured by placing identifiers on the human body. As the human skeleton is a highly articulated structure, twists and rotations make the movement fully three-dimensional. As a consequence, each body part continuously moves in and out of occlusion from the view of the cameras, leading to inconsistent and unreliable tracking of the human body. As a good solution to this situation, marker-based vision systems have attracted the attention of researchers in medical science, sports science and engineering [Sturman and Zeltzer, 94].

In vision based tracking system a digital camera is used to collect the raw data in a sampling process. Based on sampling theory in processing of any time varying data, the processed signal must be sampled at a frequency at least twice as high as the highest

frequency present in the signal itself. It has been shown that kinetic and energy analysis can be done with negligible error using a standard 24-frame per second movie camera [Winter, 82]. However, to add more detail and accuracy, it is better to use higher speed recording cameras.

Figure 3-1 An infrared camera used for recording the motion of a human. [Vicon©]

3.1.3. Data collection

In this research, to capture the kinetic data of human motion, a subject who had reflective markers on the lateral second metatarsal, the lateral malleolus, the heel, the center of rotation of the knee and the greater trochanter was asked to walk in the Gait Lab surrounded by eight infrared cameras. Infrared cameras do not use a visible light and therefore are not influenced by reflection from light sources other than those sources required to get the desired circular reflection from the markers.

As shown in Figure 3.1, the active infrared lights form a ‘donut’ shape around each camera lens. These lights are pulsed at 120 Hz for a period less than a millisecond. Thus, the reflected infrared light from the markers is the only light that is picked up by the camera, and since it is a pulsed source, the marker images are frozen in time.

The camera provides a two-dimensional image of a three-dimensional situation. To determine the three-dimensional spatial coordinates, eight different cameras are used to provide eight images at a single instant. The 3D analysis can be performed by using Direct Linear Transformation method (DLT) [Abdel Aziz and Karara, 71]. For 'm' markers, the DLT method provides a linear relationship between the two-dimensional coordinates of the i^{th} marker on the film and its three-dimensional location in space. For 'n' cameras, the relationship between the coordinates of the marker on the film of the j^{th} camera and the spatial three-dimensional coordinates of each marker are determined by:

$$X_{ij} = \frac{a_{1j}x_i + a_{2j}y_i + a_{3j}z_i + a_{4j}}{a_{9j}x_i + a_{10j}y_i + a_{11j}z_i + 1} \qquad (i = 1,...m) \qquad (3.1)$$

$$Y_{ij} = \frac{a_{5j}x_i + a_{6j}y_i + a_{7j}z_i + a_{8j}}{a_{9j}x_i + a_{10j}y_i + a_{11j}z_i + 1} \qquad (j = 1,...n) \qquad (3.2)$$

Where (X_{ij} , Y_{ij}) is the coordinate of the i^{th} marker on the film measured with the j^{th} camera, (x_i , y_i , z_i) is the coordinate of the i^{th} marker in the three-dimensional space and ' a_{kj} 'is the k^{th} coefficient in the transformation formula, which is calculated through calibration techniques.

3.1.4. Filtering

The collected data (raw data) contain additive noise from many possible sources. Noise could be from optoelectric devices, calibration processes, or human error in manual digitizing. Therefore, it is essential that raw data be filtered and smoothed.

Normal walking has been analyzed by several researchers and the harmonic content of the trajectories of the seven leg and foot markers has been determined [Winter et al., 74].

The highest harmonic was found to be in the toe and heel trajectories, and it was found that 99.7% of the signal power was contained in the lower seven harmonics (below 6 Hz). This results in selecting 6 Hz as a cutoff frequency for the filter (f_c = 6). Capturing the human motion at 120 Hz indicates a sampling frequency (f_s = 120). Therefore a ratio of 20 for the sampling frequency, over low-pass cutoff frequency, is effective at rejecting noise and passing data. Positional data are digitally filtered independently in X, Y, Z direction with a Butterworth low-pass filter. This filter passes, unattenuated, the lower frequency signal while at the same time attenuating the higher frequency noise. The data is then passed through the filter a second time in reverse order to eliminate phase distortion. This eventually created a fourth-order, zero-phase shift, double-pass filter with the same cutoff frequency.

The mathematical form of a second order Butterworth low-pass filter is as follows:

$$X^{f}_{(nT)} = a_0 X^{r}_{(nT)} + \sum_{i=1}^{2} [a_i X^{r}_{(n-i)T} + b_j X^{f}_{(n-i)T}] \tag{3.3}$$

Where ' X_f ' is the filtered output coordinate, ' X_r ' is the raw coordinate data, ' nT ' is the nth sample, ' $(n-i)T$ ' is the (n-1)th sample and ' a_i, b_i ' are filter coefficients listed in Table 3.1.

Table 3-1 Coefficient for Butterworth Low-Pass Filter

f_s / f_c	a_0	a_1	a_2	b_1	b_2
6	0.15505	0.31010	0.15505	0.62021	-0.24041
8	0.09763	0.24247	0.09763	0.94281	-0.33333
10	0.6746	0.19526	0.6746	1.14298	-0.41280
12	0.04949	0.09898	0.04949	1.27963	-0.47759
14	0.03789	0.07578	0.03789	1.37889	-0.53045
16	0.02995	0.05991	0.02995	1.45424	-0.57406
18	0.02428	0.04856	0.02428	1.51338	-0.61051
20	0.02008	0.04017	0.02008	1.56102	-0.64135

3.1.5. Joint Angle Calculation

Given the coordinate data from anatomical markers at either end of a segment, it is an easy step to calculate the absolute angle of that segment in the space. Figure 3.2 shows the limb and joint angles in the spatial reference system.

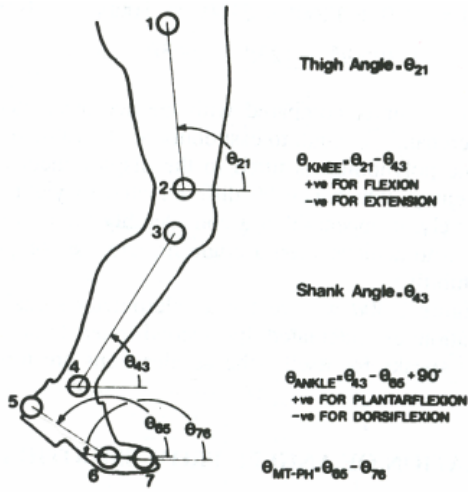

Figure 3-2 Limb and joint angles in the spatial reference system [Winter, 04]

The angles of ankle, hip and knee can be calculated based on the position of the markers and through Equation 3.4 to 3.6.

$$\theta_{Ankle} = \tan^{-1}\left(\frac{z_3 - z_4}{x_3 - x_4}\right) - \tan^{-1}\left(\frac{z_6 - z_5}{x_6 - x_5}\right) + \frac{\pi}{2} \tag{3.4}$$

$$\theta_{Knee} = \tan^{-1}\left(\frac{z_2 - z_1}{x_2 - x_1}\right) - \tan^{-1}\left(\frac{z_3 - z_4}{x_3 - x_4}\right) \tag{3.5}$$

$$\theta_{Hip} = \tan^{-1}\left(\frac{z_2 - z_1}{x_2 - x_1}\right) \tag{3.6}$$

3.2. Simulation of Walking

Human locomotion has attracted the attention of many researchers. Because of complexity and the linked segment model, certain oversimplifications were made or the

simulation was considereed to short periods of the movements. Townward and Seireg [Townward, 72] modeled the human with massless rigid lower limb with one degree of freedom (DOF) at each hip (flexion/extension). Hemami [Hemami, 80] proposed a three-segment three-dimensional model with rigid legs and no feet, and Pandy and Berme [Pandy, 88] simulated single support only using a five-segment planar model with no feet. Such simplification would not produce realistic results. Even with more complete models, many researchers constrained parts of their model's kinematics [Beckett and Chang, 68; Chao and Rim, 73; Townsend, 81].

Kooman et al. used an inverse dynamics model for the analysis, reconstruction ans prediction of bipedal walking [Koopman, et al., 95]. They combined the inverse dynamics model with optimization techniques in order to predict walking pattern or to reconstruct non-measured rotation when only a part of the three-dimensional joint rotation is measured. Gilchrist and Winter used a 3D nine-segment model of walking in ADAMS software. This model demonstrated some success using the inverse dynamic joint moments as input [Gilchrist and Winter, 97].

After the pioneer works in early 80s, the optimization techniques were introduced to use muscle forces in the modeling of human walking.

Anderson and Pandy combined a three-dimensional, neuromusculoskeletal model of the body and dynamic optimization theory to simulate normal walking on level ground [Anderson and Pandy, 2001].

There are two well known approaches for simulating the human walking, inverse dynamics and forward dynamics. The next two sections will provide some information and difficulties in using each approach. In this study the stability criterion is selected to

check the performance of the AAFO instead of generating the simulation of walking and the reason is the difficulties associated with Inverse and Forward Dynamics. This approach is introduced in section 3.3.3

3.2.1. Inverse Dynamics

The first approach is using inverse dynamics to study the human movements. This type of analysis takes the kinematic measurements and combines them with measured external forces such as ground reaction forces, to estimate the internal joint reaction forces and moments. This, of course, is the inverse of what really happens, hence the name inverse dynamics.

The main problem with the inverse dynamics method is that it is required to measure all the joint angles as well as the ground reaction force. However, for a patient with drop foot, these measurements are completely different than a normal person. Running another experiment with a subject who has a drop foot problem may provide the missing information. By using an AAFO, however, both GRF and joint angles will change in time and this information is not predictable. In addition to these limitations, the main purpose of the simulation in this work is to study the effectiveness of the AAFO in improving the patient's walking condition. Obtaining this information is not possible with the inverse dynamics approach.

3.2.2. Forward Dynamics

In this approach, a time-varying joint moment will be applied to each joint. The net effect of all muscle forces acting at each joint generate this moment, which in turn accelerates (or decelerates) the adjacent segments and ultimately cause displacement. The constraints

of forward solution models are considerable when compared with inverse solutions. These constraints and assumptions are listed as follows [Winter, 04]:

1. There must be no kinematic constraints; the model must be permitted to fall over, jump or collapse as dictated by the inputs.
2. The initial conditions must include the position and velocity of every segment.
3. The only inputs to the model are externally applied forces and internally generated moments.
4. External reaction forces such as GRF must be calculated and applied to the system during a simulation.

Using forward dynamics, simple human body motions have been modeled with reasonable success. Philips et al. modeled the swinging limbs of a human using the accelerations of the swing hip along with the moments about the hip [Philips et al. 83]. Hemami et al. (1982a) modeled the sway of the body in the coronal plane with each knee locked. With adductor/abductor actuators at the hip and ankle as input, the stability of the total system was defined.

More recent modeling of three-dimensional gait has been more successful. One of the major problems with previous attempts was the modeling of initial contact. These earlier models employed springs to represent the elastic characteristics of the bottom of the feet, which resulted in extremely large accelerations of the foot segment and similarly large spikes in the ground reaction forces. This was solved with a viscoelastic model of the foot with an array of parallel spring and dampers under the rigid foot model [Gilchrist and Winter, 96].

However, even with using more realistic model for the initial contact, it becomes apparent that in the forward dynamics approach any small errors in the joint moments after about 500 ms results in accumulating kinematic errors that ultimately becomes too large, and the model either becomes unbalanced or collapses. The accumulation of these errors is an inherent characteristic of any forward dynamics model. The double integration of the segment accelerations caused by the input and reaction moments and forces, cause displacement errors that increase over time. To overcome this problem a new approach is presented in the next section.

3.3. Stability Criterion to Check the Performance AAFO

In this work, the purpose of simulating human walking motion is to develop an environment that a SMA AAFO can be tested on a patient with drop foot. The main assumption in this approach is that, the patient with drop foot has the same joint angles at all the joints but ankle.

The proposed method consists of two parts, trajectory generation and stability criterion. In the first part, the trajectory of all joints except the ankle is applied to the corresponding joint. For the ankle, the recorded normal human walking data is assumed as a desired trajectory for the control systems. Based on the dynamics of the SMA actuator and control systems, the actuator will have a response to that of the desired trajectory. This response is calculated off-line and then applied to the ankle joint.

3.3.1. Trajectory Generation

Using a vision-based recording system; it is possible to capture the data of human walking for a specific person at a specific speed. However to have information about the

joint angle at different walking speed, it is required to run the experiment again. At the same time, it is necessary to ensure that the subject maintains the desired walking speed, which is not an easy task. To overcome this problem, a trajectory generation method is presented in this section. The generated trajectory by this method can both fit the sample data of the experiment and also predicts the joint trajectories at the other speeds.

Interpolation between some key points (gait parameters) and defining the whole trajectory based on two control parameters (' x_{ed} ' and ' x_{sd} ') is the main idea of the presented method [Tarkesh, 07]. Most of the parameters used for formulating the walking motion, are shown in Figure 3.3.

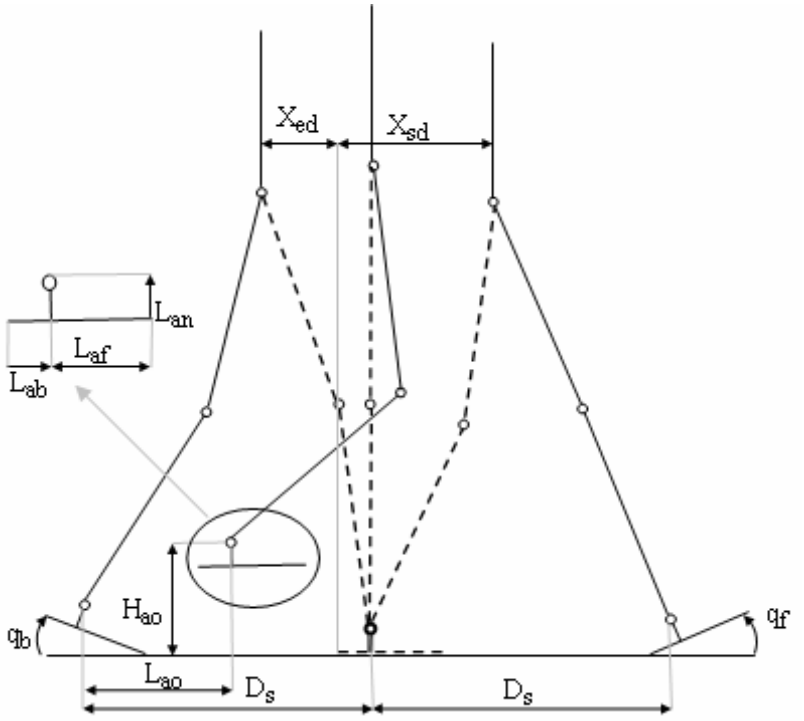

Figure 3-3 The gait and geometrical parameters

In the proposed method for trajectory generation, the whole joint trajectory will be dependent on three sets of parameters: geometrical parameters, gait parameters and control parameters. The list of all these parameters is given in Table 3.2.

Table 3-2 All the parameters and their definition in trajectory generation

Parameter	Definition	How to calculate
x_a, y_a	Ankle coordinates in XY plane	
x_h, y_h	Hip coordinates in XY plane	
θ_a, θ_h	Ankle and hip relative sagital rotational angles	
	Geometrical Parameters:	
L_{th}	Length of thigh segments	Given in Table3.3
L_{sh}	Length of shank segments	Given in Table3.3
L_f	Length of foot segments	Given in Table3.3
L_{ab}	Distances from back of the foot to the ankle along the X-axis	Given in Table3.3
L_{af}	Distances from front of the foot to the ankle along the X-axis	Given in Table3.3
L_{an}	Distances along the Y-axis from foot to the ankle	Given in Table3.3
	Gait Parameters:	
T_c	The Instant in that one walking cycle is completed	It defines the speed of walking so for different speed, it is given
T_d	The instant in that double support phase is finished	Defined based on T_c
T_m	The instant in which x_a, y_a reach L_{am} and H_{am}	Based on the recorded data, represented based on T_c
D_s	Length of each step	Based on the recorded data, assumed to be constant at any speed
H_{am}	Maximum height of the ankle during its motion	Based on the recorded data
L_{am}	Corresponding x position for H_{am}	Based on the recorded data
$h_{\min}, h_{\max}$	Min and Max height of the hip during its motion	Based on the recorded data
q_b, q_f	Foot departing and foot landing angle	Based on the recorded data
	Control Parameters:	
x_{ed}, x_{sd}	Distances along the x-axis from the hip to the ankle of the support foot	See Section 3.2.3

The first set is geometrical parameters, such as the length of each segment. In Table 3.3, physical properties of the body for each segment are given with respect to the mass and height of the body. 'M' and 'H' are the total body's mass and height, respectively while 'L' denotes length of the segment.

Table 3-3 Physical properties of the segments of the human body [Winter, 04]

	Head, Arms and Trunk (HAT)	Thigh	Shank	Foot
Mass	0.678 M	0.1M	0.0465M	0.0145M
Radius of Gyration	$1.142\,L_{tr}$	$0.323\,L_{th}$	$0.302\,L_{sh}$	$0.475\,L_f$
Length	$L_{tr}=0.52H$	$L_{th}=0.24H$	$L_{sh}=0.24H$	$L_f=L_{ab}+L_{af}$
Foot's Length	$L_f=0.152H$	$L_{ab}=0.33L_f$	$L_{af}=0.67L_f$	$L_{an}=0.39H$

The second set of parameters is the set of gait parameters, which are '$T_c, T_m, q_b, q_f, L_{ao}, H_{ao}, h_{\min}, h_{\max}$'. All these parameters are calculated based on sampled data which is recorded and will be fixed for other speeds. Because it is assumed that the step length is constant, different walking speeds will need different time cycles. Therefore, 'T_c' will be defined based on the speed of walking. It can be shown that having ankle and hip trajectories is sufficient to formulate the trajectories of all leg joints uniquely [Huang et. al, 01].

Here, all the calculations are carried out for one leg but it can simply be repeated for the other leg. Using experimental data captured from real human motion, it was possible to consider each joint's location at specific points. Interpolating these points by a particular function that both matches human motion and is compatible with geometrical and boundary conditions, one could plan trajectories for the ankle and hip. The functions used here must behave smoothly. To satisfy this condition, the functions must be differentiable and their second derivative continuous. For this purpose, polynomial spline and sinusoidal functions are used that normally satisfy these requirements.

3.3.1.1. Ankle Trajectory

A fourth degree polynomial is used for the ankle trajectory when the foot is in the swinging motion, while a sinusoidal function is used for the interval of foot-ground

contact as shown in Equations 3.7-3.11. The use of the latter function makes the foot trajectory compatible with geometrical constraints.

$$0 < t < T_d : \begin{cases} x_a = L_{af}\left(1-\cos\theta_a\right) - L_{an}\sin\theta_a \\ y_a = -L_{af}\sin\theta_a + L_{an}\cos\theta_a, \qquad \theta_a = -q_b\left(\frac{t}{T_d}\right)^p \end{cases} \tag{3.7}$$

$$T_d < t < T_m : \{x_a = F_1(t), \quad y_a = F_2(t), \quad \theta_a = G_1(t) \tag{3.8}$$

$$T_m < t < T_c : \{x_a = F_3(t), \quad y_a = F_4(t), \quad \theta_a = G_2(t) \tag{3.9}$$

$$T_c < t < T_c + T_d : \begin{cases} x_a = 2D_s - L_{ab}\left(1-\cos\theta_a\right) - L_{an}\sin\theta_a \\ y_a = L_{ab}\sin\theta_a + L_{an}\cos\theta_a \\ \theta_a = q_f\left(\frac{T_c + T_d - t}{T_d}\right)^p \end{cases} \tag{3.10}$$

$$T_c + T_d < t < 2T_c : \{x_a = 2D_s, \quad y_a = L_{an}, \quad \theta_a = 0 \tag{3.11}$$

Applying transitional conditions (given in Equations 3.13-3.9), these two curves are joined smoothly as in Figure. 3.4. In these trajectories, the foot angle is designed to vary in motion to better match human motion. This assumption is a distinctive feature of this work. In most previous works, it is assumed that the foot angle is constant and the foot always remains level with the ground. Assuming constant angle for the foot has the limitation that the biped's speed will be reduced due to shorter steps.

$F_i(t)$ and $G_j(t)$ are 4th and 5th order polynomial functions given in Equation 3.12 and 'p' is used for adjusting swing acceleration.

$$\begin{aligned} F_i(t) &= a_4t^4 + a_3t^3 + a_2t^2 + a_1t + a_0 \qquad i = 1,2,3,4 \\ G_j(t) &= b_5t^5 + b_4t^4 + b_3t^3 + b_2t^2 + b_1t + b_0 \qquad j = 1,2 \end{aligned} \tag{3.12}$$

The coefficients of the polynomial functions in the Equations 3.12 are calculated using the constraints given by Equations 3.13-3.15.

$$t = T_d : \begin{cases} x_a = L_{af}\left(1 - \cos q_b\right) + L_{an} \sin q_b \\ y_a = L_{af} \sin q_b + L_{an} \cos q_b, \quad \theta_a = -q_b \end{cases} \tag{3.13}$$

$$t = T_m : \{x_a = L_{am}, \quad y_a = h_{am}, \quad \theta_a = q_m \tag{3.14}$$

$$t = T_c : \begin{cases} x_a = 2D_s - L_{ab}\left(1 - \cos q_f\right) - L_{an} \sin q_f \\ y_a = L_{ab} \sin q_f + L_{an} \cos q_f \\ \theta_a = q_f \end{cases} \tag{3.15}$$

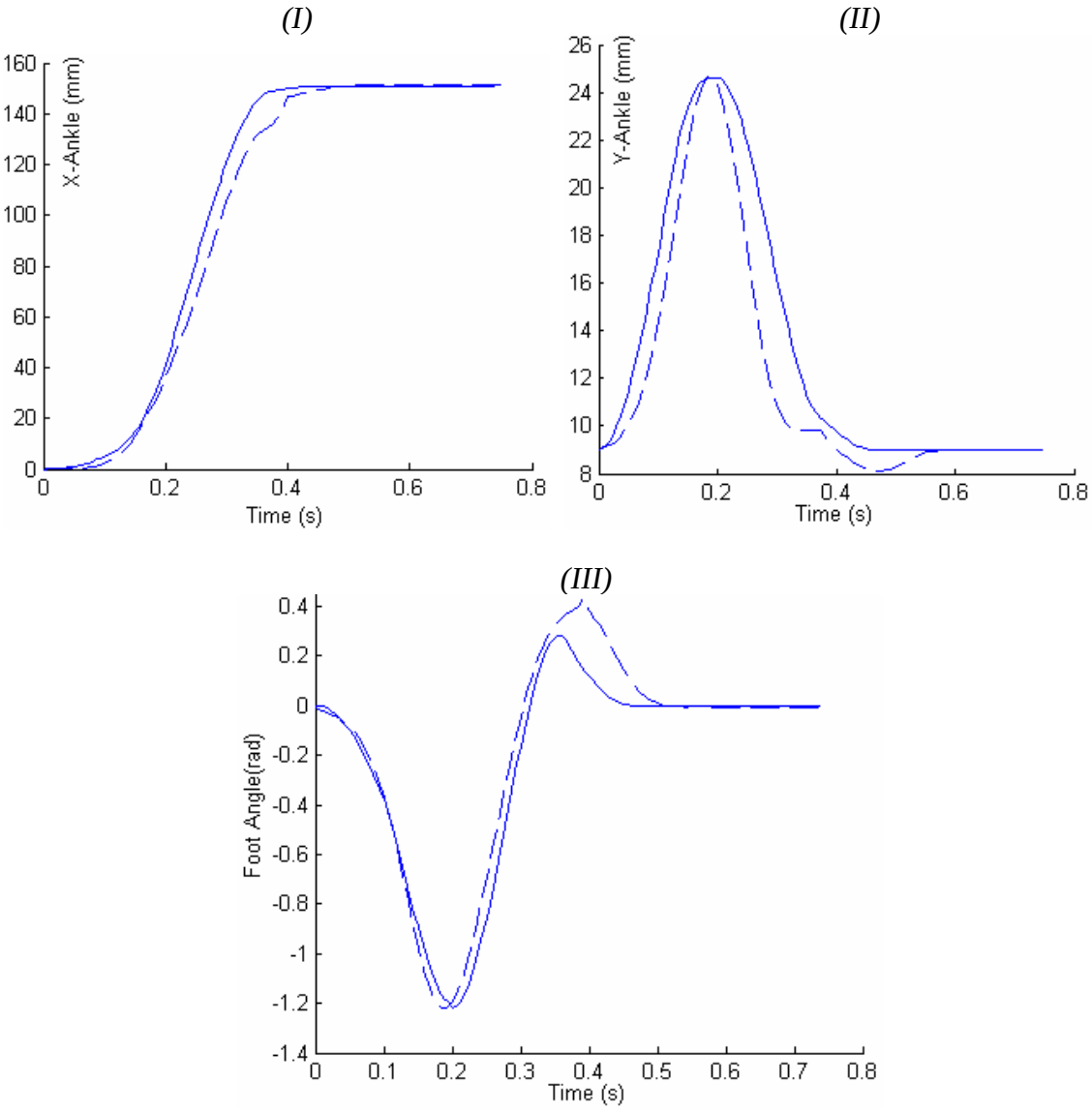

Figure 3-4 (I)-Ankle Trajectory in X-Direction, (II)-Ankle Trajectory in Y-Direction (III)-Foot angle (Dashed line is the human recorded data and the solid line is the generated trajectory)

3.3.1.2. Hip Trajectory

The hip trajectory is interpolated with third–order splines assuming to have its highest position midway in the single support phase and its lowest midway in the double support phase. This choice of trajectory minimizes the energy consumption of the body. This is because of the fact that the body has minimum height while it has maximum velocity and vice versa [Azimi et. al, 05]. This trajectory is represented in Equation 3.16 and is shown in Figure 3.5. Transitional conditions for hip equations are listed in Equations 3.17-3.18. Equations of hip motion in sagital plane in x and y positions are given as:

$$
\begin{aligned}
&0 < t < T_d : \begin{cases} x_h = X_{[1,1]}t^3 + X_{[2,1]}t^2 + X_{[3,1]}t + X_{[4,1]} = F_x \\ y_h = Y_{[1,1]}t^3 + Y_{[2,1]}t^2 + Y_{[3,1]}t + Y_{[4,1]} = F_y \end{cases} \\
&T_d < t < T_c : \begin{cases} x_h = X_{[5,1]}t^3 + X_{[6,1]}t^2 + X_{[7,1]}t + X_{[8,1]} = G_x \\ y_h = Y_{[5,1]}t^3 + Y_{[6,1]}t^2 + Y_{[7,1]}t + Y_{[8,1]} = G_y \end{cases} \\
&X_{8x1} = A_{8X8}{}^{-1} \times B_{8x1}, \\
&Y_{8x1} = C_{8X8}{}^{-1} \times D_{8x1}
\end{aligned}
\tag{3.16}
$$

A, B, C, D matrices are formed according to the constrained equations, given as:

A & B	$F_x(T_d) = D_s - x_{sd}$	$F_x'(T_d) = G_x'(T_d)$
$F_x(0) = x_{ed}$	$G_x(T_d) = D_s - x_{sd}$	$F_x''(T_d) = G_x''(T_d)$
$F_x'(0) = G_x'(T_c)$	$G_x(T_c) = D_s + x_{ed}$	$F_x''(0) = G_x''(T_c)$

(3.17)

C & D	$F_y(T_f) = h_{\max}$	$F_y'(T_s) = G_y'(T_o)$
$F_y(T_s) = h_{\min}$	$G_y(T_f) = h_{\max}$	$F_y''(T_s) = G_y''(T_o)$
$F_y'(T_f) = G_y'(T_f)$	$G_y(T_o) = h_{\min}$	$F_y''(T_f) = G_y''(T_f)$

(3.18)

$$T_s = 0.5T_d, \quad T_f = 0.5(T_c - T_d), \quad T_o = T_c + 0.5T_d$$

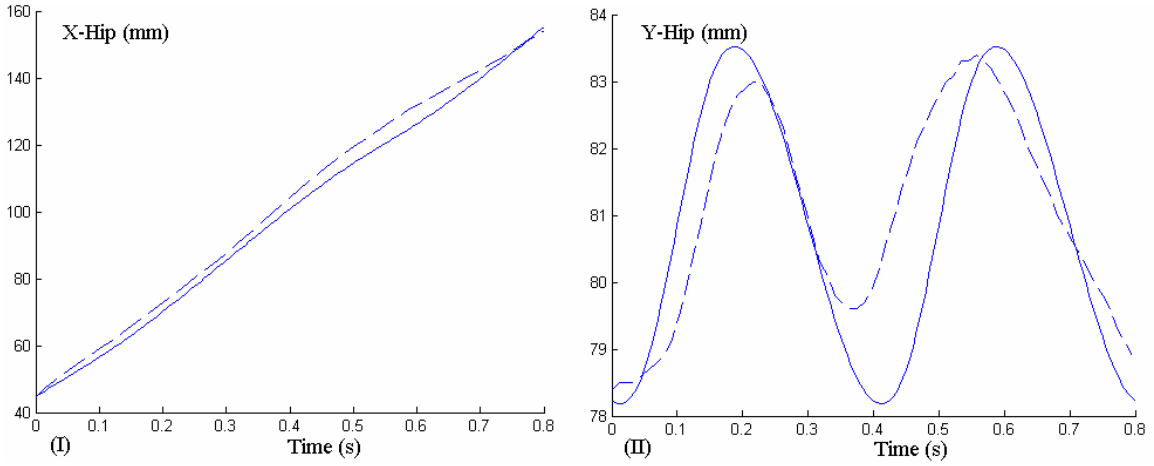

Figure 3-5 (I)-Hip Trajectory in X-Direction, (II)-Hip Trajectory in Y-Direction (dashed line is the human recorded data and the solid line is the generated trajectory)

3.3.1.3. Calculating Control Parameters

It was shown that having sample data of human walking, one can generate the trajectory of walking for another subject with a different height and/or walking speed. This trajectory generation is based on two parameters (control parameters). Since changing the value of control parameters will affect the whole joint trajectories, it is important to find the best value for these parameters. To this end, an optimization method is needed. It is assumed that a normal human chooses the most stable walking pattern during walking. Therefore, using a stability criterion [Tarkesh, 2007] for a different range of control parameters, the most stable walking pattern and the optimum control parameters associated with them can be found.

There are several methods to ensure the stability of a particular walking trajectory. In this study, the Zero Moment Point (ZMP) criterion is utilized. For stable walking, ZMP is a well known concept for the synthesis of a walking pattern. The ZMP is the point where the resultant of all reaction forces is applied. In other words, it is a point, about which the total moment of all the external forces is zero.

To find the safest trajectory, it is necessary to evaluate all possible trajectories planned by the method described above to satisfy the selected stability criterion. The pattern in which the largest stability margin is gained will be selected as the optimum walking pattern.

Section 3.3.2 will talk more about ZMP stability criterion in detail.

3.3.2. Stability Criterion

Depending on the analysis method, two different approaches are used for stability verification of the walking robots. In the first approach the, Center of Gravity (COG) is used as a stability criterion for static walkers with low speed. Such a system can be modeled as a static system at each instant. The similar concept for dynamic analysis is the Zero Moment Point (ZMP), which was introduced by Vukobratovic and Borovac in 1968. The ZPM criterion states that as long as the zero moment point is within the convex hull of all contact points, stability of walking is satisfied [Vukobratovic, 04]. In a biped, the stable region is the surface of the support foot (feet). The location of the ZMP is given by Equation 3.19.

$$x_{zmp} = \frac{\sum_{i=1}^{n} m_i(\ddot{y}_i + g)x_i - \sum_{i=1}^{n} m_i \ddot{x}_i y_i - \sum_{i=1}^{n} I_i \ddot{\theta}_i}{\sum_{i=1}^{n} m_i(\ddot{y}_i + g)} \qquad (3.19)$$

The distance between the boundaries of the stable region and the ZMP is called the stability margin. The stability is directly affected by this distance.

To check the performance of the AAFO the experimental data of tracking the ankle angle will be applied to the ankle joint while the other joint are following the data coming from the trajectory generation block. All these information will be used to check the stability

of motion based on the ZMP criterion. A summary of this approach is illustrated in Figure 3.6.

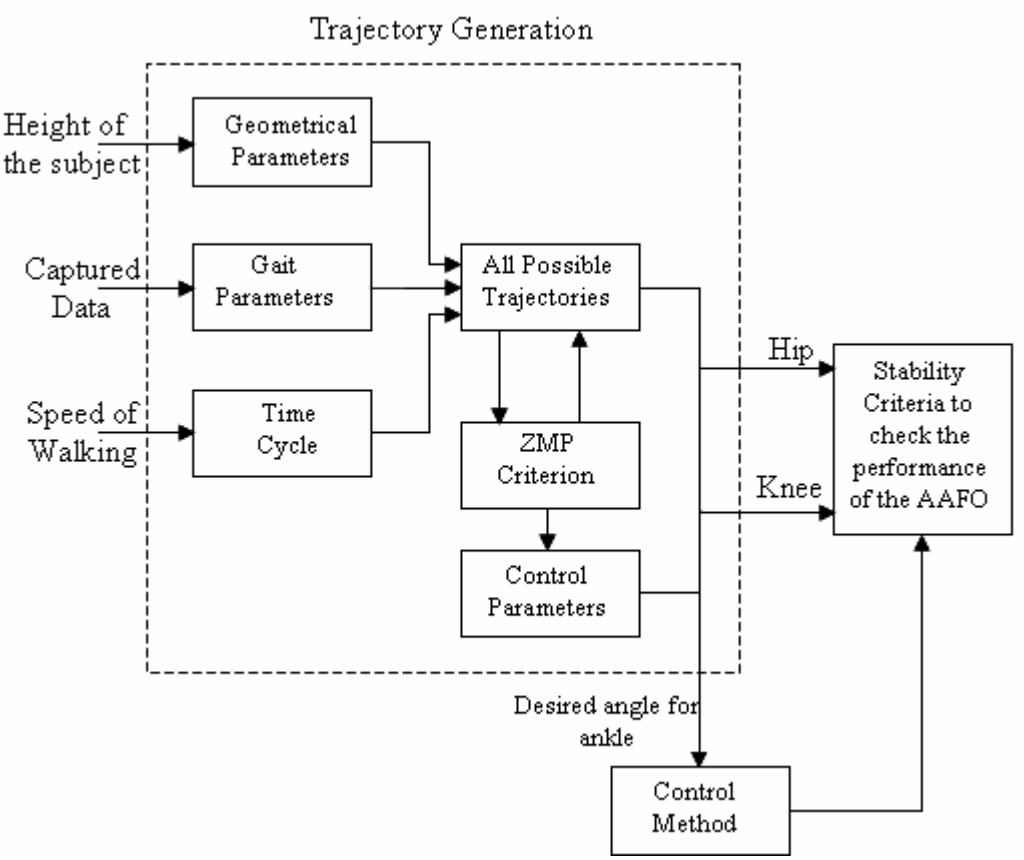

Figure 3-6 The algorithm to check the performance of the AAFO

3.3.3. Human Body Model

Biomechanical models of the entire human body are normally composed of rigid segments linked by simple kinematic connections [Bobbert and van Soest, 94; Gerritsen et al., 96]. However, the segments of the human body are not rigid and such an assumption can lead to some errors in both inverse and direct dynamics analyses, especially those associated with high accelerations and impulsive loading [Nigg and Bobbert, 90]. This error is the main reason of using wobbling mass models.

Typically in wobbling mass models, segments are separated into two elements: a rigid component, and a soft tissue component-the wobbling mass. In some studies [Minetti and Belli, 94; Wright et al., 98] only a single wobbling mass is included to represent the visceral mass. Gruber et al. [Gruber et al., 98] used a two-dimensional, three segment wobbling mass model to recreate the vertical ground reaction force for a subject landing from a drop. A similar model was used by another group to study the influence of soft tissue movement of ground reaction forces, joint torques and joint reaction forces in drop landing [Pain and Challis, 06]. Their results showed that peak joint torques and forces were much greater for the rigid body model compared with the wobbling mass model. Peak vertical ground reaction force increased to 40.5 bodyweights, compared with 16.2 bodyweights for the wobbling mass model. With rigid legs, and only a wobbling mass for the trunk, as stated by Wright [Wright et al., 98], the peak vertical ground reaction force was 31.4 bodyweights.

Since in our study we are not dealing with high acceleration (e.g running) or high impact loading (e.g drop landing), a rigid body model is used. The human body is modeled two dimensionally with four segments (foot, shank, thigh and HAT) connected with revolute joints (hip, knee and ankle). Each segment is representing by a rigid body model. The physical parameter of the human body is used for the proper segment which was given in Table 3.3.

Chapter 4

4. Modeling the AAFO

AAFOs have the potential to allow for significant improvement in the gait of those individuals who experience drop foot. As reported in Chapter 1, several studies have been published documenting the design of various prototypes. However, due to the types of actuators that have been employed in these prototypes and their overall design, the practicality of such designs is quite limited. Using DC motors in the Series Elastic Actuator at MIT shows promising results in a lab environment [Blaya, 04]. However it should be noted that the actuator weighs 2.6 kg and requires bulky batteries and electronics for operation. In addition, it was observed that patients may be unable to sit while wearing this AAFO.

The size and weight of the pneumatic auxiliary components such as the compressor would appear to be the main difficulty in using pneumatic actuation used in the AAFO at University of Michigan [Ferris, 05].

In order for an AAFO to be functional at a level that would allow it to be commercially viable, it must be light-weight, adaptable to a wide range of patients who vary in age, size, and type of disability, reliable and relatively uncomplicated. The need of light

weight and flexible actuation with a high power to mass ratio brings the idea of using novel actuators such as Shape Memory Alloys (SMA).

In order to check the feasibility of using Shape Memory Alloys as an actuator in AAFOs, a brief introduction of shape memory alloys is presented in the first section. It is then followed by conceptual design and introducing an experimental setup based on SMA actuation and ankle dynamics in section 2. Also, to check the functionality of SMA-AAFO in simulation environments as described in the previous chapter, the entire actuation mechanism is modeled in the last section.

4.1. Shape Memory Alloys

In 1932, a Swedish physicist by the name of Arne Olander discovered an interesting phenomenon when working with an alloy of gold (Au) and cadmium (Cd). The Au-Cd alloy could be plastically deformed when cool and then be heated to return to, or remember, the original dimensional configuration [Elahinia, 2004]. This phenomenon is known as the Shape Memory Effect (SME) and the alloys that exhibit this behavior are called Shape Memory Alloys (SMA) [Mavroidis et al., 99]. In 1961, a group of U.S. Naval Ordnance Laboratory researchers lead by William Beuhler stumbled across a significant discovery in the field of SME and SMA. While testing an alloy of Nickel and Titanium for heat and corrosion resistance, they found that it too exhibited the SME. The Ni-Ti SMA proved to be significantly less expensive, easier to work with, and less dangerous (from a health standpoint) than previously discovered alloys. These factors refreshed interest and research in SME and its applications.

Shape Memory Alloys consist of a group of metallic materials that demonstrate the ability to return to some previously defined shape or size when subjected to the

appropriate thermal procedure. Some examples of these alloys are AgCd, AuCd, CuAlNi, CuSn, CuZn(X), InTi, NiAl, NiTi, FePt, MnCu, and FeMnSi. The SME occurs due to a temperature and stress dependent shift in the materials crystalline structure between two different phases called Martensite and Austenite. Martensite, the low temperature phase, is relatively soft whereas Austenite, the high temperature phase, is relatively hard [Elahinia, 04].

For a simple example of the SME in action, consider the following: If a straight bar of some SMA in its austenitic (high temperature) phase is allowed to cool below the phase transition temperature, the crystalline structure will change to Martensite. If the bar is subsequently plastically deformed, by say bending, and then reheated above the phase transition temperature, it will return to its original straight configuration (Figure 4.1).

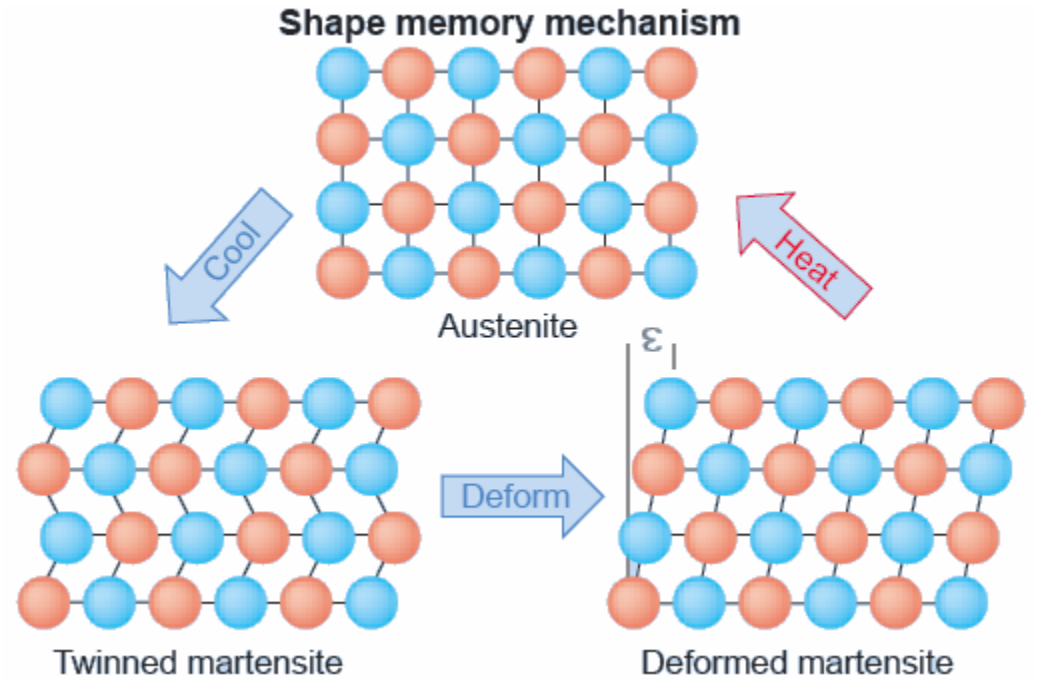

Figure 4-1Shape Memory Mechanism [Lombardi, 04]

The change that occurs within a SMAs crystalline structure is not a thermodynamically reversible process. In other words, there is energy dissipation due to internal friction and

structural defects. As a result, a temperature hysteresis occurs which is shown in Figure 4.2.

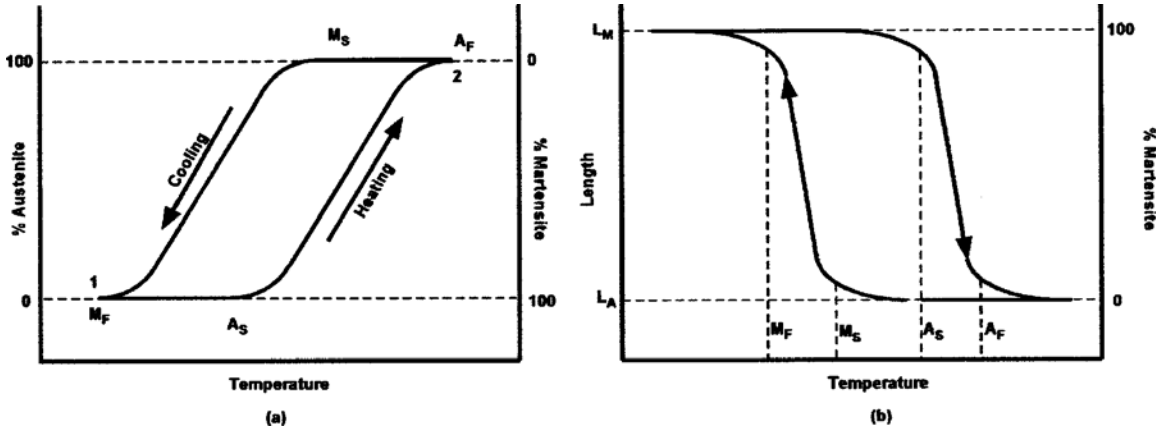

Figure 4-2 Hysteresis loop in shape memory alloy actuators [Mosley, 01]

Of all the Shape Memory Alloys that have been discovered to date, Nickel-Titanium (Ni-Ti) has proven to be the most flexible and beneficial in engineering applications. The following characteristics of Ni-Ti make it stand out from the other SMAs: greater ductility, more recoverable motion, excellent corrosion resistance (comparable to series 300 stainless steels), stable transformation temperatures, high biocompatibility, and the ability to be electrically heated for shape recovery.

Their advantages include drastically reduced size, weight, and mechanical complexity. SMAs also have disadvantages, which must be thoroughly considered prior to application. Compared to more conventional actuators, they operate with a low efficiency, at low bandwidths and with small displacements.

4.1.1. SMA Applications

Typical SMA applications fall into two large categories based on the specific properties that are considered: superelastic applications and shape memory effect applications. Superelastic (pseudoelastic) properties are used primarily in the biomedical field, for

stents, guidewires, orthodontic wires, osteosynthesis, etc. Another typical and important application exploiting the superelastic property is that for eyeglass frames. Shape memory effect, on the other hand, is primarily used in the industrial field for Joule effect actuators, which can take advantage of the stroke, force and durability characteristics of SMAs. A simple SMA wire can replace an electromagnetic motor, enabling cost savings and design simplicity, especially when simple mechanical movements are required. More effective actuators can be obtained by using SMA wires showing the two-way effect. This types of actuators can be used, for instance, in locks, both for automotive and several other industrial applications, for electronics-related applications (such as plug-in devices for PCs), for the movement of small parts in toys, and broadly speaking, when a simple mechanical movement is required and space, weight, and cost set severe production constraints. Another important application is related to sensor- actuators, in which the SMA wire, both in wire and in spring formats, can react to a room temperature change by modifying its shape, and in doing so actuating specific devices, such as sprinklers for fire prevention [Otsuka, 99].

SMA Blood-clot filters have been developed that can be easily deformed and inserted in a vein while cold. Upon heating by the body, the filter that is made of NiTi wire, is functionally shaped and anchors itself in the vein and catches the passing clots [Miyazaki, 98].

Cryofit hydraulic coupling are SMA cylinders made by Raychem Corporation. They are expanded while in martensite phase. When they warm up to austenite they shrink in diameter and strongly hold the tube ends. The tube diameter prevents the SMA sleeve

from fully recovering its original shape. The stress created by the sleeve is strong enough to create a joint that, in many ways, is superior to a weld [Gilbertson, 2000].

For force actuation, excluding robotic applications, SMA materials have been used as circuit board edge connectors. The SMA is biased by a linear spring. In this electrical connector system, when the connector is heated, the SMA component opens the spring. This allows force free insertion or removal of the circuit board. Upon cooling the SMA releases the spring which then closes the circuit to form the connections. SMAs have found other application based on the same idea. One such example is fire safety valves that use an SMA element to shut off the toxic or flammable gas flow when a fire occurs [Melton, 98].

Another class of SMA actuators is designed to use a portion of the shape recovery for accurate positioning. An example of such an actuator is a flow rate control valve. The flow rate is adjusted by raising the temperature of a SMA component such the valve close to a desired amount [Otsuka, 99].

The pseudoelastic property of shape memory alloys has been used in a number of commercially available products. An example is an eyeglass frame that is made of NiTi. The shape memory alloy can undergo large deformations without damaging the frame. Another example is guide wires for steering catheters that have been developed using NiTi wires into vessels in the body. The guide wire resists permanent deformation if bent severely [Miyazaki, 98].

SMAs are extremely corrosion resistant, demonstrate excellent biocompatibility, can be fabricated into very small sizes and have properties of elasticity and force delivery. These properties make these materials a natural candidate for biomedical applications

[Gilberson, 2000]. The biological compatibility is of paramount importance in using any material in vivo environment. Therefore many studies on the biocompatibility of NiTi have been performed in vitro and in vivo, including their behavior during sterilization [Thierry, 98]. A number of medical applications that make use of the SMA's mechanical properties have been proposed [Lipscomb, 96; Yhia, 2000]. Among them are orthodontic wires [Natrass, 98; Schneevoigt, 99], orthopedic implants for osteosynthesis [Reyhanen, 99], stents for various applications [Kulkarni, 90; Marks, 99; Venugopalan, 99; Shih, 2000], and bone substitution materials [Ayers, 99; Kang, 02].

4.1.2. SMA Actuators

SMA actuators are an effective way to reduce weight and to minimize the complexity of various systems. As actuators, these materials have been used in a wide range of applications from thin film actuators [Roch, 03] to helicopter rotor actuators [Chopra, 02]. Using Shape Memory Alloy actuators provides an interesting alternative to conventional actuation methods. Their advantages create a means to drastically reduce the size, weight, and complexity of robotic systems. First of all, SMA actuators possess an extremely high force to weight ratio. A NiTi actuator can apply an actuation stress of 500 MPa (72.5 Psi). So, a 150 μm diameter NiTi wire can apply a force of 8.8 N, which is 0.897 kgf (1.99 lbf). If the wire is 10 cm (3.94 in.) long it would weigh 11.4 mg (0.025 lbm) and could contract 0.85 cm. So, the actuator can lift an object 78,000 times its own weight nearly 1 cm! Granted, a simple electrical circuit is needed to heat the wire, but the force to weight ratio is still remarkable. Shape Memory Alloy actuators also are incredibly compact and simple. In the example described above, the actuator itself has a volume of only $0.002\,cm^2$. A SMA actuation system consists only of the SMA element

and a heating and cooling method. The cooling method can be as simple as a combination of natural convection, conduction and radiation. A final advantage is silent operation. Whereas conventional actuators produce a significant amount of noise, the SMA actuator is completely silent.

Several researchers have implemented shape memory alloy technology for use in articulated hands. In 1984, Hitachi Co. developed a four fingered robotic hand that incorporated twelve groups of 0.2mm fibers that closed the hand when activated. Dario et al. [Dario, 87] proposed an articulated finger unit using antagonistic coils and a heat pump. An SMA actuator has been used in eye prostheses to execute horizontal and vertical actuation [Wolfe, 05].

4.2. Conceptual Design of SMA AAFO

Most of the SMA actuators utilize these alloys in the wire form. Designing a wire based actuator requires selecting the following design parameters:

- The length of the wire
- The diameter of the wire
- The number of wires, and
- The mechanism used for actuation.

SMA elements provide actuation when the temperature exceeds a certain limit. Reverse actuation takes place when the temperature of a previously active element decreases below another value. As a result, SMA actuators have speed limitations, which must be thoroughly considered and analyzed prior to designing an actuation system. By considering this limitation, it is possible to find the required length, diameter and the number of necessary wires for the selected mechanism as explained in the next sections.

4.2.1. Actuation Mechanism and Wire Length

The first step in designing a SMA actuator is the design of a mechanism to use the relatively small absolute strain of the material to generate the desired motion. The typical strain of a Ni-Ti SMA element is about 8%. A SMA actuator, through the shape memory effect (SME), provides one-way actuation. In other words the actuation is not reversible. The SMA wire, therefore, must be deformed by a bias force in martensite in order to achieve repetitive motions. There are two ways of providing the bias force and therefore two types of SMA actuators. One actuator called bias type is composed of an SMA element and a bias spring. The other, called differential type, is made of two SMA elements. In the present design, a bias-type SMA wire actuator is selected where the bias force (torque) is provided by a linear spring and the weight of the moving body. The reason behind this selection is explained in more detail in section 4.2.3.

In a bias type SMA actuator, the useful actuation torque is the difference between the bias torque and SMA wire torque. In designing the SMA actuator for the AAFO, the mechanism used by Elahinia and Ashrafiuon is adopted [Elahinia, 02]. This Mechanism is showed in Figure 4.3.

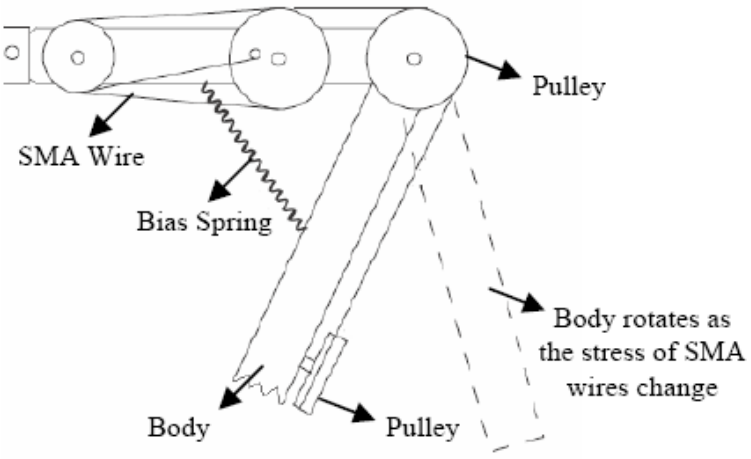

Figure 4-3 The mechanism used for actuation

The initial length of the SMA wire that is guided by the pulleys should be chosen in such a way that upon full contraction it can rotate the foot from its minimum position at -25^o to the maximum position at $+15^o$. The ankle range of motion was previously shown in Figure 2.7. The initial length of the wire can be calculated through kinematic a relationship, as described in Equation 4.1.

$$l_0 = 2r_p \frac{\Delta\theta}{\varepsilon_{\max}} \tag{4.1}$$

Where 'l_0' is wire initial length, 'r_p' is pulleys radius and '$\Delta\theta$' is the range of motion at ankle joint which is 40^o. Having the maximum strain ($\varepsilon_{\max} = \%8.5$) and assuming the radius of pulley equals to 4 cm, the initial length of the wire will be about 70 Cm.

4.2.2. Diameter and Number of Wires

SMA actuation is the result of increased stress in the wire as a consequence of martensite to austenite phase transformation. Maximum achievable stress of a NiTi SMA wire ($\sigma_{\max}$) is about 400MPa. Therefore the maximum torque ($T_{\max}$) generated by 'n' wires with a diameter of 'd' is given in Equation 4.2.

$$T_{\max} = n r_p \sigma_{\max} \frac{\pi d^2}{4} \tag{4.2}$$

Since '$T_{\max}$' should be equal to the maximum required torque during walking, the number of wires; times the diameter squared is a constant in the case of the AAFO with known required torque (Equation 4.3).

$$n d^2 = \frac{4T_{\max}}{\pi\ r_p \sigma_{\max}} = CONSTANT \tag{4.3}$$

It may seem that the best design is to reduce the number of wires and increase the diameter. However the bandwidth is another criterion is affected by the diameter of the wire.

One of the parameters that greatly affect the bandwidth of a SMA wire actuator is the diameter. This is due to the fact that the hear transfer rate, as the underlying mechanism for actuation, is a function of the aspect ratio of the SMA actuator. As an example, a 0.006 in (150 μm) diameter wire may lift 0.728 lbs (330 gm) and require 2 seconds before it is ready to cycle again whereas a 0.012 in (300 μm) diameter wire may lift 2.76 lbs (1250 gm) and require 8 seconds before it is ready to cycle again.. The cycling time is primarily dependent on the heat transfer characteristics of the SMA cooling system. The parameters that affect bandwidth are the temperature and type of surrounding medium, the convection of the surrounding medium and the surface to volume ratio of the SMA elements. Depending on the environment, heat dissipation can be a problem. In a high temperature, low convection environment, the heat transfer to the surrounding medium is reduced resulting in a lower bandwidth. On the other hand, for a low temperature or high convection environment, the heat transfer is improved and bandwidth is increased.

Since the actuation of SMA wires is the result of the heating and cooling process, the heat transfer model can be used to estimate the response time of the actuator. The assumed SMA wire heat transfer equation consists of electrical heating and natural convection as shown in Equation 4.4 and the response time of the SMA in Equation 4.5.

$$mc_p \frac{dT}{dt} = \frac{V^2}{R} - h_c A_c (T - T_\infty) \tag{4.4}$$

$$\tau = \frac{\rho c_p}{4h_c} d \tag{4.5}$$

Where ' R ' is the resistance, ' c_p ' is the specific heat, ' m ' is the mass, ' ρ ' is the density, and ' A_c ' is the circumferential area of the SMA wire. ' V ' is the applied voltage, ' T_∞ ' is the ambient temperature, and ' h_c ' is the heat convection coefficient.

Equation 4.2 and 4.5 show that having a larger diameter will results in generating more torque at the expense of a slower response time. Considering Equation 4.1 to 4.5, the relationship between response time and the number of wires as well as initial length of wire can be found (Equation 4.6).

$$\tau = \frac{\rho c_p}{4h_c}\sqrt{\frac{8\Delta\theta T_{\max}}{nl_0\pi\varepsilon_{\max}\sigma_{\max}}} \rightarrow \tau = K\sqrt{\frac{1}{n}} \qquad (4.6)$$

where 'K' is a constant which depende on the physical properties of the SMA wire and the maximum required moment at the ankle joint.

The moment at the ankle joint during normal walking of a healthy subject with overall weight of 67.5 kg is shown in Figure 4.4.

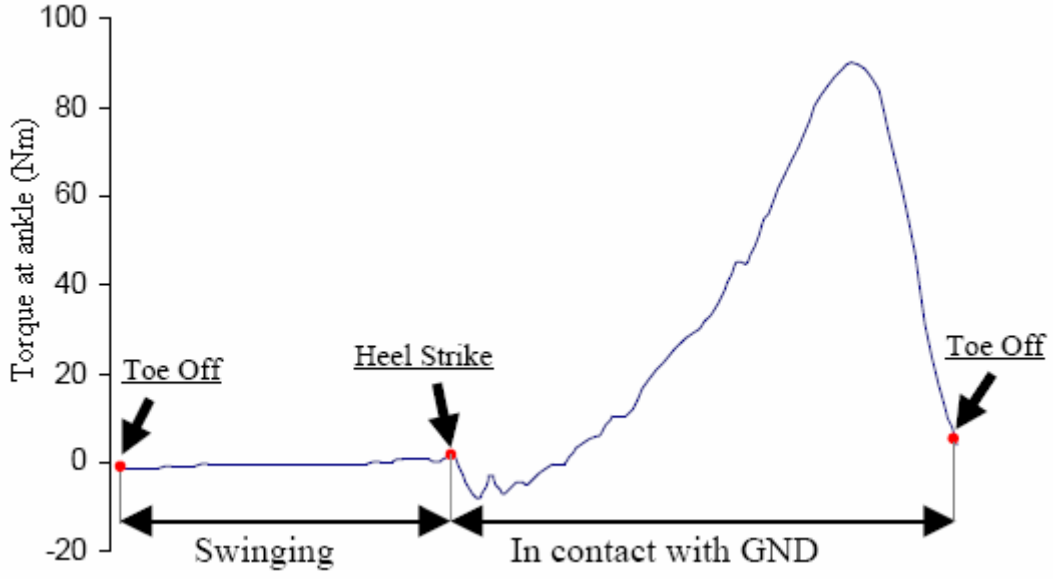

Figure 4-4 Ankle moment vs walking events [Winter, 04]

Based on Figure 4.4, the maximum ankle moment for a 67.5 kg healthy subject is around 85 Nm. Assuming that muscles around the ankle of a drop foot patient can provide up to 80 percent of this amount, SMA wires should generate the rest which is 17Nm. Since the pulley mechanism will double the force of wire, this amount will reduce to 8.5Nm. Using the physical properties of SMA wire given in Table 4.1, the relationship between number of wires and response time is shown in Figure 4.5.

Table 4-1Physical properties of SMA

Parameter	Description	Unit	Value
h_c	Heat convection coefficient	$J/m^2.°C\,Sec$	150
c_p	Specific Heat of Wire	$Kcal/Kg.°C$	0.2
ρ	Density	gr/cm^3	6.5
σ_{max}	Maximum allowed stress	MPa	400

It is desired for any actuator to be designed in such a way as to have a minimum time constant. The relationship between number of wires, response time and diameter of the wire is shown in Figure 4.5.

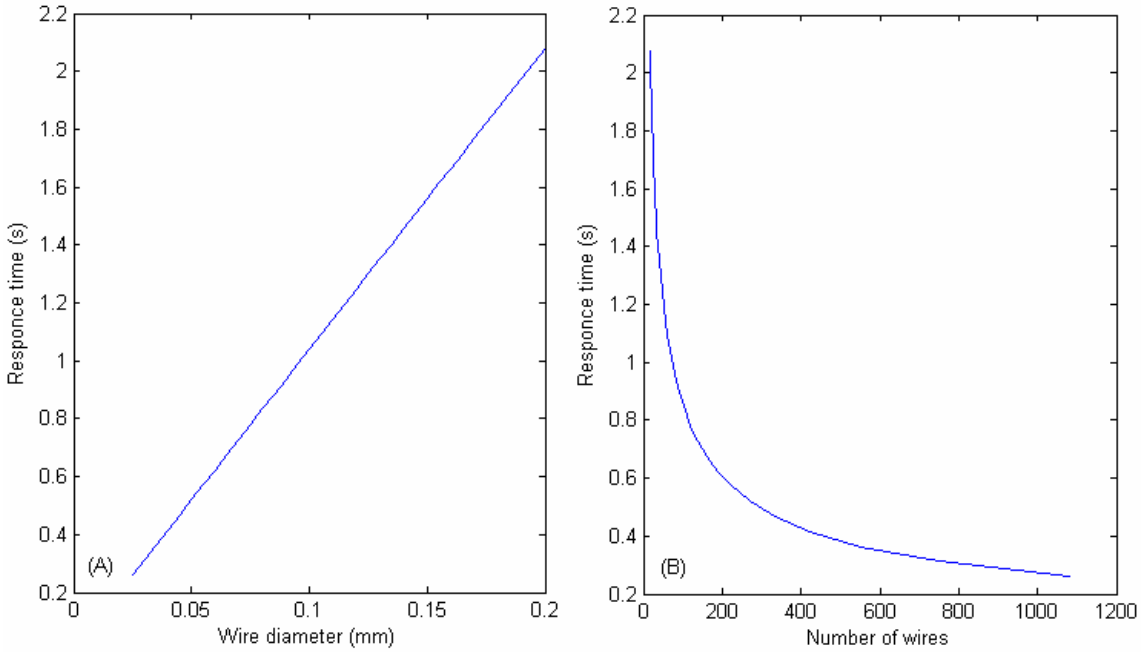

Figure 4-5 A-Relationship between diameter of SMA wire and it's response time B-Relationship between the number of wires and response time (initial length is 0.7m)

Figure 4.5A indicates that in order to have a response time less than 0.5 s the wire diameter should be less than 0.05 mm. Available SMA wire diameter that fits in this category can be found in Table 4.2 where other physical properties such as Electrical resistance are provided as well.

Table 4-2 Design parameters of commercially available SMA wires

Diameter Size (In)	Diameter Size (mm)	Resistance (Ohms/Inch)	Maximum Pull Force (grams)	Approximate current at room temperature (mA)
0.0010	0.0254	45.0	7	20
0.0015	0.0381	21.0	17	30
0.002	0.0508	12.0	35	50
0.003	0.0762	5.0	80	100
0.004	0.1016	3.0	150	180
0.005	0.127	1.8	230	250

The best way to increase the force capability without sacrificing actuation time is to connect many thin wires mechanically in parallel with enough space between the wires for heat dissipation to create a bundle actuator.

The electrical connection of SMA wires in the bundle actuator is another criterion which should be considered during the design procedure. The effective linear resistance of a SMA bundle with all wires in parallel is inversely proportional to the number of wires in the bundle. As an example, a bundle consisting of 50, 12 in (30.5 cm) long, 0.006 in. (150 μ m) diameter wires (R = 1.27 Ω/in (0.0323 Ω/mm) all in a parallel circuit would have R_{eff} = 0.0254 Ω/in (0.01 Ω/cm) and a total bundle resistance R_{eff} = 0.305 Ω. Given a required actuation current of 0.4 A through each wire (i.e. 20 A for the bundle due to the entirely parallel arrangement), the resulting voltage drop across the bundle is 6.1 V. The combination of low voltage and very high current can be avoided by creating a circuit where the wires are arranged electrically in a combination of series and parallel

paths while remaining mechanically connected in parallel. Equation 4.6 can be used for a combination of wires in series and parallel electrical connections:

$$V_B = I_{SMA}\frac{nL\overline{R}}{P} \quad \text{and} \quad I_B = PI_{SMA} \tag{4.6}$$

Where 'V_B' and 'I_B' are the voltage drop and current through the bundle, respectively. 'I_{SMA}' is the single wire actuation current, 'N' is the number of wires in the bundle, 'P' is the number of parallel paths, 'L' is the bundle length, and 'R' is the single wire linear resistance. It is worth noting that the ratio 'N/P' must be equal to an integer if identical paths are constructed.

In summary, for actuating a large number of SMA wires that are connected in parallel, a low voltage and high current is needed. On the other hand, for a small number of parallel paths, a high voltage and low current is needed. This means that in order to optimize the power consumption of all the SMA wires in a bundle actuator should be mechanically in parallel while using a small number of electrical parallel paths.

Selecting the length of wire equal to 70 cm and the electrical to 0.5 A, the required number of wires, the number of parallel path in the bundle actuator and the voltage drop across the bundle is summarized in Table 4.3

Table 4-3Summary of conceptual design for a SMA wire with length of 70cm

Diameter (μm)	**Resistance of Wire (Ω)**	**Current, I_{SMA} (mA)**	**Number of wires, N**	**Parallel Wires, P**	**τ_s, Time response**	**V_B, Voltage drop (v)**
25.4	45	20	1146	14.43	0.23	28.87
38.1	21	30	509	6.73	0.345	14
50.8	12	50	220	4.62	0.46	9.24
76.2	5	100	128	4.48	0.69	8.96
101.6	3	180	73	4.96	0.92	9.2

In order to have the fastest actuation, the lowest possible diameter should be chosen for the SMA wires. This diameter is 25.4 μm . Fabrication of a bundle actuator with more than one thousand SMA wires and a diameter less than a human hair is beyond the scope of this work. In order to test the concept a simple SMA actuated device is used. Dynamics of this device, as shown in the next sections, is similar to the dynamics of the ankle joint.

4.2.3. Experimental Setup

There are two basic elements which are necessary for any form of biped walking, regardless of the existence and the level of possible physical disabilities:

- Periodic movement of each foot from one position of support to the other in the direction of progression.
- Continuing ground reaction forces (GRF) that support the body.

Therefore, it is necessary to study the two parameters for the ankle joint to select an experimental setup with a similar behavior. Figure 4.6 illustrates the torque generated at the ankle joint of a healthy person at constant walking speed. As this figure shows, the ankle torque is a function of the angular position of the ankle.

Figure 4.6 illustrate that a relationship between the ankle moment versus ankle angle follows a hyperbolic pattern, where after midstance till the second Toe off it experiences an almost linear relationship (constant stiffness). This behavior can be exhibited by either an active or passive mechanical system. In the human ankle–foot system, active musculoskeletal components are likely utilized with passive components at all walking speeds. However, an ankle prosthesis consisting of a rotational spring–damper system

could be used to mimic the behavior at slow walking speeds and this was the main reason to choose the bias spring mechanism in the conceptual design.

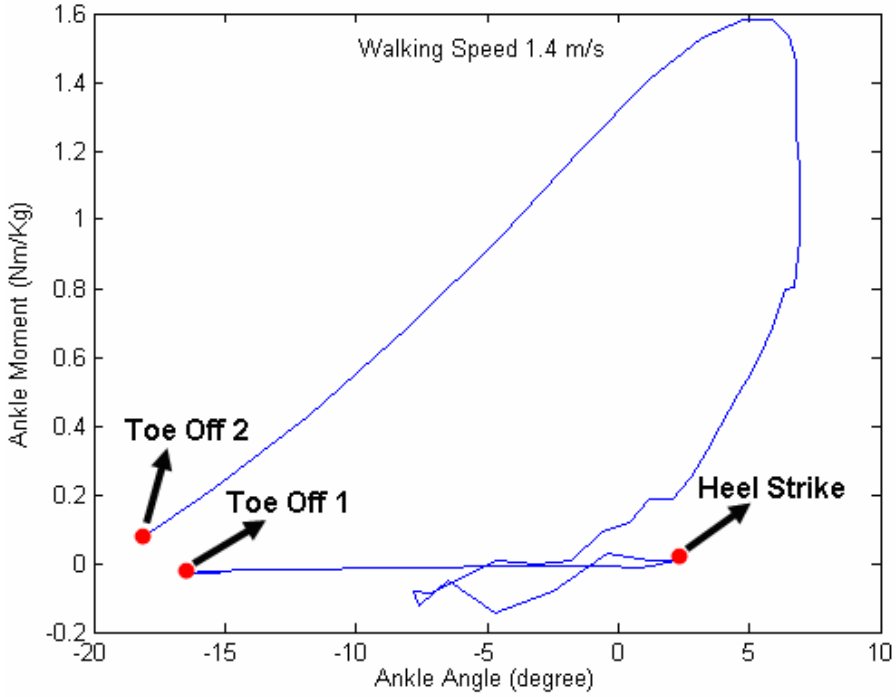

Figure 4-6Healthy foot ankle joint behavior during one walking cycle [Winter, 04]

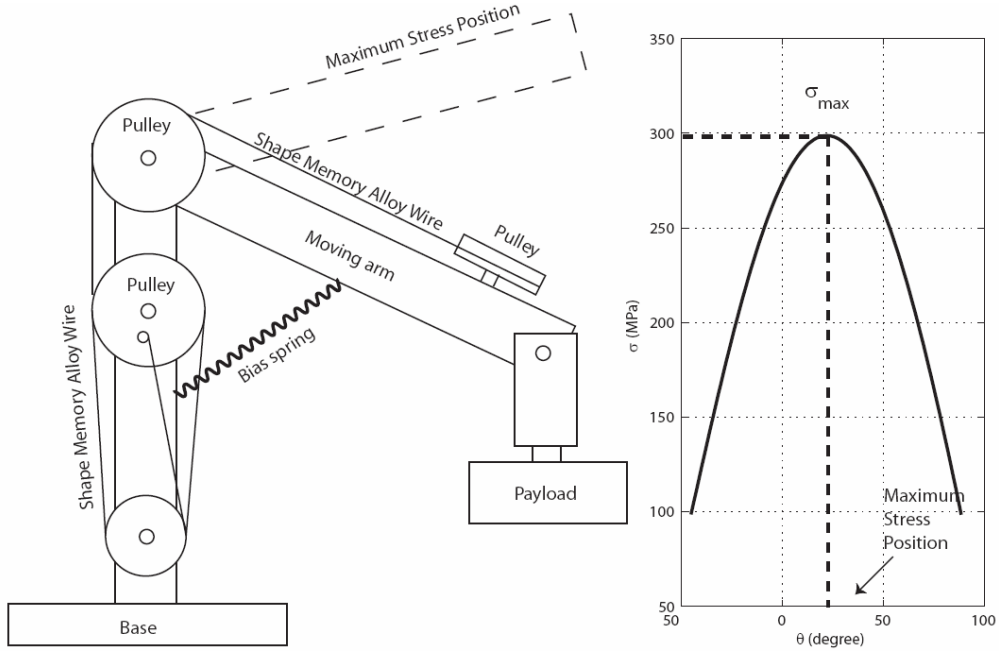

Figure 4-7 One DOF SMA actuator for experimentally evaluation of the SMA actuated AAFO, which has a biocompatible torque-angular displacement [Elahinia, 2001]

The system shown in Figure 4.7 is a one-degree-of-freedom shape memory alloy actuator. Initially this system will be used to investigate the possibility of using SMA wires to actuate the AAFO. The main reason for choosing this system is the similarity between the torque-angle at the ankle (Figure 4.6) and the torque-angle of this device as shown in Figure 4.7.

This actuator is used in this research to investigate the design of a SMA actuated active foot orthosis devices. The arm is actuated by a bias type actuator constructed with SMA wire, pulleys, and a linear spring. The SMA wire is Flexinol with a diameter of 150 μm. Heating the SMA wire induces a negative strain in the material creating a positive torque and the arm rotates counterclockwise. Conversely, cooling the wire induces positive strain causing the arm to rotate in a clockwise direction. By adjusting the electrical current to the SMA wire and with proper control logic it is possible to position the actuator at desired angular positions or track desired trajectories. A proper control algorithm enables the SMA actuator to provide suitable actuation. To investigate the control algorithms for mimicking normal walking gait, this system uses the angle measurement feedback provided by an encoder and adjusts the voltage to SMA wire to create the required level of force and torque at each stage of the walking cycle.

An accurate model of this SMA actuated 1 DOF arm is required for simulation and evaluation of different control algorithms. Modeling of the SMA arm is the topic of the next section and the control algorithm will be explained in Chapter 5.

4.3. SMA Actuator Modeling

.The model is constructed from several related parts (blocks), each representing an element of the physical system's behavior. For numerical simulations, the model is built

in Dymola. The model consists of phase transformation, heat transfer, SMA wire constitutive and arm dynamic sub-models. The input is voltage and the outputs are arm angular position, angular velocity of arm, the SMA wire's temperature, stress, and the Martensite fraction as shown in Figure 4.8. Elements of the models are bilaterally connected forming an algebraic loop. One reason for this is that physical properties of the SMA wire are dependent on stress and temperature of the wire. Thus bilateral causality exists between the dynamic model and the constitutive equation as well as wire's constitutive equation and Martensite fraction (phase transformation) equations.

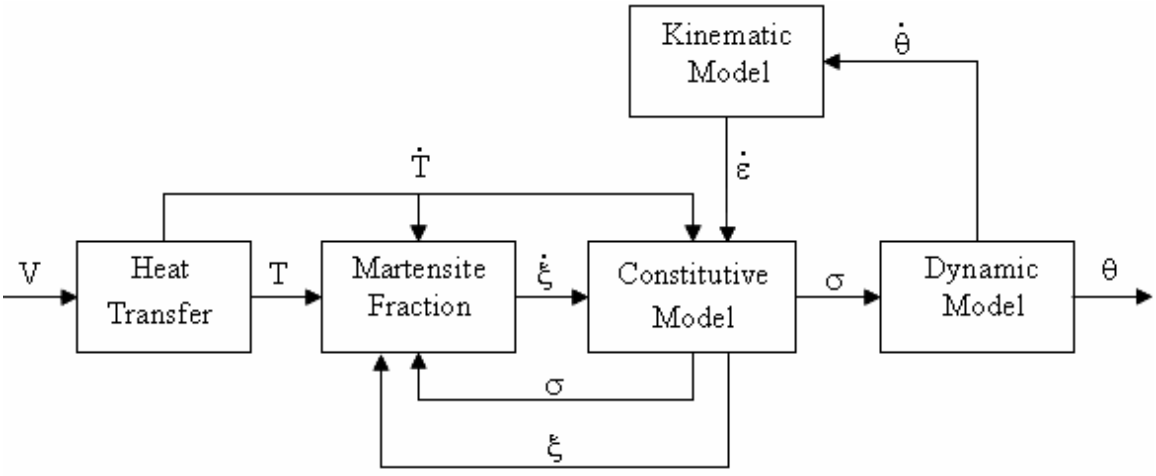

Figure 4-8 Modeling of the SMA actuator

4.3.1. Heat Transfer Model

The SMA wire heat transfer equation consists of electrical (joule) heating and natural convection:

$$mc\frac{dT}{dt} = I^2R - hA(T - T_\infty) \tag{4.7}$$

The parameters in the heat transfer equation are: 'm' mass per unit length of wire, 'd' diameter of wire, 'A' circumferential area of the unit length of wire, 'c' specific heat, 'I'

electrical current, 'R' resistance per unit length of wire, 'T' temperature of wire, 'T_∞' the ambient temperature and 'h' heat convection coefficient.

4.3.2. Wire Constitutive Model

The Wire constitutive model shows the relationship between stress, strain and temperature [Tanka, 86; Liang and Rogers, 90]. The basic equation is:

$$\dot{\sigma} = D\dot{\varepsilon} + \theta_T \dot{T} + \Omega\dot{\xi} \tag{4.8}$$

Where 'D' is the average Young's modulus and is represented by Equation 4.9, 'θ_T' is the thermal expansion factor and 'Ω' is the phase transformation contribution factor which is defined in Equation 4.10.

$$D = \frac{D_M + D_A}{2} \tag{4.9}$$

$$\Omega = -(D_M + D_A)\bar{\varepsilon}_L \tag{4.10}$$

Where 'D_A' is the Austenite Young's modulus, 'D_M' is Martensite Young's modulus and '$\bar{\varepsilon}_L$' is the transformation strain.

4.3.3. Martensite Fraction Model

In the constitutive equation, it is required to know the Martensite fraction derivative at each instant of time. Based on hysteresis behavior of SMA wires, a cosine curve-fitting model is developed. It needs temperature and stress to determine the fraction. Due to hysteresis behavior of SMA wires the equations are different for heating and cooling cases.

4.3.3.1. Reverse Transformation

Reverse transformation from Martensite to Austenite (heating) is represented by:

$$\xi = \frac{\xi_M}{2}\{\cos[a_A(T - A_s') + b_A\sigma] + 1\} \tag{4.11}$$

Where 'ξ' is Martensite fraction which has a value between '$\xi_M = 1$' (Martensite phase) and '$\xi_A = 0$' (Austenite phase), 'a_A' and 'b_A' are curve fitting parameters shown in Equation 4.12, 'T' is wire temperature and 'σ' is wire stress.

$$a_A = \frac{\pi}{A_f' - A_s'} \qquad b_A = \frac{a_A}{C_A} \tag{4.12}$$

Where 'A_s'' and 'A_f'' are Austenite phase start and final temperature respectively, and 'C_A' is a curve fitting parameter.

4.3.3.2. Forward Transformation

The forward transformation equation from Austenite to Martensite (cooling) is:

$$\xi = \frac{1 - \xi_A}{2}\cos[a_M(T - M_f') + b_M\sigma] + \frac{1 + \xi_A}{2} \tag{4.13}$$

Where 'ξ_A' here is the minimum Martensite fraction obtained during heating, 'a_M' and 'b_M' are curve fitting parameters shown in Equation 4.14.

$$a_M = \frac{\pi}{M_s' - M_f'} \qquad b_M = -\frac{a_M}{C_M} \tag{4.14}$$

Where 'M_s'' and 'M_f'' are Martensite phase start and final temperature, respectively and 'C_M' is a curve fitting parameter.

4.3.3.3. Heating Time Derivative

Derivative equation for heating:

$$\dot{\xi} = \begin{cases} \frac{-\xi_M}{2} \sin[a_A(T - A_s') + b_A\sigma][a_A\dot{T} + b_A\dot{\sigma}] & \text{if } A_s < T < A_f \\ 0 & \text{otherwise} \end{cases} \tag{4.15}$$

Where 'A_s' and 'A_f' are stress modified Austenite start and final temperature, respectively (Equation 4.16)

$$A_s = (A_s' + \frac{\sigma}{C_A}) \qquad A_f = (A_f' + \frac{\sigma}{C_A}) \tag{4.16}$$

4.3.3.4. Cooling Time Derivative

Derivative equation for cooling:

$$\dot{\xi} = \begin{cases} \frac{\xi_A - 1}{2} \sin[a_M(T - M_f') + b_M\sigma][a_M\dot{T} + b_M\dot{\sigma}] & \text{if } M_f < T < M_s \\ 0 & \text{otherwise} \end{cases} \tag{4.17}$$

Where 'M_s' and 'M_f' are stress modified Martensite start and final temperature, respectively (Equation 4.18)

$$M_f = (M_f' + \frac{\sigma}{C_M}) \qquad M_s = (M_s' + \frac{\sigma}{C_M}) \tag{4.18}$$

4.3.4. Kinematics Model

The kinematic model includes the relationship between strain "and angular displacement 'θ'. Measuring a positive angle as clockwise, the equation is:

$$\dot{\varepsilon} = -\frac{2r\dot{\theta}}{l_0} \tag{4.19}$$

Where ' r ' is pulleys radius and ' l_0 ' is wire initial length.

4.3.5. Dynamics Model

The dynamic model of the arm including the spring and the load of the segments is represented by:

$$I_e\ddot{\theta} + c_r\dot{\theta} + [\tau_g(\theta) + \tau_s(\theta)] = \tau_w(\sigma) \tag{4.20}$$

' τ_w ', ' τ_g ' and ' τ_s ' are the resulting torques from the SMA wire, gravitational loads, and the bias spring, respectively and ' σ ' is the wire stress. ' I_e ' is the effective mass moment of inertia of the segment and ' C_r ' is the torsional damping coefficient approximating the joint friction.

4.4. Simulation and Model Verification

Computer simulations of the SMA arm model are performed in MATLAB/Simulink and Dymola; dSPACE hardware-in-the-loop solution is used for the experiments. All the parameters used in modeling the SMA are listed in Table 4.4.

To verify the model, a series of experiments is done for various inputs to the system. These results demonstrate reasonable accuracy of the actuator model, as shown in Figure 4.9. The figure compares simulation and experimental results of Equation 4.21 as an input voltage.

$$V = \begin{cases} 18\sin 0.1t & t \le 10\pi \\ 0 & 10\pi < t \le 40 \end{cases} \tag{4.21}$$

Table 4-4 Modeling Parameters and their numerical value [Liang, 90]

Parameter	Description	Unit	Value
m	SMA wire's mass per unit length	Kg	$1.14e^{-4}$
A	SMA wire's circumferential area per unit length	m^2	$4.712e^{-4}$
C	Specific heat of wire	$Kcal/(Kg.\ ^oC)$	0.2
R	SMA wire's resistance per unit length	Ω	45
T_∞	Ambient temperature	^oC	20
h	Heat convection coefficient	$J/(m^2.^oC.Sec)$	150
D_A	Austenite Young modulus	GPa	75
D_M	Martensite Young modulus	GPa	28
θ_T	SMA wire's thermal expansion factor	$MPa/\ ^oC$	0.55
Ω	Phase transformation contribution factor	GPa	-1.12
σ_0	SMA wire's initial stress	MPa	75
ε_0	SMA wire's initial strain		0.04
T_0	SMA wire's initial temperature	^oC	20
ζ_0	SMA wire's Martensite fraction factor		1
A_s	Austenite start temperature	^oC	68
A_f	Austenite final temperature	^oC	78
M_s	Martensite start temperature	^oC	52
M_f	Martensite final temperature	^oC	42
C_A	Effect of stress on Austenite transformation	$MPa/\ ^oC$	10.3
C_M	Effect of stress on Martensite transformation	$MPa/\ ^oC$	10.3
l_o	Initial length of SMA	mm	900
r	Radius of pulley	mm	8.25
m_p	Payload mass	gr	57.19
m_a	Moving link mass	gr	18.7
K	Bias spring stiffness	N/m	3.871

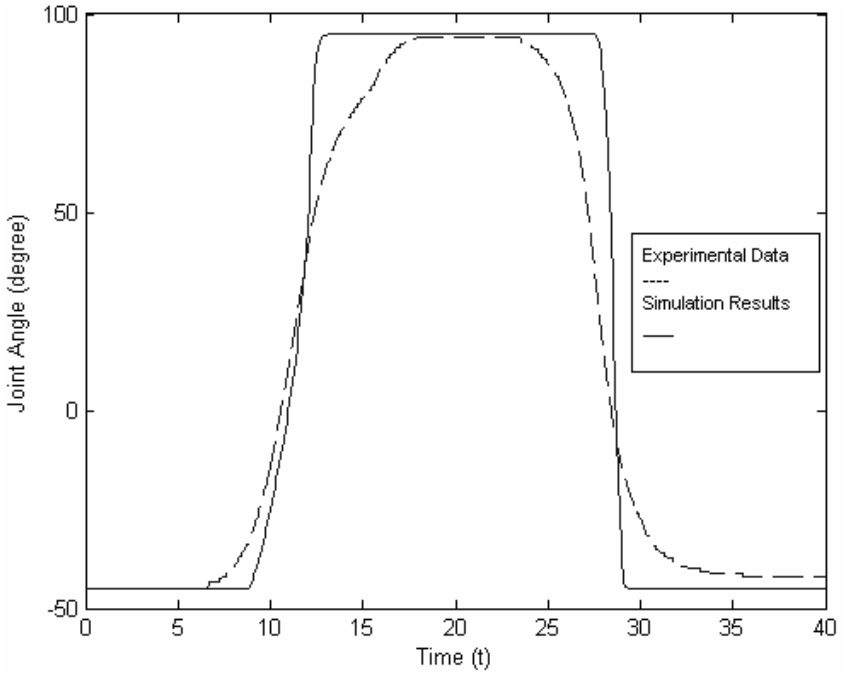

Figure 4-9 Comparing Simulation and experimental result for a sine wave input

In another experiment, constant voltages were used as an input. Figure 4.10 illustrates the response of the system to 14 and 14.4 volts as an input.

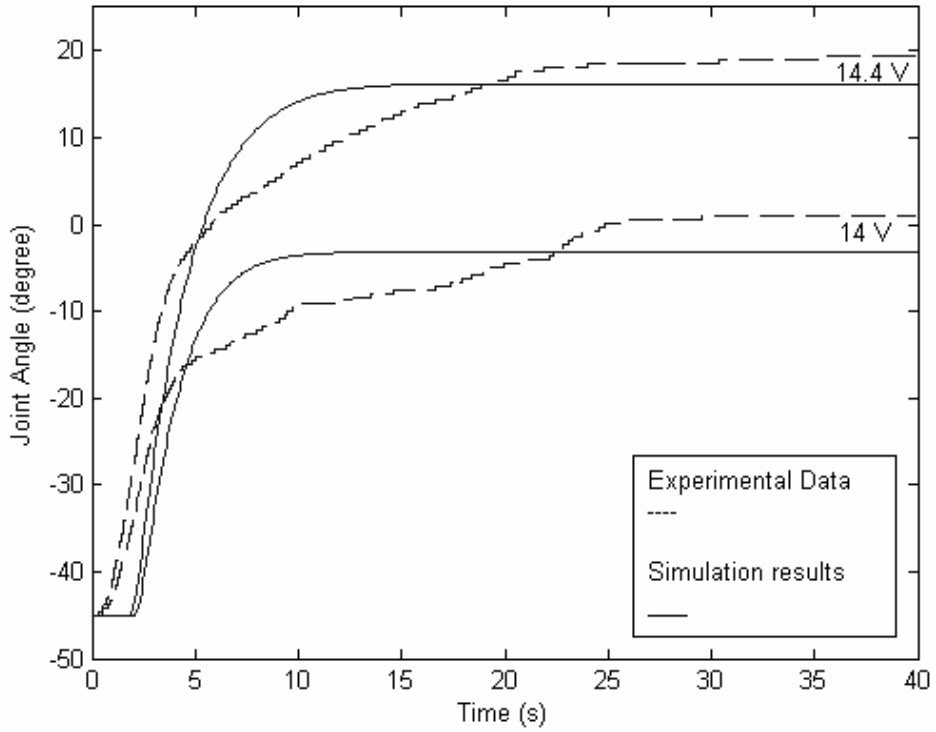

Figure 4-10 Verification of the model by comparing the simulation results with experimental data for two constant inputs

Some of the differences between the simulation and experimental results are due to parameter uncertainties and model simplifications. Specifically, the modulus, transformational tensor and thermal coefficient were all assumed to be constant. The assumptions of a linear spring force and viscous friction contributed to the discrepancy of the results. Figure 4.10 shows that a slight increase in the applied voltage causes a sudden jump in the joint angle. The main reason of this behavior can be more understood by comparing the Martensite fraction of the two experiments in Figure 4.11 and temperature plots in Figure 4.12.

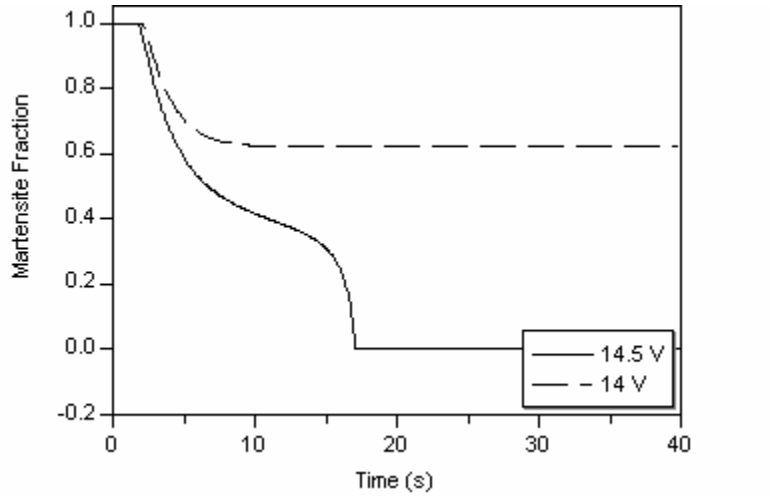

Figure 4-11 Phase transformation in the two experiment

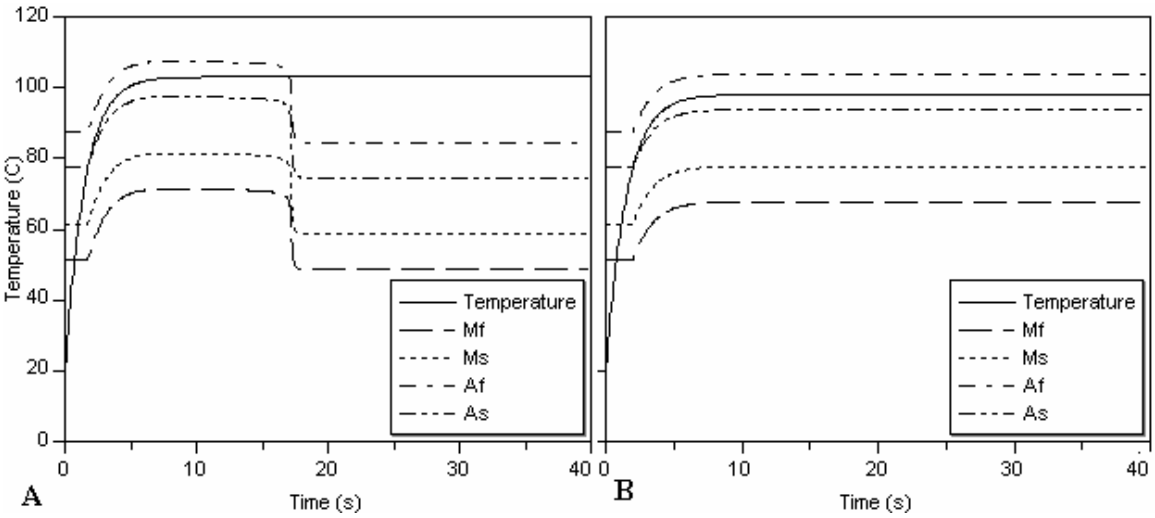

Figure 4-12 A-Temperature plots for 14.4V input B-Temperature plots fo 14V input

By increasing the temperature, the molecular structure of the SMA begins to change from Martensite to Austenite where SMA can be formed to its memorized shape. This behavior can be studied by introducing four temperatures, starting and final temperature of Martensite transformation (‘ M_s ’, ‘ M_f ’) as well as Austenite transformation temperatures (‘ A_s ’, ‘ A_f ’). According to Figure 4.12, the temperature of the wire is almost the same in the two experiments but the phase transformation temperatures are decreased in the second experiment. Having a lower temperature to pass for finishing the austenite transformation, the wire can get to fully Austenite mode in the second experiment where ξ=1.

This occurs because the required torque and hence SMA wire stress start decreasing after a certain angle. Recalling that the actuation limit temperatures are a function of stress and so their values also decrease Figure 4.13 and 4.14 shows the stress of the wire and ‘ M_s, A_f ’ for the experiments.

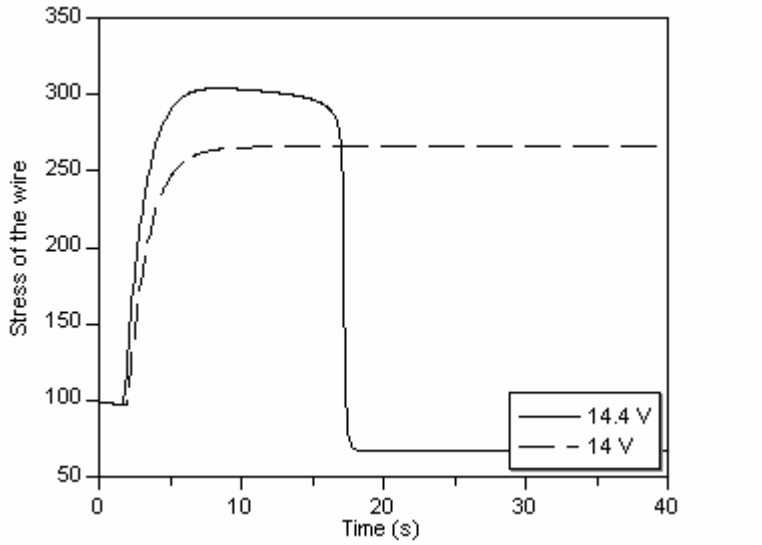

Figure 4-13 Stress of the wire in two experiments

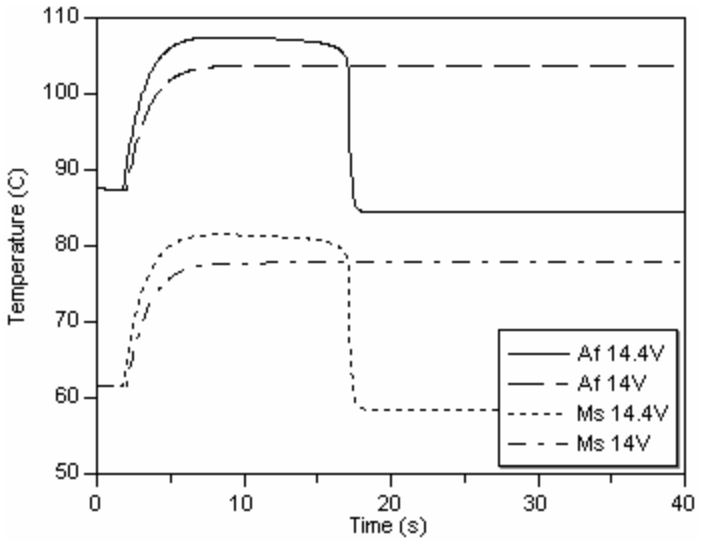

Figure 4-14 Two of the temperature transformation (' M_s , A_f ')

Chapter 5

5. Controlling Shape Memory Alloys

In order to generate the desired actuation torque with the SMA AAFO, an effective control system should regulate the actuation of the wires. As previously shown, the actuation behavior of a SMA element is a function of the external force (stress), the displacement generated (strain) and the temperature. The multi-input nature of the SMA actuators makes their control a challenging task. In most cases, Joule heating is used to adjust the temperature of a SMA actuator. A control algorithm adjusts the applied electric voltage to the SMA element to regulate the actuation. In this chapter the result of research in developing the control techniques for the SMA experimental setup are presented. This setup, as previously explained, serves as a benchmark to evaluate different aspects of the SMA AAFO design. This chapter starts with a review of state of the art SMA actuation controls and follows with a discussion on control designs.

In 1984 Honma et. al. demonstrated that it is possible to control SMA actuation by electric heating [Honma, et. al, 84]. They used an open-loop pulse width modulation (PWM) technique to operate their SMA-actuated robots. In 1986, Kuribayashi proposed an antagonistic pair of SMA wires for the operation of a rotary joint [Kuribayashi, 86]. PWM was used in a feedback controller to control both position and force. The controller

adjusted the duty cycle between the two antagonistic actuators by switching the applied voltage between the two actuators.

In the early days of Nitinol SMA, products such as fine-gauge wire were not available and this impeded work for many researchers. Recent rapid advances in SMA materials have accelerated the research and development efforts of implementing SMA materials. In the early 90s more active researches on SMA and controlling SMA based actuators bigan. This includes (1) active blade and wing shape control [Roglin and Hanagud 96, Epps and Chopra 01], (2) active shape control of beam type structures [Baz et al 94, Song et al 2000a], (3) vibration control of mechanical and civil structures [Wilde et al 99, Humbeeck 03], and (4) control of actuators for medical devices [Maeda et al 96, Duerig et al 02].

The control research applied to SMA's can be broadly divided into three categories:

- Pulse Width Modulation (PWM),
- Linear control, and
- Nonlinear control

The following section will cover the challenges in controlling SMA rotary actuators, which will be used in developing the AAFO. The next sections will talk about three different type of controller used in this study. They include linear control (PID), nonlinear control (Switching between PID and stress based sliding mode control) and finally an adaptive robust controller which is proposed as the most effective controller for this application.

5.1. Control Challenges in Rotary SMA Actuators

It is important to recognize the co-dependent relationship between stress, Martensite fraction, and transformation temperature, for it is this complex nonlinear relationship that causes many difficulties with regards to control design for SMA actuators.

When an input voltage is applied to the SMA actuator, the temperature of the wire will rise. Martensite fraction is a non-dimensional variable indicating the solid-state phase of the material. Before actuation, when the SMA element is at low temperature and at its maximum length, the Martensite fraction is equal to 1. No phase transformation takes place as the temperature increases and passes the Martensite final temperature transformation, M_f. As the SMA element temperature rises, the temperature exceeds the Austenite start temperature, A_s, and the Martensite fraction decreases resulting in contraction of the wire.

If, at steady state, the temperature falls at a temperature between the Austenite start and final temperatures, only partial phase transformation is achieved. Based on this, in the case of the SMA rotary actuator that is used to evaluate the SMA AAFO, it seems that by increasing the applied voltage and elevating the temperature it is possible to position the actuators at different desired positions. In other words, it seems there exists a monotonic is linear relationship between the applied voltage (temperature) and the position of the SMA actuator. As shown in the following, this is not the case and therefore the control of SMA rotary actuators is challenge ridden.

As shown in Chapter 4, there is a certain point (in the case of the actuator used in this research 14.4V) that only a slight increase in the applied voltage will result in a large phase transformation to Austenite. The small increased voltage heats the wire enough to

cause the arm to rotate through the angle of maximum stress. At this angle, the stress of the SMA wire due to gravitational and spring torques is maximum. As it is show in Figure 5.1, upon passing this angle, the stress in the wire begins to decrease rapidly, which results in a drop in the transformation temperatures. This drop allows the temperature of the wire to pass through the Austenite final temperature, causing the Martensite fraction to fall to zero and the wire to achieve maximum strain.

It is previously demonstrated by Elahinia that, when the SMA-actuated rotary manipulator moves beyond the angle of maximum stress, the transformation temperatures begin to decrease at a rate proportional to the change in stress [Elahinia, 04]. In terms of control design, if the desired position is beyond the maximum stress position, the controller should first apply a high enough voltage to reach the maximum stress position. Beyond this position, while the position error is still not zero, the voltage should drop rapidly in order to prevent the wire from undergoing the full transformation (see Figure 5.1). Consequently, when a control system is based solely on the position error it will apply high voltage to the wire, even when the arm is beyond the maximum- stress-position and the wire will be overheated to the point of full transformation. Although it is possible to tune such a position-based controller to work well for certain positions, it can not work well for all set points.

The other challenge in controlling SMA wires is a number of state variables which are not easy to measure. This lack of information make the implementing of model based controllers more difficult. For example, in the proposed experimental setup, to have a model based controller, it is essential to have information about state variables such as stress and temperature of the wire, Martensite fraction, joint angle and angular velocity.

Among these variables only the angle and angular velocity of the arm can readily be measured. To address this issue, Ikuta classified feedback control variables into two categories of external variables (displacement and stress) and internal variables (temperature and phase transformation). He showed that since electric resistance is almost a linear function of the phase transformation (negligible hysteresis), and is also easy to measure, it can be used as a feedback variable. Stiffness of a SMA spring is also shown to be a linear function of normalized electric resistance [Ikuta, 90]. This technique is only applicable when a relatively long SMA wire actuator is used, for the resistance variation becomes measurable.

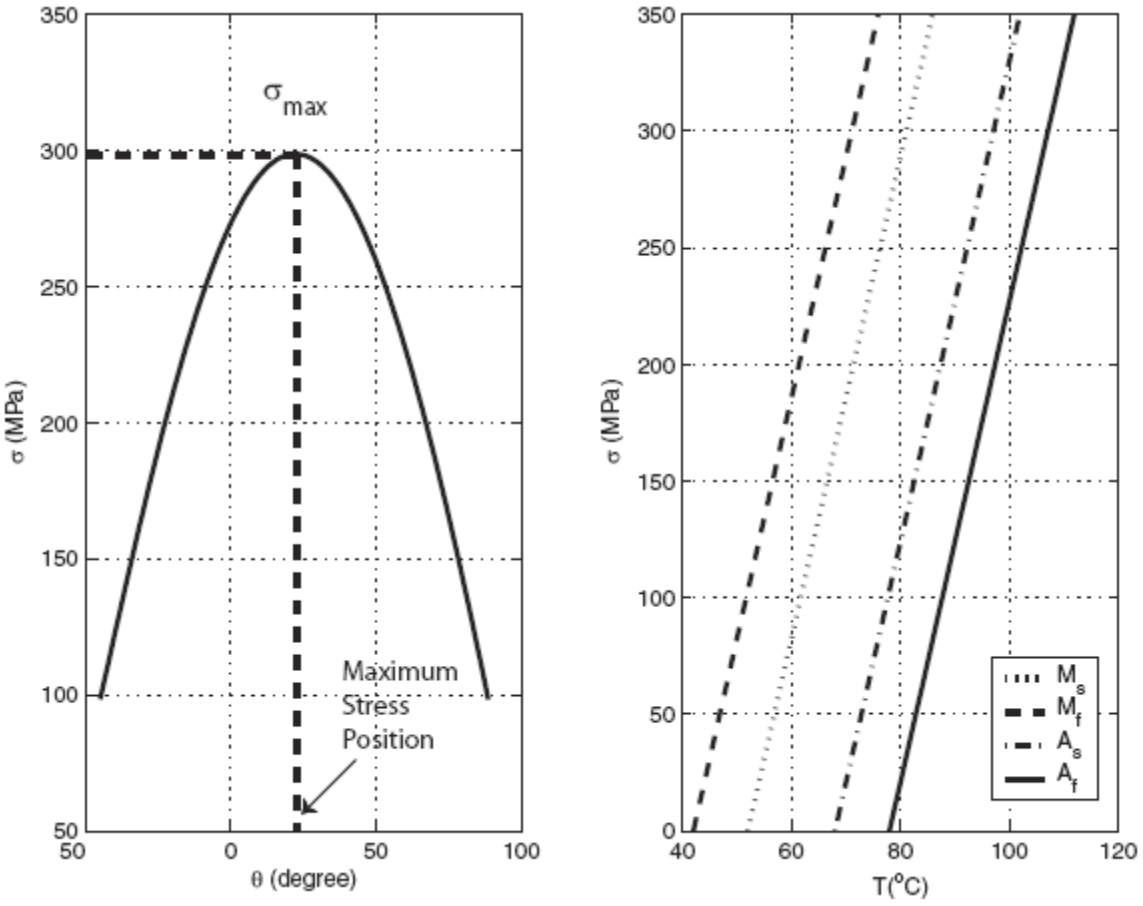

Figure 5-1The transformation temperatures decrease, when the arm cross the maximum stress position which makes the position control more difficult [Elahinia, 2004]

5.2. PID Controller

Due to the nonlinearity of both systems, the robotic arm and SMA actuator, it is not expected that a linear controller such as a PID controller can demonstrate an acceptable control performance. However, simulation and experimental results of a PID controller is used as a benchmark for comparing the effectiveness of other control algorithms. Some of the results achieved with the PID controller are presented in this section.

Since walking can be safely assumed to be a harmonic function, a sine wave is selected as another desired trajectory for testing the controllers. Since the time cycle of the gait and the range of ankle motion are proportional to the amplitude and frequency of the motion, it is possible to check the controller for different gait and walking speeds. In Figures 5.2 and 5.3 the ankle's range of motion is assumed to be 40^{o} (0.4 rad). It can be seen that PID may have a reasonable tracking in low frequencies but always have an offset about 5 degrees.

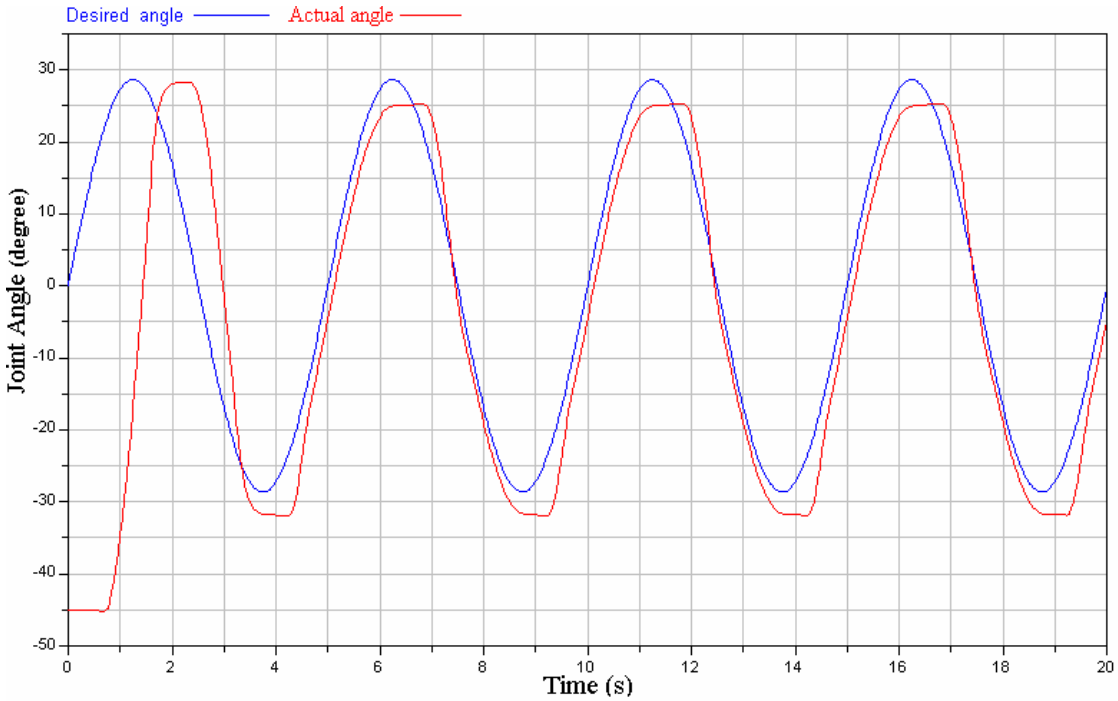

Figure 5-2 PID controller in tracking a sine wave with a frequencies of 0.2 HZ

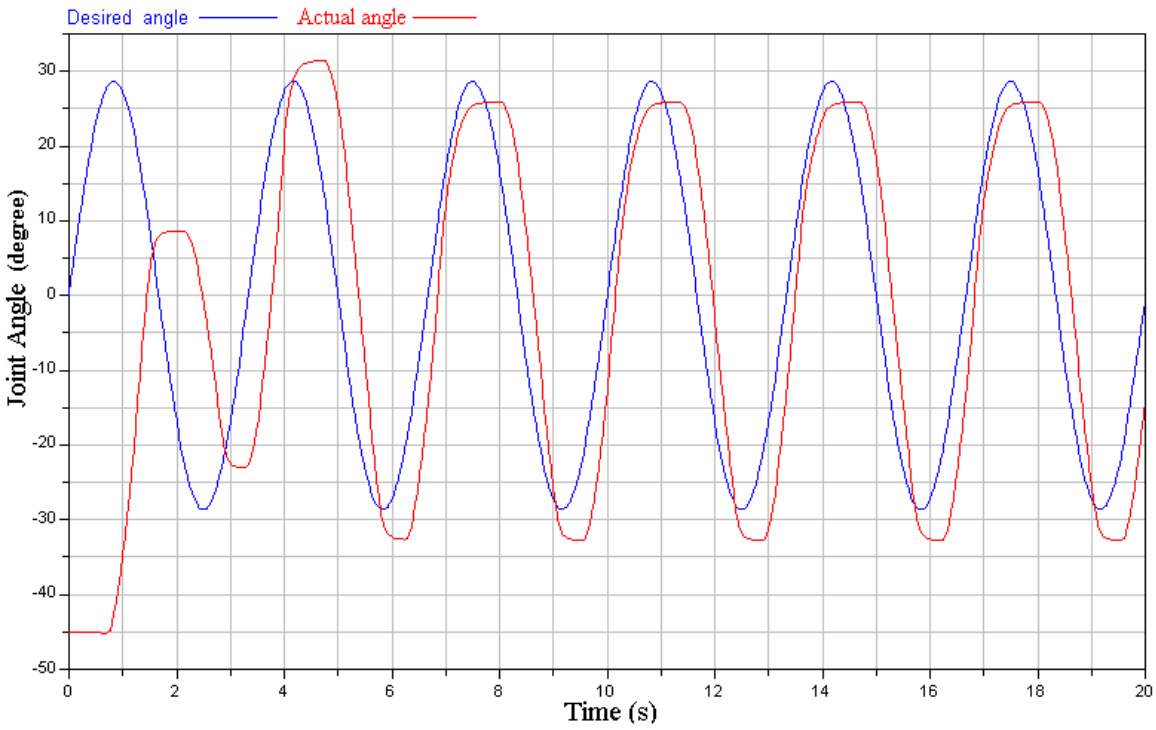

Figure 5-3 PID controller in tracking a sine wave with a of frequencies 0.3 HZ

5.3. Nonlinear Controller

More recently, nonlinear control methods have been employed for SMA-actuated systems. Nakazato et al. designed a fuzzy logic controller to control the duty cycle of a PWM controller for a SMA actuator with antagonistic wires [Nakazato et al., 93]. A neural network inverse model for a SMA wire actuator was also presented by Song et al. [Song et al., 03a]. They also used another approach with hysteresis compensation by using a neural network feedforward controller and a sliding-mode based robust feedback controller [Song et al., 03b]. Arai et al. used feedback linearization [Arai et al., 95], Elahinia and Ashrafioun applied variable structure controllers [Elahinia et al., 01].

A sliding mode controller which is known to be robust to parameter variations is formulated and used for position tracking of SMA actuators by different research groups [Elahinia et al, 05; Choi, 06].

Fuzzy logic control has also been used for differential SMA actuators based on position and temperature measurements [Nakazato et al., 93]. Experimental results showed better control performance compared with a PID controller. In this section, two nonlinear approaches (1-stress based sliding mode controller and 2-switching control between sliding mode and PID) are used for controlling the angle of the SMA actuator.

5.3.1. Stress Based Sliding Mode Controller

As previously discussed, the transformation temperatures of the SMA wire are stress dependent. This phenomenon adds to the complexity of the position control of the SMA actuated arm. To overcome this problem, in this section, a sliding mode controller is designed to calculate the desired stress of the wire based on the desired angular position of the arm. The stress of the wire is a better set-point for the controller since the transformation temperatures and hence the Martensite fraction are both functions of the wire stress. A feedback controller maintains this desired stress by regulating the input voltage to the wire.

To do so, it is required to have an estimation of the actual stress of the wire. The estimated stress is compared with a desired stress calculated by the sliding mode controller. A PID controller regulates the applied voltage to the SMA wire to achieve the desired stress.

5.3.1.1. Estimating the Stress of the Wire

Elahinia et al. proposed an Extended Kalman filter to estimate the actual stress. The Extended Kalman Filter (EKF) is the nonlinear version of the Kalman Filter. The filter recursively predicts the state vector by using all or some of the system and sensor

dynamics, statistical description of the noise and uncertainties, and initial conditions of the system. A schematic of the EKF is shown in Figure 5.4.

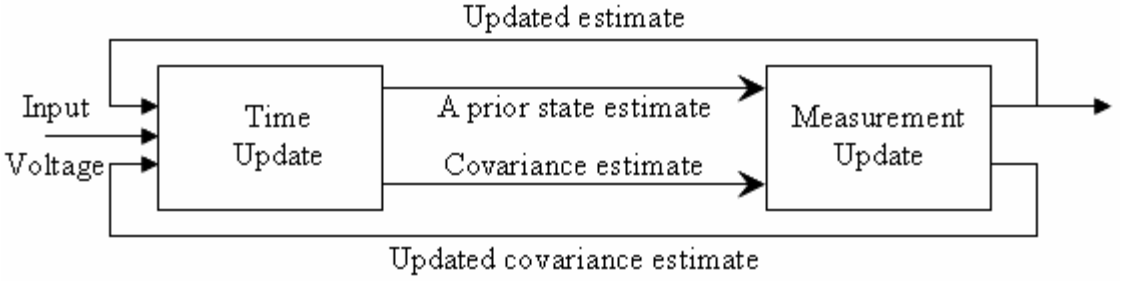

Figure 5-4 Block diagram of an Extended Kalman Filter

By using the EKF Elahinia et al. showed satisfactory results in terms of the filter estimating a state vector that closely matches the state vector generated by a nonlinear model of the system. Since the model had been previously verified against experimental data and the filter is designed based on this model, it is expected that the filter can accurately predict the state vector of the SMA actuated arm. However there is no experimental result to support the performance of EKF in estimating the stress of the wire To overcome this problem in the second approach, we intend to use the dynamic equation (relationship between the stress and angular position) to estimate the stress of the wire based on the measured angular acceleration and velocity. However to use the dynamic model, it is necessary to prove that our dynamic model is realistic.

One area of improving the dynamic model of the system is to choose a more realistic representation for the friction.

In this study the Lugre friction model is used for accurate modeling of friction.

5.3.1.1.1. Using LuGre Friction Model

It is well known that the classical friction models such as Coulomb and Karnopp, in which the relation between friction forces and the relative velocity between contact

surfaces are discontinuous, generate discontinuity in the dynamic model. This could result in difficulty in integrating equations of motion into one.

When a frictional contact is in static friction phase, relative motion may exist. This arises with tangential compliance and, because there is no true sliding, it is called pre-sliding displacement. A friction model renders pre-sliding displacement if variations in applied force below the breakaway force produce elastic deformation and movement. A friction model renders static friction, if, for applied forces smaller than a breakaway force, there is no steady-state relative motion.

In the LuGre model, in order to remove the discontinuity of the contact equation, the parameter 'Z' is used to present the state of strain in frictional contact. This friction model involves a single state variable in which rigid body displacement 'X' is decomposed into its elastic 'Z' and plastic 'w' (inelastic) components.

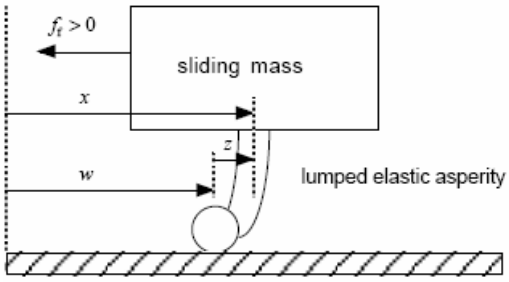

Figure 5-5 Model of block subject to friction force showing decomposition of displacement x into elastic and inelastic components, z and w.

$$x = z + w \tag{5.1}$$

Considering the pure elastic or plastic displacement we will have the following equations.

$$\begin{aligned} &\text{Sticking - Elastic displacement}: \begin{cases} \dot{x} = \dot{z} \\ \dot{w} = 0 \end{cases} \\ &\text{Sliding - Plastic displacement}: \begin{cases} \dot{x} = \dot{w} \\ \dot{z} = 0 \end{cases} \quad \Rightarrow \dot{x} = \dot{z} + \dot{w} \end{aligned} \tag{5.2}$$

Using this model, the equation of friction may be written as Equation 5.3:

$$f_f = \sigma_0 z + \sigma_1 \dot{z} + \sigma_2 v, \quad \sigma_i > 0 \tag{5.3}$$

Where ' z ' represents the state of strain in the frictional contact, and ' σ_0 ' and ' σ_2 ' are Coulomb and viscous friction parameters, respectively and ' σ_1 ' provides damping for the tangential compliance. The signal ' $\dot{z}$ ' is governed by Equation 5.4.

$$\dot{z} = \dot{x}[1 - \frac{\sigma_0}{f_{ss}(\dot{x})}\text{sgn}(\dot{x})z]^i \tag{5.4}$$

Where conditions for ' i ' are given in 5.5 and ' $f_{ss}(\dot{x})$ ' is represented by 3.25.

$$i \in \text{Z} \text{ and } \frac{\sigma_0}{f_{ss}(\dot{x})} > 0 \tag{5.5}$$

where ' $f_{ss}(\dot{x})$ ' represents the Stribeck curve, or steady-state friction-velocity curve. The Stribeck curve describes friction as a function of steady state sliding velocity. (5.6)

$$f_{ss}(\dot{x}) = f_c + (f_{ba} - f_c)e^{-(\dot{x}/v_s)} \tag{5.6}$$

Where ' f_c ' is obtained by Coulomb law, ' $\dot{x}$ ' is the relative velocity between the two contact surfaces, ' f_{ba} ' is the breakaway force and ' v_s ' is the characteristic velocity.

Initially it was assumed that the friction loss at the joint can be modeled as viscous damping. Using a Lugre friction model rather than viscous friction, it is possible to have a more realistic dynamic model. Comparing the simulation results with two models, one using the Lugre and the other using the viscous model, with experimental result, shows that the Lugre model can follow the experimental results much better than viscous.

Figure 5.6 compares the experimental and simulation results when applying 14 V to both the Lugre friction model and the viscous friction model.

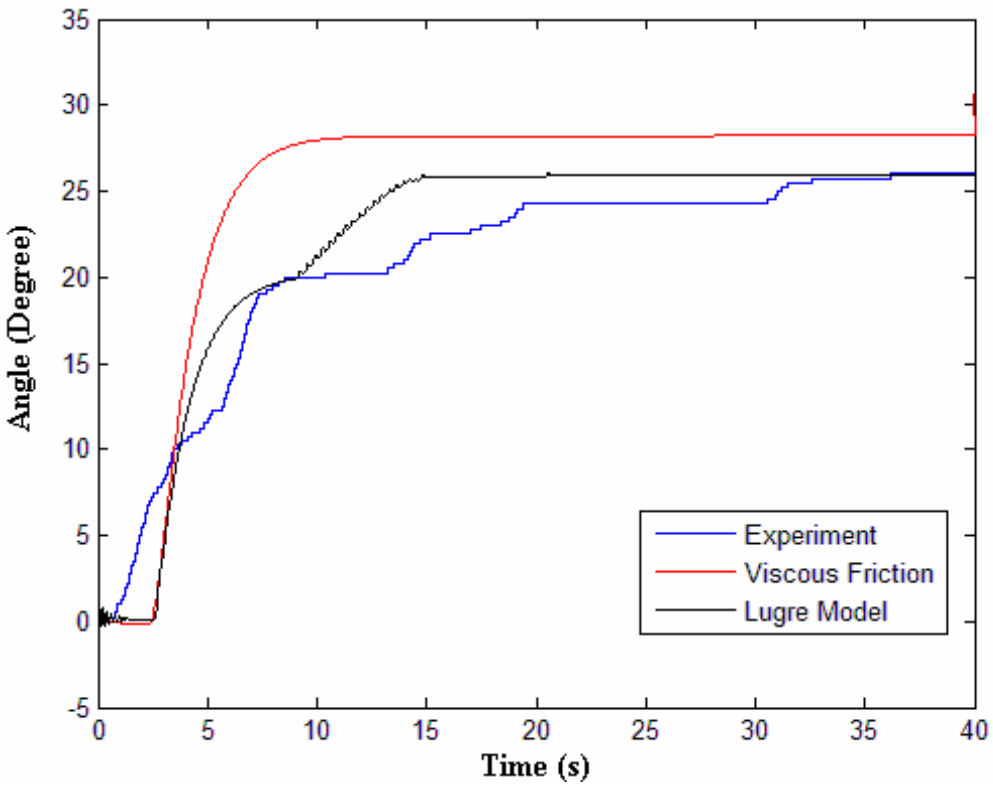

Figure 5-6 Comparison of the performance of the Lugre and viscous model

5.3.1.2. Sliding Mode Controller

Sliding control is a robust nonlinear Lyapunov-based control algorithm in which an nth order nonlinear and uncertain system is transformed to a 1st order system. Considering a SISO system

$$x^{(n)} = f(x) + b(x)u \tag{5.7}$$

where 'u' is the scalar input and 'x' is the state vector. For this system the nonlinear functions '$f(x)$'and '$b(x)$' are not exactly known. The control objective is for the system to follow a desired state vector '$\dot{x}$'. Furthermore, consider the surface '$S(t)$'in the state-space as:

$$S(x,t) = (\frac{d}{dt} + \lambda)^{n-1}\tilde{x} \tag{5.8}$$

where '$\tilde{x} = x - x_d$' is the tracking error and 'λ' is a positive constant. It can be shown that tracking the desired state vector is equivalent to that of remaining on the surface $S(t)$ [Slotin and Li, 90]. Therefore the control law should be selected in such a way that the distance to this surface decreases along all system trajectories (sliding condition):

$$\frac{1}{2}\frac{d}{dt}S^2 \le \eta s \tag{5.9}$$

where 'η' is a positive constant. As a result, all the trajectories are forced to reach the sliding surface in finite time and stay on the surface for all future times, hence the name sliding mode control. $S(t)$ is called the sliding surface and the system's behavior once on the surface is called sliding mode ($\dot{s} = 0$). It can be shown that the reach time from the initial state to the surface is:

$$t_{reach} \le S(t=0)/\eta \tag{5.10}$$

Thus, a typical motion under sliding mode control consists of a reaching phase and a sliding phase. During the sliding phase, the motion is confined to the sliding surface.

The sliding controller for the SMA rotary actuator is deigned to find the desired stress of the SMA wire. Referring to the equation of motion (Equation 5.8), the sliding surface can be defined as:

$$s = (\frac{d}{dt} + \lambda)\tilde{\theta} \tag{5.11}$$

where '$\tilde{\theta} = \theta - \theta_d$'. The dynamic of the system at sliding surface can be written as:

$$\dot{s} = 0 \tag{5.12}$$

This Equation 5.12 describes the dynamics of the system while it is in the sliding mode.

$$\dot{s} = \ddot{\theta} - \ddot{\theta}_d + \lambda\dot{\tilde{\theta}} = 0 \tag{5.13}$$

The dynamics model of the SMA arm can be used to derive the '$\ddot{\theta}$' which is the angular acceleration.(Equation 5.14). In Equation 5.14 'τ_{Fr}' is the resistance torque due to Lugre friction in the system.

$$\ddot{\theta} = \frac{\tau_w(\sigma) - \tau_{Fr}(\theta, \dot{\theta}) - \tau_s(\theta)}{I_e} \tag{5.14}$$

Using Equation 5.7 and 5.8 it is possible to find desired torque of the wire.

$$\tau_w = \tau_g + \tau_{Fr} + I_e\ddot{\theta}_d - I_e\lambda\dot{\tilde{\theta}} + Ksat(s) \tag{5.15}$$

where 'K' is the control gain and '$Sat(s)$' is the saturation term that is added to the desired torque of the SMA wire to address the uncertainties in the model. Also, for the case that the initial state of the system is not on the sliding surface, the saturation terms forces the trajectories to merge to the sliding surface. Having the desired torque, the desired stress of the SMA wire can be readily calculated as:

$$\sigma_d = \frac{\tau_w}{2r_p A_w} \tag{5.16}$$

where 'r_p' is the radius of the pulley and 'A_w' is the cross-section area of the SMA wire. In the proposed control design, the sliding mode controller calculates the desired stress of the wire based on the desired position. A second feedback controller, which is a PID controller, maintains the desired stress by applying the required voltage to the wire. Since the controller tracks the desired stress of the wire when the arm reaches the maximum stress position, the controller adjusts the control input accordingly. Therefore, the wire temperature remains in the actuation range. Figure 5.7 shows the proposed control system schematically.

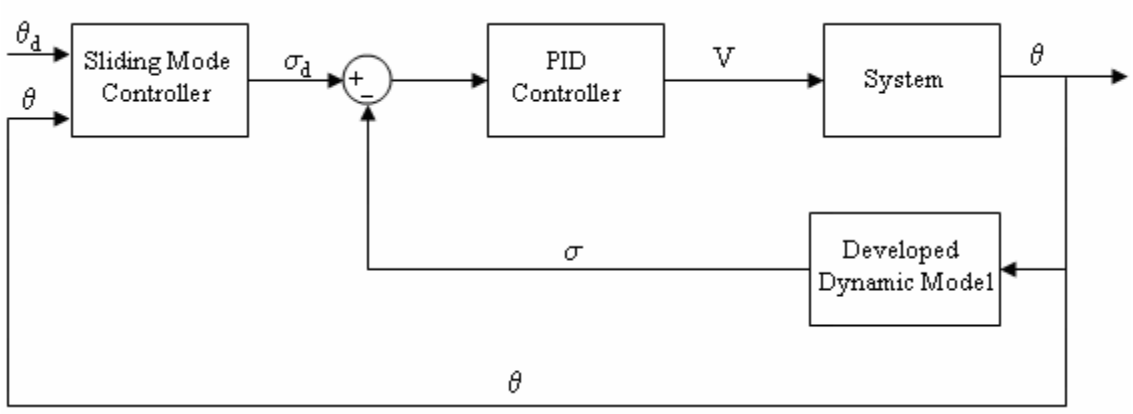

Figure 5-7 Block diagram of the stress based sliding mode control

The simulation results with the stress based sliding mode controller (SMC) is presented here and compared with a PID controller. Figure 5.8 and Figure 5.9 illustrate the performance of the proposed controller with that of a PID controller in tracking a sine wave.

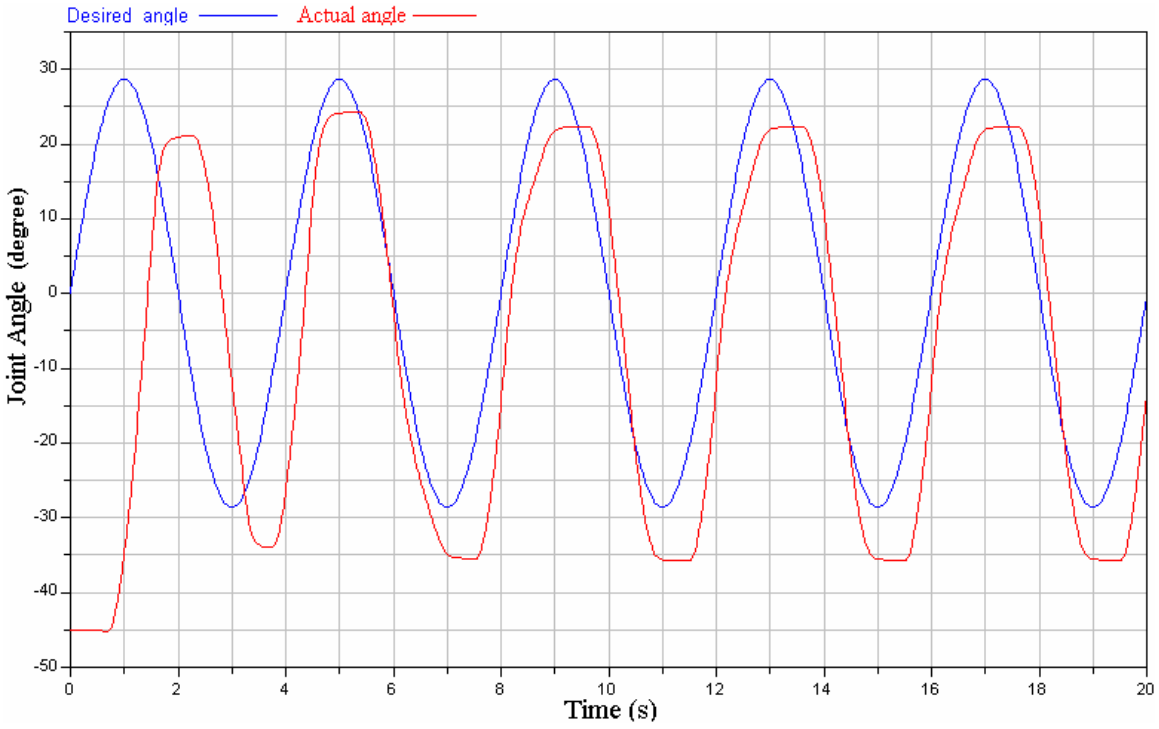

Figure 5-8 PID Performance in tracking a sine wave with frequency of 0.25HZ

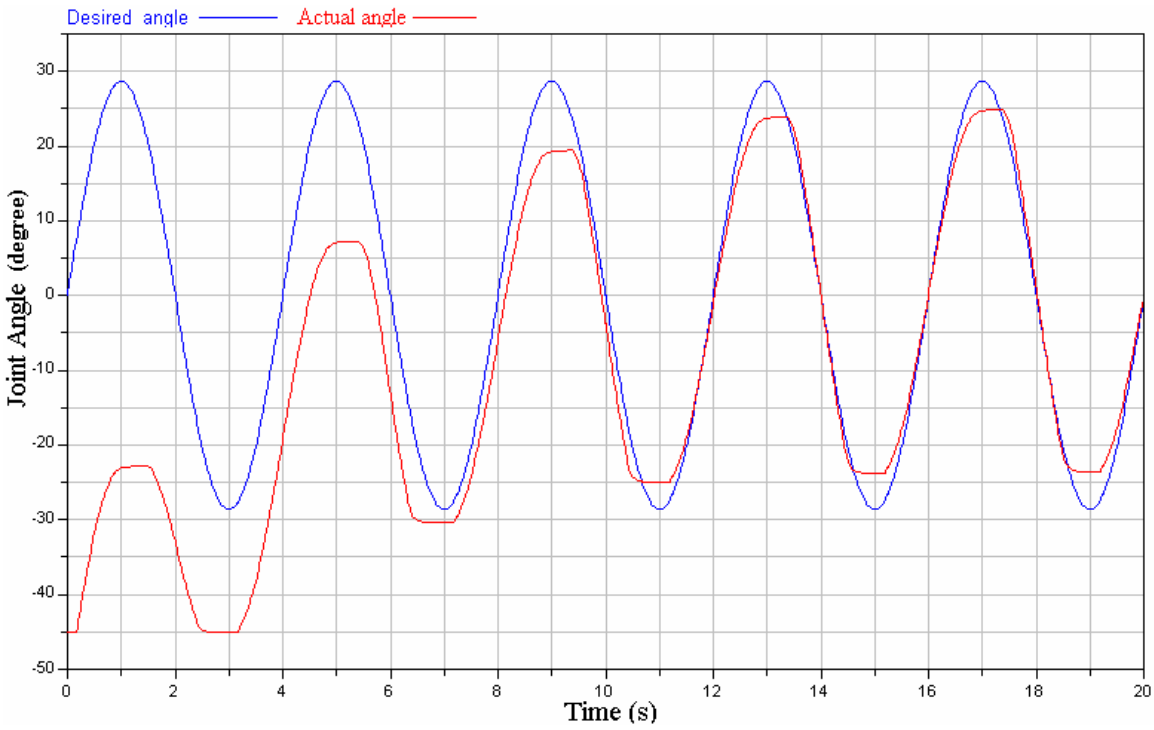

Figure 5-9 SMC performance in tracking a sine wave with frequency of 0.25HZ

5.3.2. Switching Sliding Mode Controller

Comparing Figures 5.8 and 5.9, it can be seen that with PID control, the actual angle reaches the desire one quickly, but cannot track the trajectory very well. However, with sliding mode control the opposite is true. With the sliding mode control, it takes more time to reach the desired value, but as it does it can follow the trajectory very well. The reason for the delay in time is that while the temperature of the wire is less than Martensite starting transformation temperature, no actuation takes place. Therefore, to shorten this delay time it is important to apply a high voltage first and when the transformation begins, the controller takes its role. In Equation 5.15 the 'K' factor can be used to push the system closer to the sliding surface. However the 'K' factor will change the desire stress and therefore the stress error. It should be notified having a larger desired

stress will ends to a lower raise time but at a same time it will cause chattering as the system get closer to the sliding surface.

Based on this observation, a switching control is proposed in which both a PID and sliding mode controller are working at the same time under a main switching criterion. This criterion is based on 'S' value (the sliding surface).

When the system is far from the sliding surface, a PID with a large gain will control and as the system approached the sliding surface, the control system will switch to the sliding mode controller. This combined controller is both robust and precise in tracking. The proposed switching controller is shown schematically in Figure 5.10.

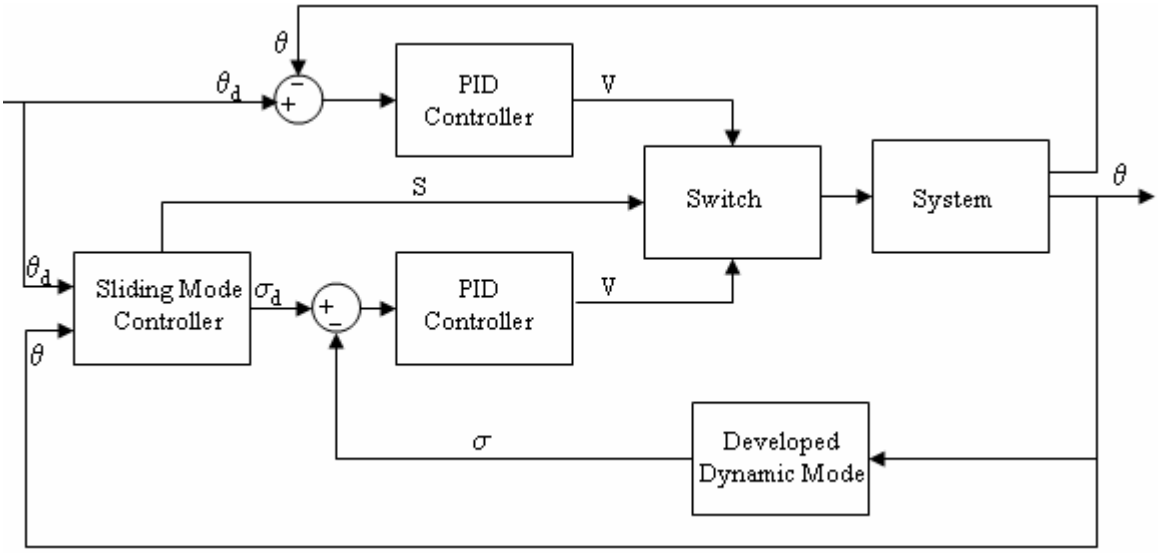

Figure 5-10Block diagram of the switching control

Figure 5.11 shows the performance of the switching control where the reaching time of the system is faster than a SMC controller and it can also follow the trajectory very well.

In chapter 6 the performance of all these controllers are compared with each other more in detail.

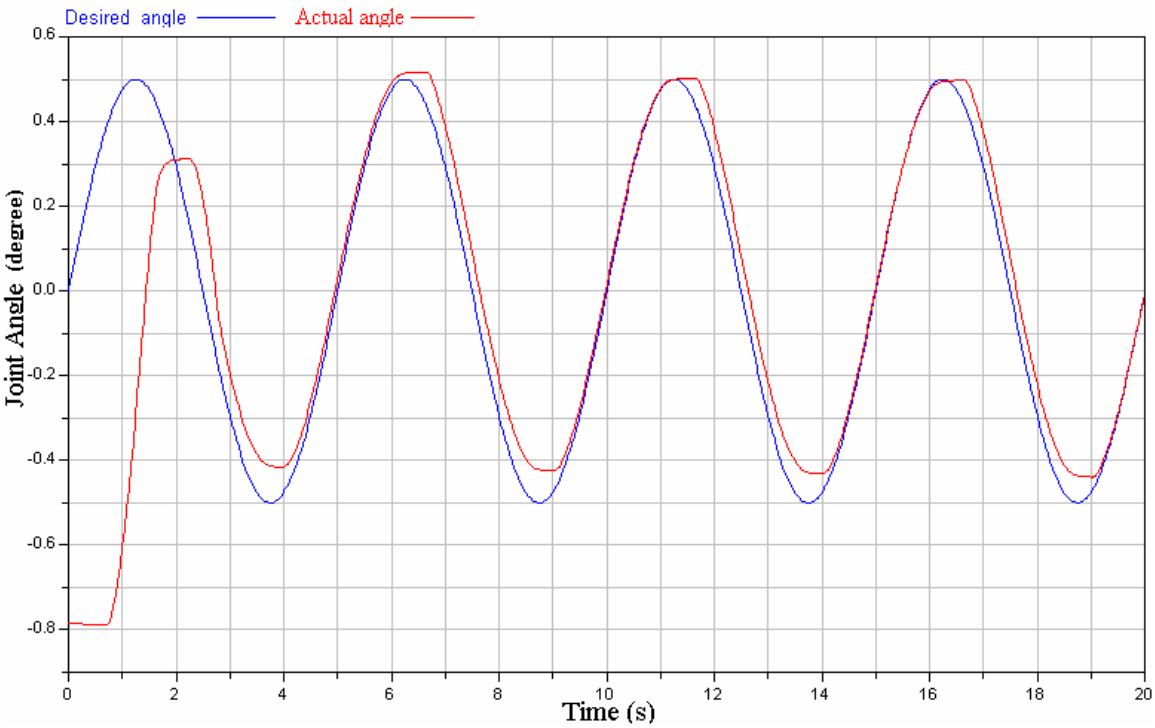

Figure 5-11 SMC-PID switching control tracking a sine wave with frequency 0.2HZ

5.3.3. Adaptive PID

Although switching control between a stress-based sliding mode and a position-based PID controller shows improved results, its implementation is difficult. This hybrid controller requires accurate simulation of the system dynamics which is computationally intensive. This limits the application of this hybrid control for experimental evaluation. Therefore another control technique based on the sliding mode controller is presented in this section, which is less computationally intensive. The experimental results of this controller are provided in chapter 6.

A robust adaptive PID controller design motivated from sliding mode control is used here for the uncertain system of SMA arm. In this approach, three PID control gains, K_p, K_i, and K_d are adjustable parameters and will be updated online with an adaptation mechanism to minimize a previously designed sliding condition. By introducing a

supervisory controller, the stability of the closed-loop PID control system under the effect of plant uncertainty and external disturbance can be guaranteed [Chang and Yan, 04].

The dynamic model of the system can be represented by a second order uncertain system. Applied voltage as a function of stress of the SMA wire '$u(t)=\sigma(t)\in R$' is the input and rotation angle of the arm is the output of the system '$y(t)=\theta(t)\in R$'. The state vector of the system is given by $X=\begin{bmatrix}\theta & \dot{\theta}\end{bmatrix}^T$ therefore:

$$\begin{aligned}\dot{x}_1(t) &= x_2(t)\\ \dot{x}_2(t) &= f(X,t)+\Delta f(X,t)+\delta(t)+u(t)\\ y(t) &= x_1(t)\end{aligned} \tag{5.17}$$

The control input of the system is defined by Equation 5.18:

$$u(t)=u_{PID}+u_s \tag{5.18}$$

Where '$u_{PID}(\cdot)$' is an adaptive PID controller based on the concept of sliding mode control. A proper adaptation law that is based on the use of gradient method is used to minimize a designed sliding condition for updating PID control gains. '$u_s(\cdot)$' is the extra supervisory controller that will be fired only when the states of the system exceed some bound in order to guarantee stability of the system [Chung and Yan, 04].

In this study because of having a physical constraints that limit the maximum applied voltage the state of the system will never exceed the designed bound and therefore there is no need to use the supervisory controller.

The continuous form of a PID controller, with input '$e(\cdot)$'and output '$u_{PID}(\cdot)$', is generally given as:

$$u_{PID}(t)=K_P(t)e(t)+K_I(t)\int_0^t e(\tau)\,d\tau+K_D\frac{d}{dt}e(t) \tag{5.19}$$

Where ' K_P, K_I, K_D ' are proportional, integral and derivative gains, respectively. In order to derive a proper adaptation law to update the PID controller gains, a sliding surface is used which is defined by:

$$S = \dot{\tilde{\theta}}(t) - k_1 \tilde{\theta}(t) - k_0 \int_0^t \tilde{\theta}(\tau)\, d\tau \tag{5.20}$$

Where ' $\tilde{\theta}$ ' is a tracking error defined as ' $\tilde{\theta} = \theta - \theta_d$ ' and ' k_1 ' and ' k_0 ' are designed in such a way that roots of Equation 5.21 are placed at the open left-hand side of the complex plane.

$$S^2 + k_1 S + k_0 = 0 \tag{5.21}$$

If the sliding mode occurs, i.e, ' $\dot{S} = 0$ ', then

$$\ddot{\tilde{\theta}} + k_1 \dot{\tilde{\theta}} + k_0 \tilde{\theta} = 0 \tag{5.22}$$

This implies that ' $\tilde{\theta} \to 0\ (or\ \theta \to \theta_d)$ ' as ' $t \to \infty$ '. The sliding condition that ensure the hitting and existence of a sliding mode is derived according to Lyapunov stability theory. In general, the Lyapunov function candidate for the sliding mode control is simply given by $V = \frac{1}{2} S^2$, and therefore the sliding condition is defined as:

$$\dot{V} = S\dot{S} < 0 \tag{5.23}$$

Equation 5.21 guarantees that ' $S(t) \to 0$ ' as ' $t \to \infty$ '. To derive an adequate adaptation mechanism for tuning three PID control gains, a gradient search method is used to minimize the sliding condition in Equation 5.23.

The gradient search algorithm is calculated in the direction opposite to the energy flow and obtains the convergence properties of the PID controller for tuning. Based on the

gradient method, the adaptation laws for three control gains 'K_P, K_I, K_D' is defined as follow:

$$\dot{K}_P = -\gamma \frac{\partial S\dot{S}}{\partial K_P} = -\gamma \frac{\partial S\dot{S}}{\partial u_{PID}} \frac{\partial u_{PID}}{\partial K_P} = -\gamma\, Se \tag{5.24}$$

$$\dot{K}_I = -\gamma \frac{\partial S\dot{S}}{\partial K_I} = -\gamma \frac{\partial S\dot{S}}{\partial u_{pid}} \frac{\partial u_{pid}}{\partial K_i} = -\gamma\, S \int_0^t e(\tau)\, d\tau \tag{5.25}$$

$$\dot{K}_D = -\gamma \frac{\partial S\dot{S}}{\partial K_D} = -\gamma \frac{\partial S\dot{S}}{\partial u_{PID}} \frac{\partial u_{PID}}{\partial K_D} = -\gamma\, S \frac{de}{dt} \tag{5.26}$$

Where '$\gamma > 0$' is the learning rate and '$e = \theta - \theta_d$' is the tracking error. It is worth noting that if the learning rate or the initial values of the PID control gains are not selected adequately, the resulted PID controller could potentially make the states of the system divergent.

Using Equations 5.24 to 5.26 it is possible to update the gains of the controller in order to reduce the predefined sliding condition. The schematic of this controller is given in Figure 5.12.

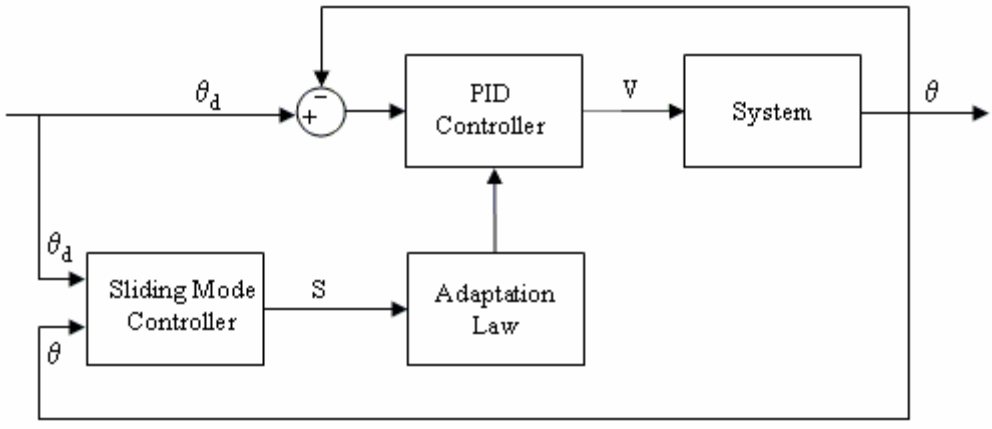

Figure 5-12Block diagram of adaptive PID control

Figure 5.13 shows that like the SMC-PID controller, the adaptive PID can follow the desired trajectory quickly and accurately.

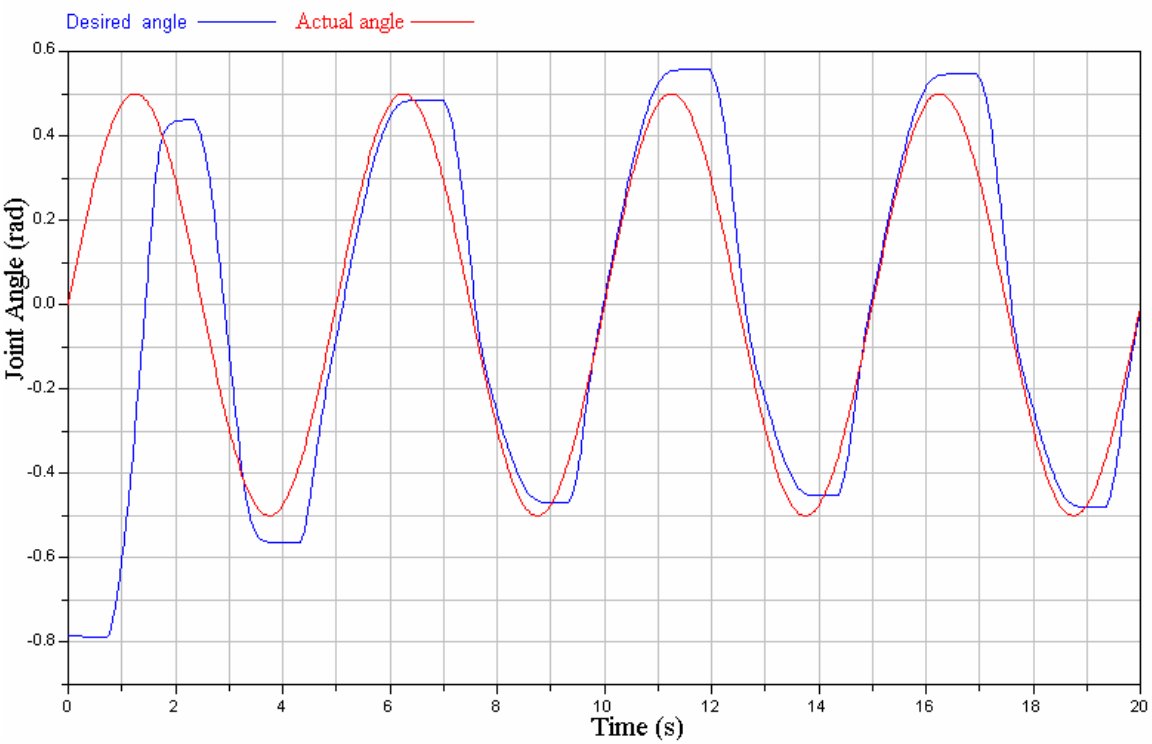

Figure 5-13 Adaptive PID controller tracking a sine wave with frequency of 0.2Hz

Chapter 6

6. Results

In Chap 5, the control problem of the SMA actuated experimental setup was investigated and an adaptive PID controller was proposed to regulate the position of the system. In this chapter the performance of the proposed controller, is compared with that of the other control techniques such as PID, stress based sliding mode controller (SMC) and switching sliding mode controller (SMC-PID). The simulation results are provided in the first section and the experimental results are provided in the second section. In the second section the robustness of the controller are experimentally examined. In the third section the experimental results are applied to the walking simulation model to check the stability of motion at different conditions. The result of this analysis provides the walking stability limitations of using SMA actuators for the AAFO.

6.1. Simulation Results

To compare the performance of adaptive PID with PID, SMC and SMC-PID controllers, three different desired trajectories are used. These trajectories are chosen to represent the different walking and gait conditions. The first trajectory to track, is an exponentially damped sine wave with an amplitude of 1 rad (57^o), a frequency of 0.2 Hz and a

damping factor of $0.1 s^{-1}$. Figures 6.1 and 6.2 show the response of the system with SMC and SMC-PID controller in tracking the desired trajectory. It is shown that sliding mode controller can not follow the desired trajectory for the first 4 seconds of simulation. This delay is mostly due to the delay associated with raising the temperature of the SMA wire beyond the Austenite start temperature. However by switching between PID and SMC in Figure 6.2, the combined controller applies a higher voltage at the beginning of the simulation and as a result the system can reach the desired trajectory faster. Additionally, the tracking error of the system is reduced.

Performance of the next two controllers: PID and Adaptive PID controllers are shown in Figures 6.3 and 6.4. The tracking error for these two controllers is compared in Figures 6.5 and 6.6. Figure 6.5 shows the tracking error for the whole time history and Figure 6.6 shows the tracking error after 4 seconds, when the actual angle is converged to the desired one. It is worth noting since the basic design of these two controllers is the same the tracking error has the same pattern but different amplitude. In adaptive PID because of the adaption law the gains are changing to enhance the performance of the system and therefore the tracking error is smaller than that of the PID controller.

The tracking error of the SMC, SMC-PID and Adaptive PID are compared in Figure 6.7 and 6.8. Figure 6.7 shows the tracking error for the whole time history and Figure 6.8 for the convergence region. Comparing the tracking errors in Figure 6.8, the effect of switching control can clearly be seen. The SMC has an error about 6^o at $t = 10s$, which decreases to 1^o after 40s while the tracking error of the combined SMC-PID is about 2^o at $t = 10s$ and decreases to less than 0.5^o at $t = 40s$. It is also clear that the tracking of SMC is better than Adaptive PID and Adaptive PID's one better than SMC.

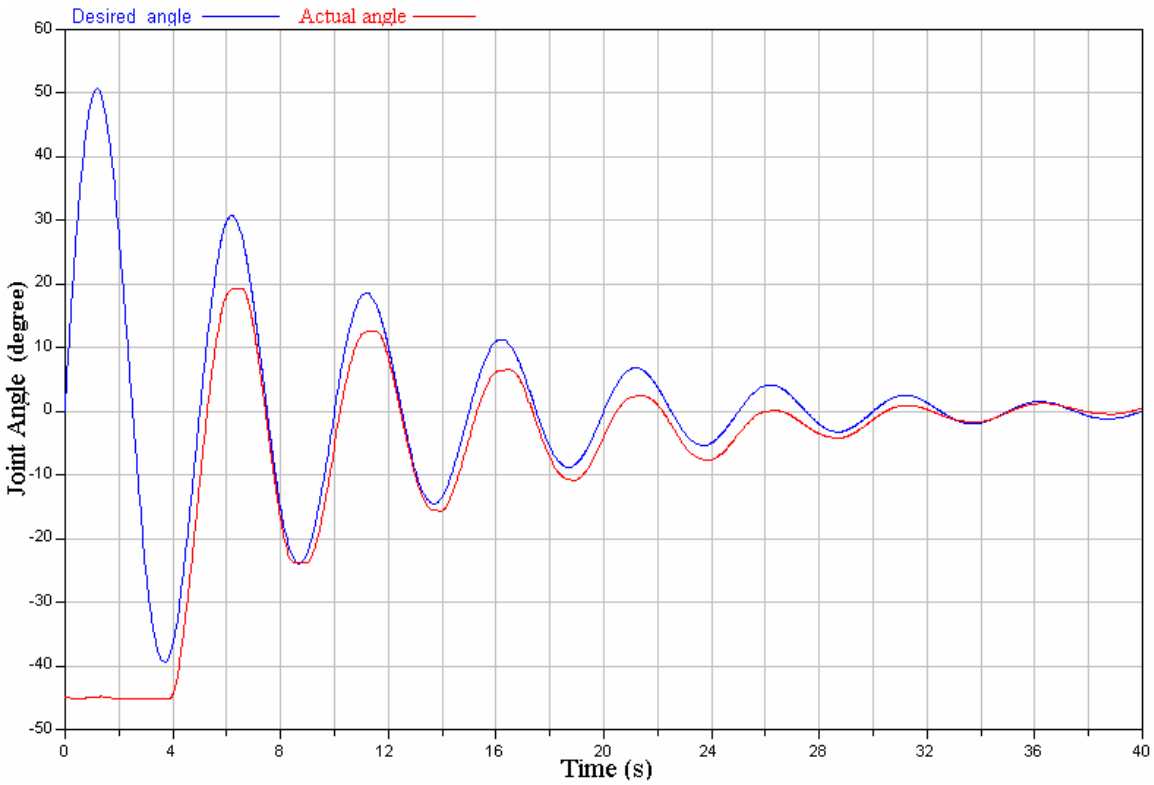

Figure 6-1 Sliding Mode Controller (SMC) simulation in tracking a damped sine wave

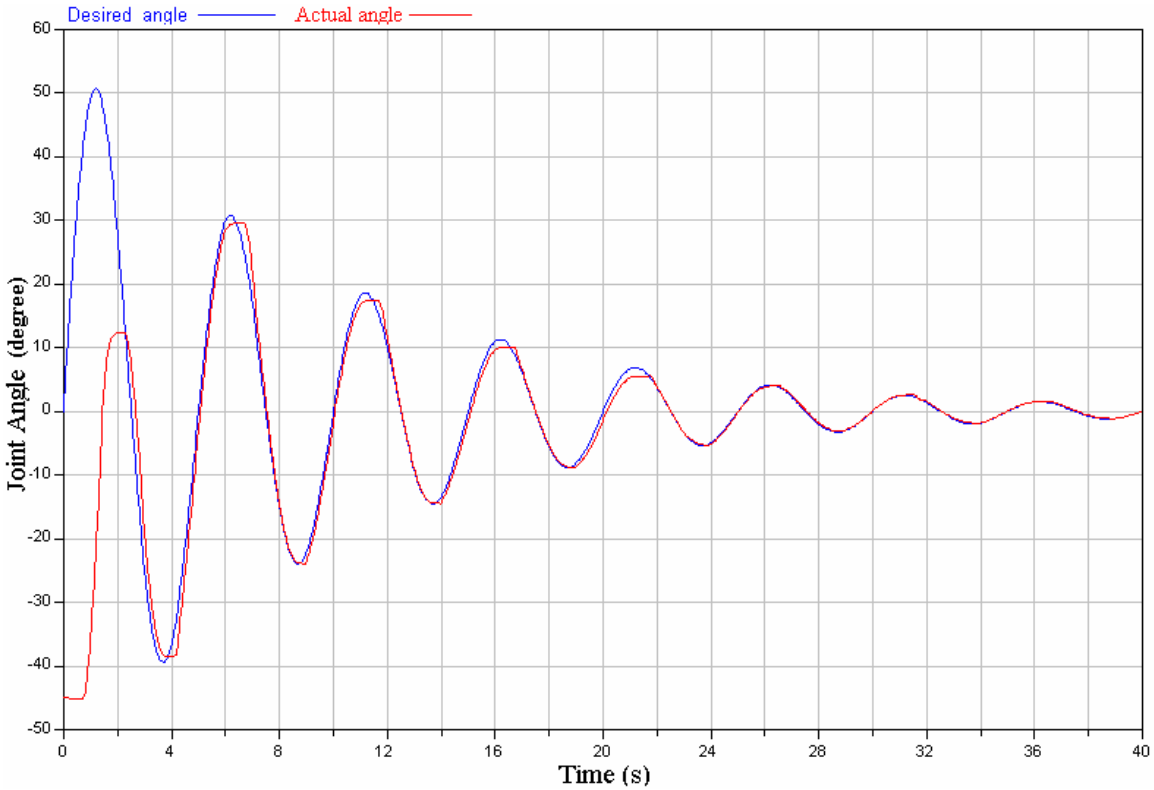

Figure 6-2 Simulation of switching control between SMC and PID in tracking a damped sine wave

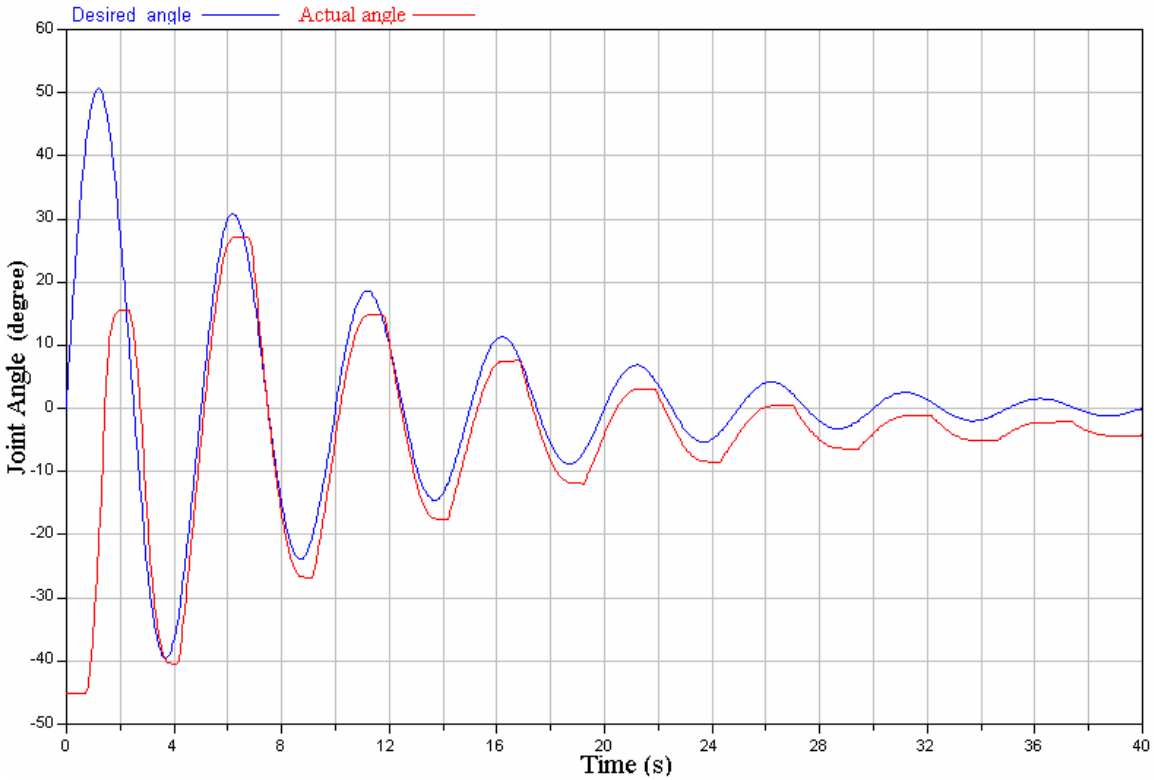

Figure 6-3 PID Controller simulation in tracking an exponentially damped sine wave

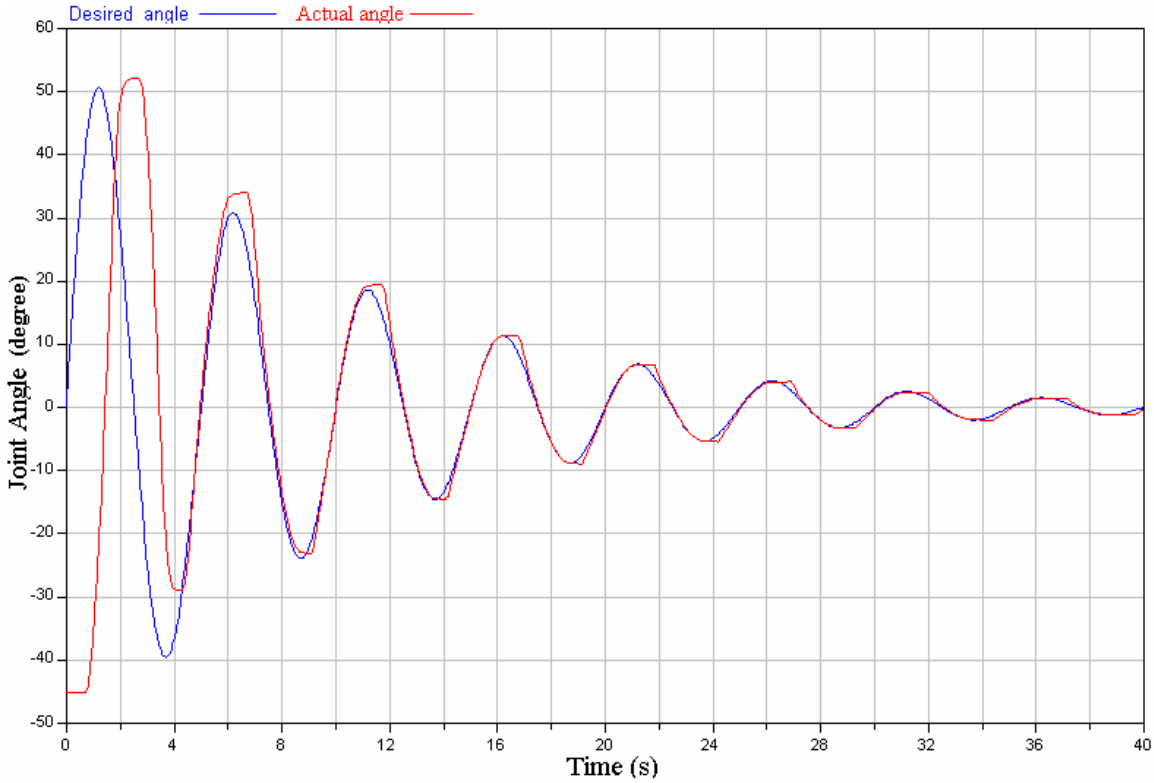

Figure 6-4 Adaptive PID simulation in tracking an exponentially damped sine wave

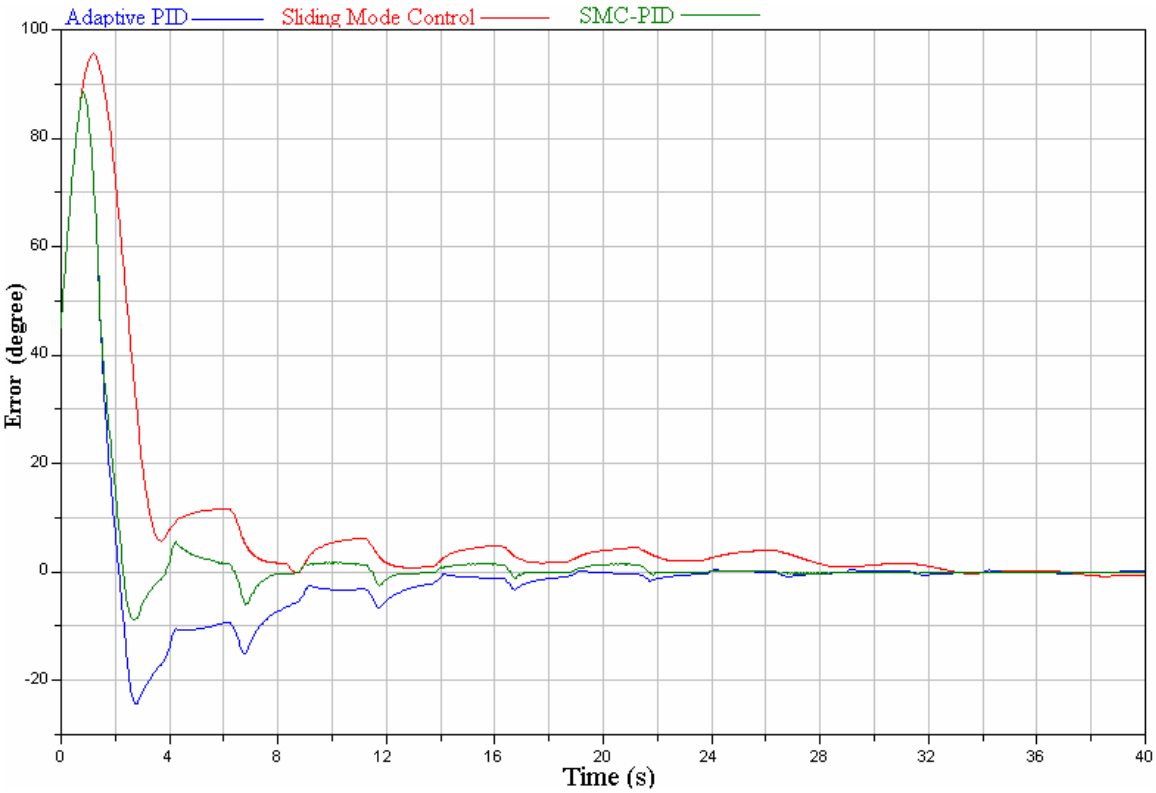

Figure 6-5 Angle error of SMC, SMC-PID and adaptive PID

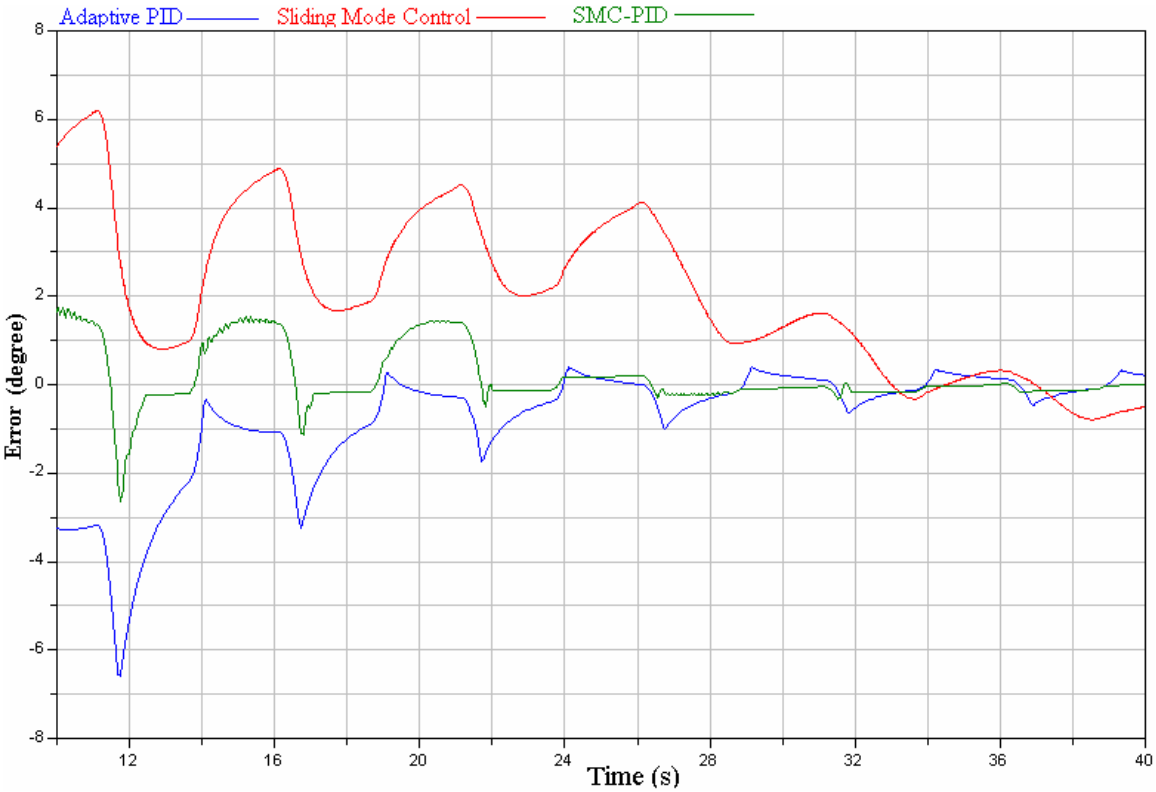

Figure 6-6 Angle error of SMC, SMC-PID and adaptive PID in tracking an exponentially damped sine wave at convergence region

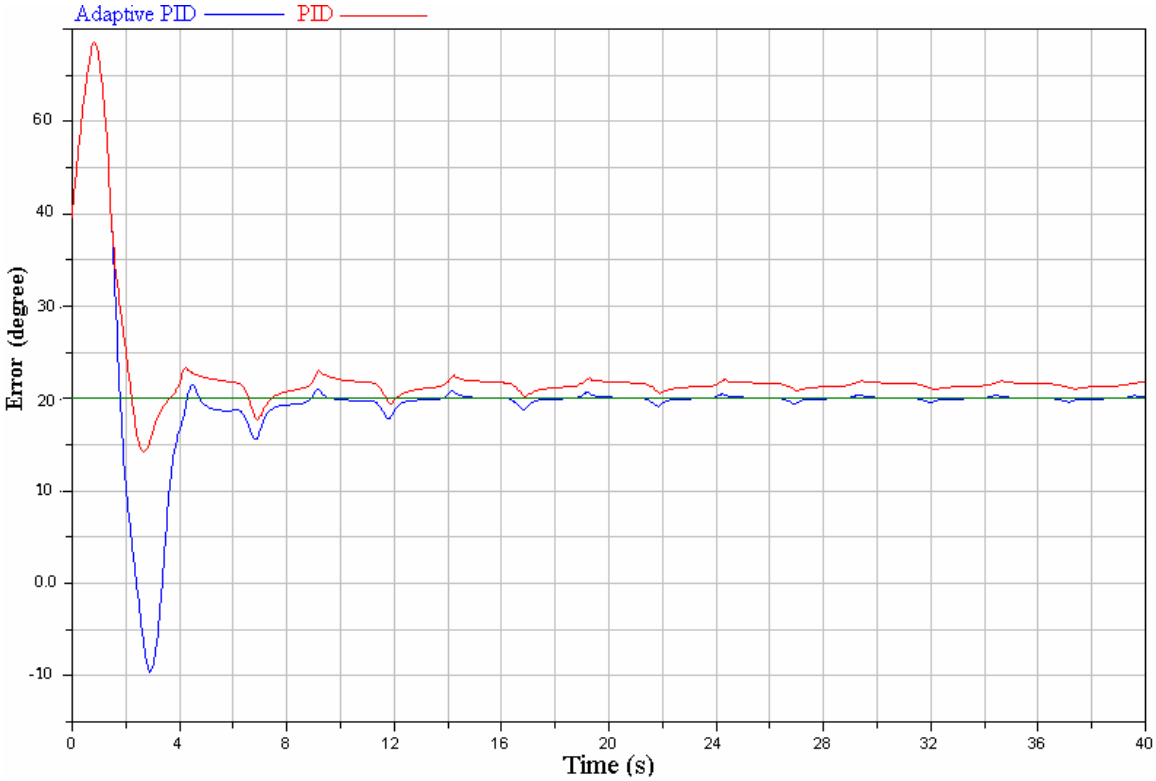

Figure 6-7 Angle error of PID and adaptive PID in tracking a damped sine wave

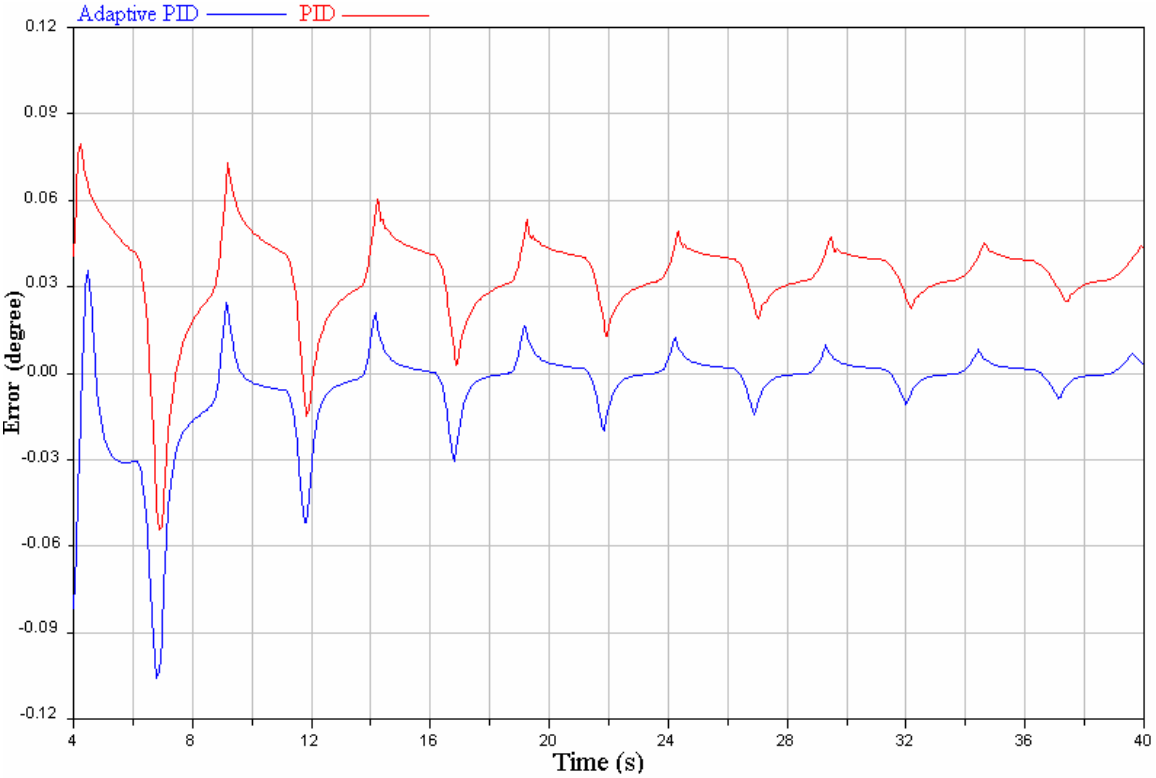

Figure 6-8 Angle error of PID and adaptive PID in tracking a damped sine wave at convergence region

The simulation results show that the switching controller between stress based sliding mode controller and PID has the minimum tracking error and therefore the best results. As it was mentioned earlier due to using a realistic model or Kalman filter and a massive calculation associated with them it is difficult to experimentally test the SMC-PID controller. Hence in the second simulation, just adaptive PID and PID are tested.

In order to check the performance of the system for different walking speeds and walking conditions, here the desired trajectory is a sine wave with a frequency of 0.1 Hz which changes to 0.25 Hz in the middle of test. The amplitude of the sine wave is also change at a same time. Figure 6.9 and 6.10 show performance of the PID and the Adaptive PID controllers in tracking the desired angle. In these simulations the control parameters are shown in Table 6.1 The tracking error is shown in Figure 6.11 for the whole time history and in Figure 6.12 for the convergence region. In the first 4 seconds both controllers experiencing a large error which is due to both initial conditions (the initial tracking error is 45^o) and also the time required to get to the temperature that phase transformation start. In tracking the first sine wave with a lower frequency, because of not tuned control parameters, the tracking error of the adaptive PID is larger than a PID for the first 2 seconds. But the adaptation law tunes the parameters and therefore the error is reduced to less than 1^o while the PID has an error about 4^o. By increasing the frequency of the sine wave (larger walking speed) the tracking error of both controllers increases. PID errors jumps to 8^o and adaptive PID to 4^o. The gains of adaptive PID during tracking the mixed sine wave are shown in Figure 6.13 to 6.14.

The parameters of each controller used in the simulation are listed in Table 6.1.

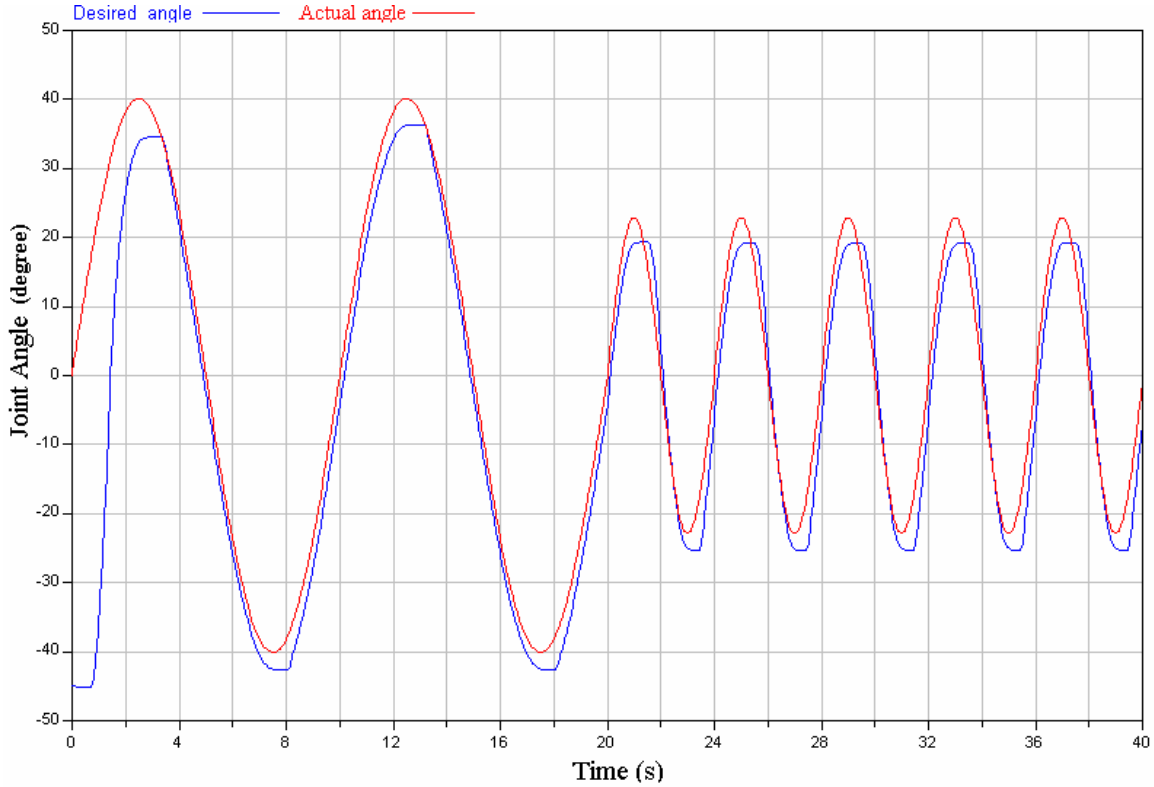

Figure 6-9 PID Controller simulation in tracking a mixed sine wave

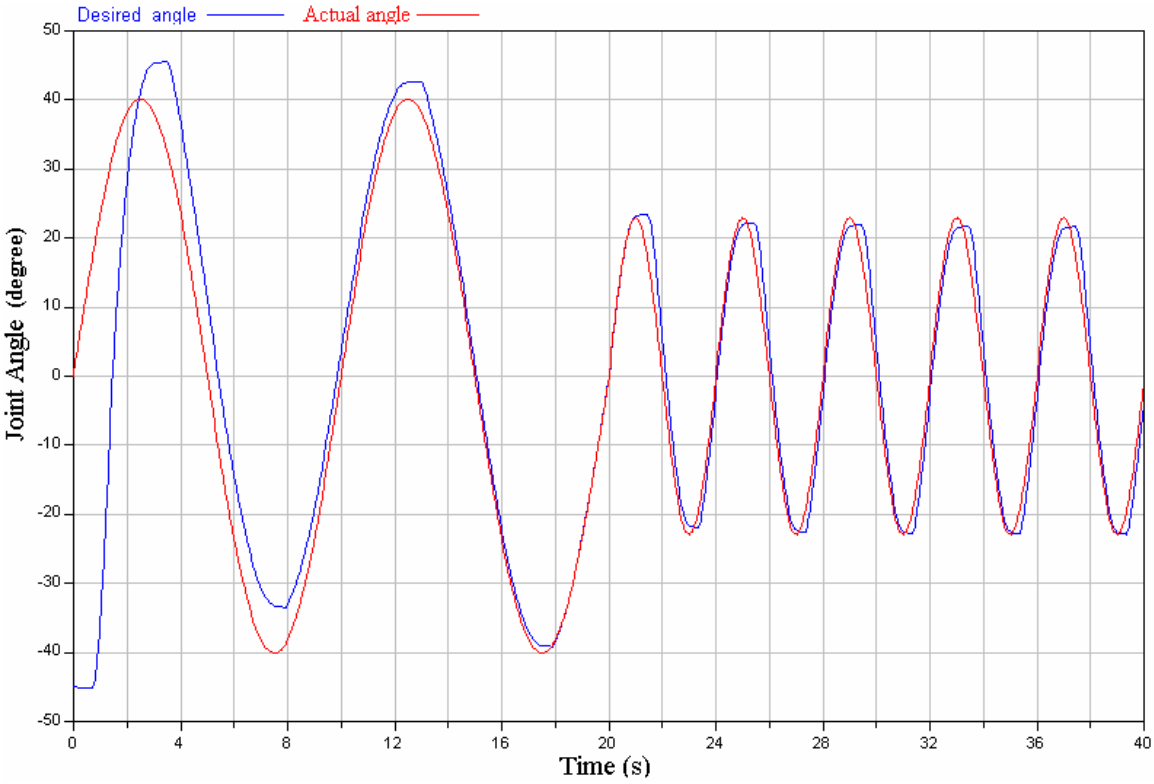

Figure 6-10 Adaptive PID simulation in tracking a mixed sine wave

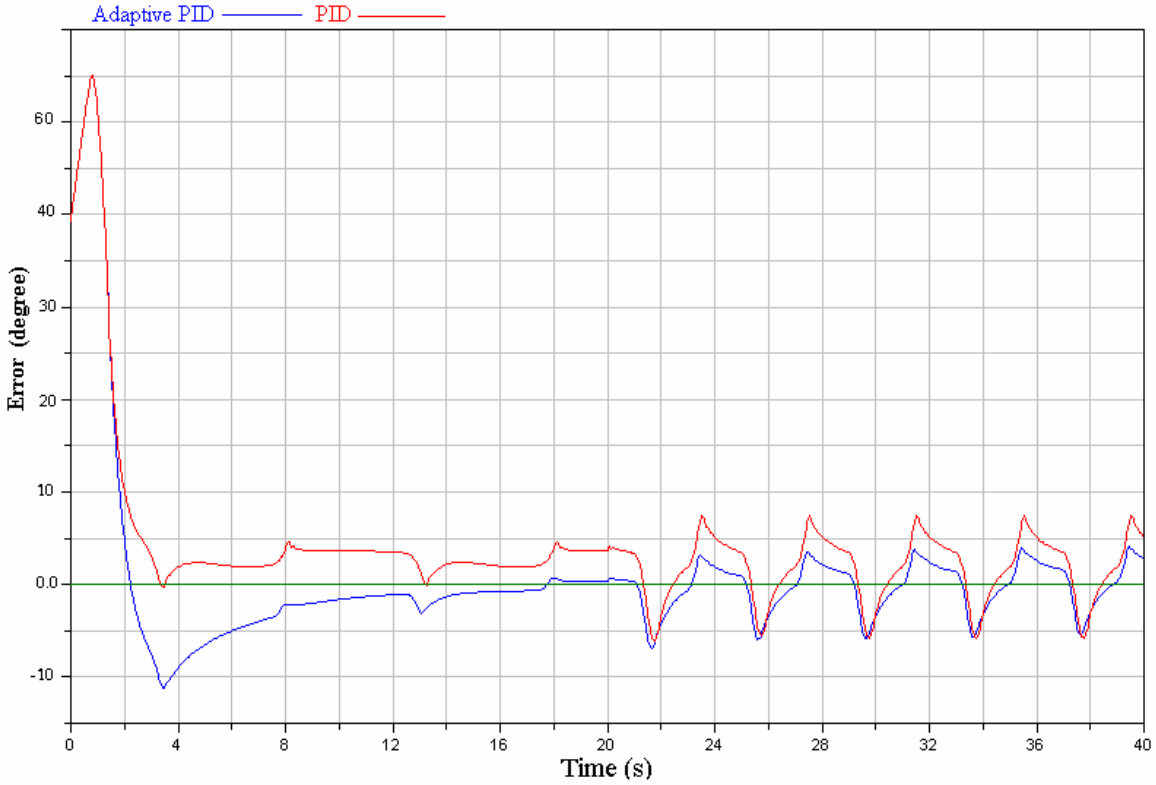

Figure 6-11 Angle error of PID and adaptive PID in tracking a mixed sine wave

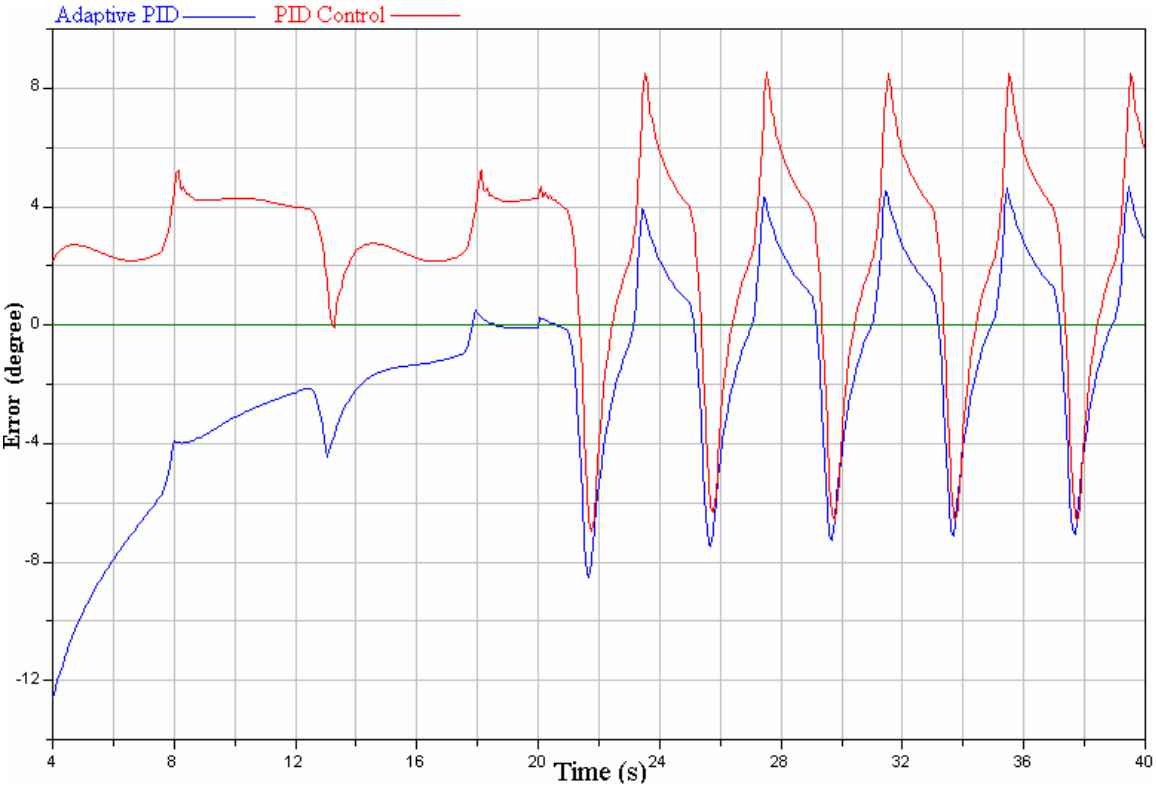

Figure 6-12 Angle error of PID and adaptive PID in tracking a mixed sine wave at the convergence region

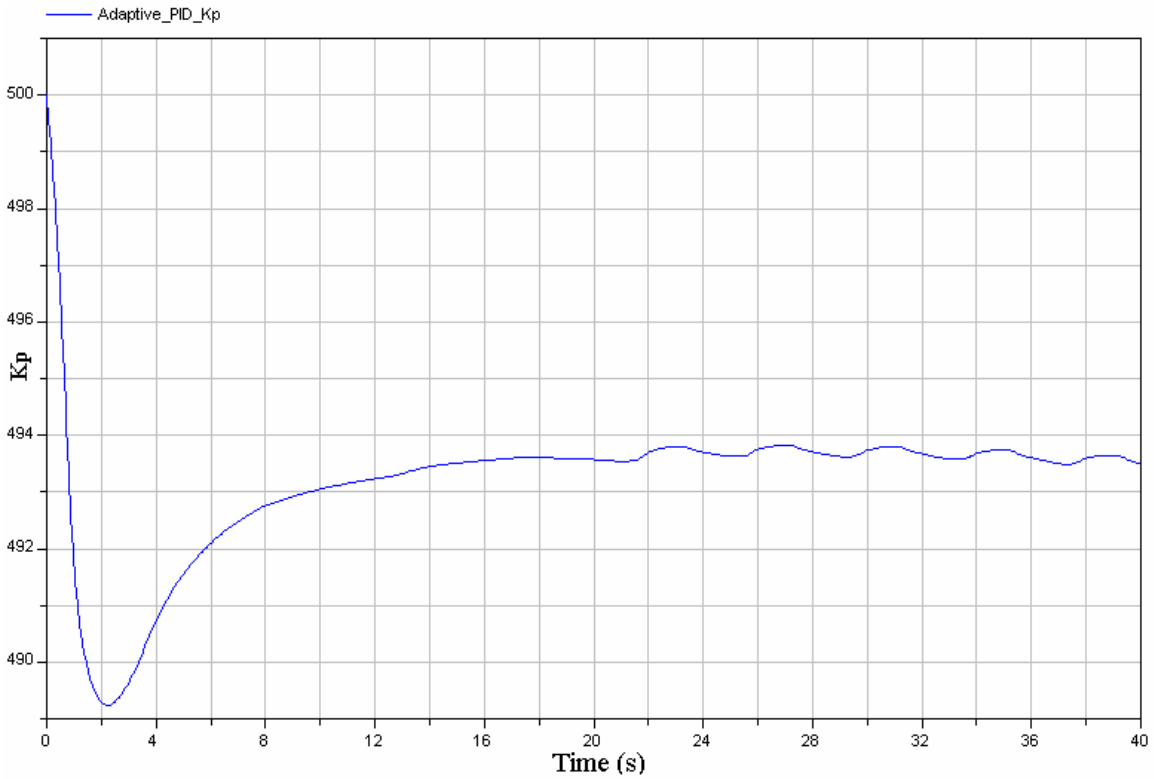

Figure 6-13 Proportional gain of Adaptive PID control in tracking a mixed sine wave

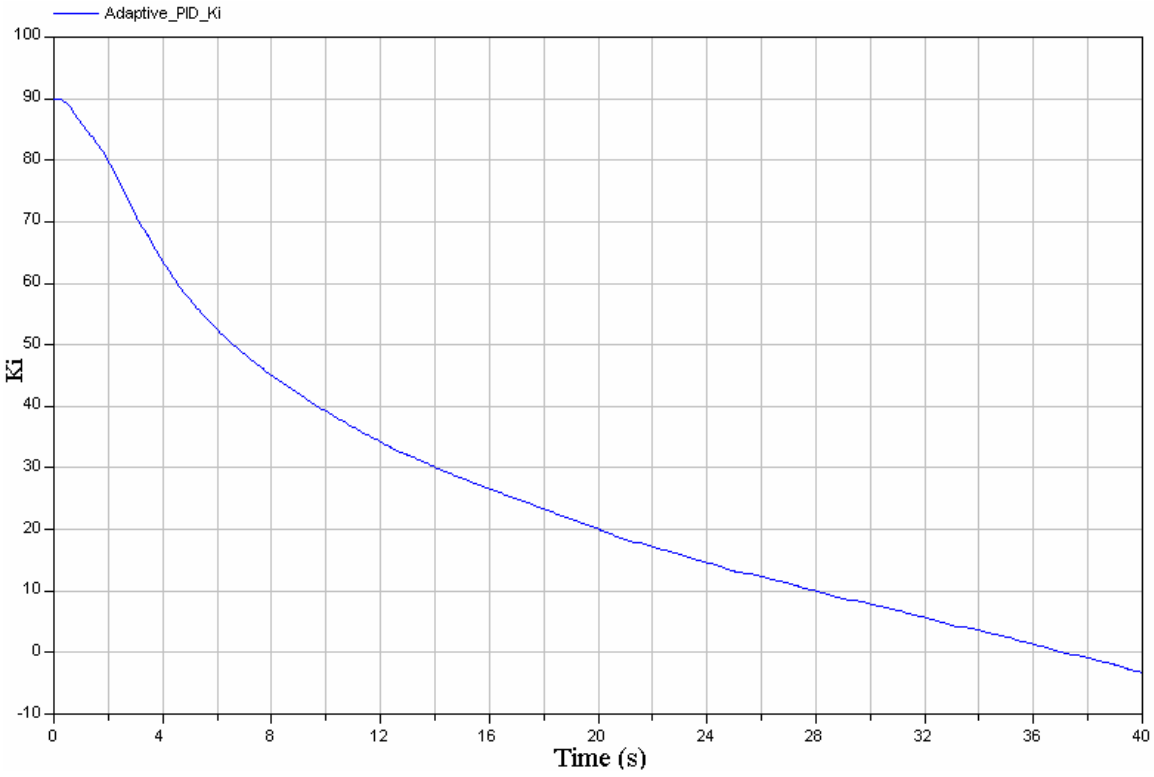

Figure 6-14 Integrator gain of Adaptive PID control in tracking a mixed sine wave

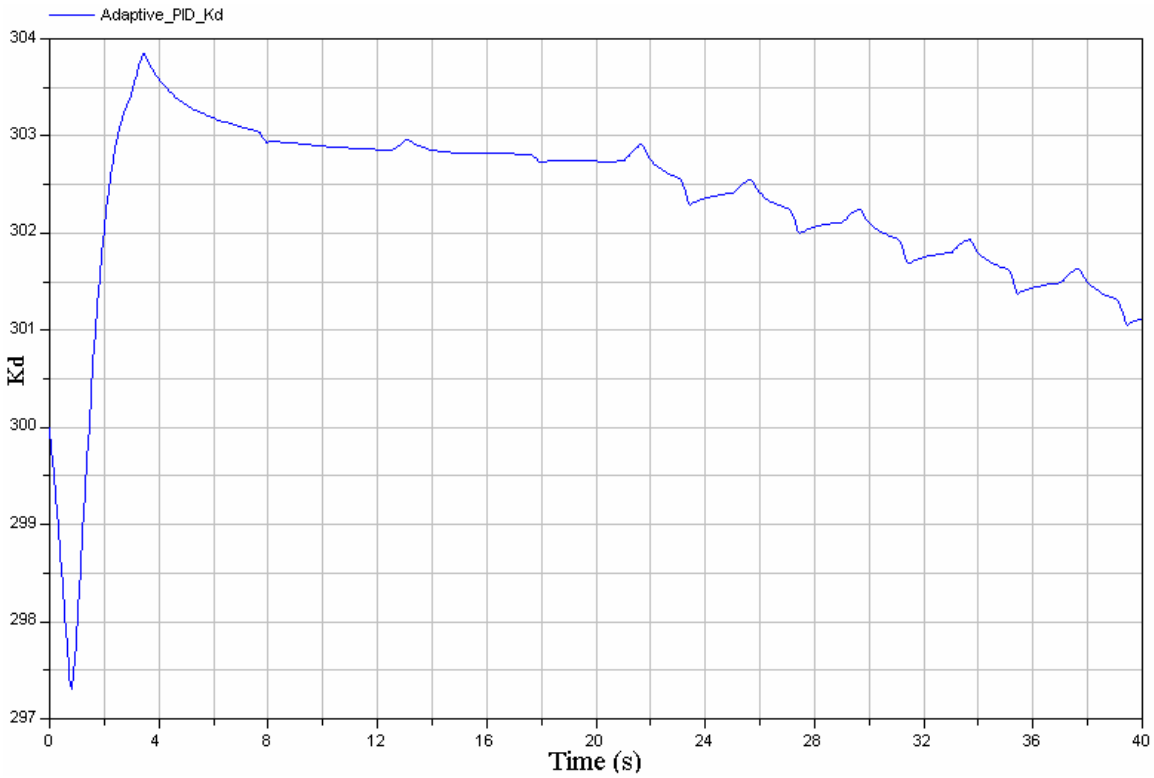

Figure 6-15 Derivative gain of Adaptive PID control in tracking a mixed sine wave

Table 6-1 Controller parameters

PID Controller	Tracking the desired angle:	$K_p = 200$	$K_i = 0.2$	$K_d = 80$
SMC	Tracking the desired stress:	$K_p = 300$	$K_i = 0$	$K_d = 30$
	Designing the desired stress	$\lambda = 10$	$b = 3$	
PID-SMC	Designing the desired stress	$\lambda = 10$	$b = 3$	$S_{cr} = 0.4$
	Tracking the desired stress:	$K_p = 300$	$K_i = 0$	$K_d = 30$
	Tracking the desired angle:	$K_p = 300$	$K_i = 3$	$K_d = 150$
Adaptive PID	Tracking the desired angle:	$K_p = 500$	$K_i = 90$	$K_d = 300$
	Design the Sliding Condition:	$\lambda = 5$	$K_0 = 1$	$K_1 = 1$

6.2. Experimental Results

The experimental results of the Adaptive PID control algorithm are presented in this section. For all the experiments, dSpace hardware-in-the-loop solution is used experiments. This solution allows MATLAB/Simulink models to be run, while the system (1-dof SMA manipulator) is part of the control/data acquisition loop. Hence real time data can be collected and also system parameters can be changed through its graphical interface. An optical encoder is used to measure angular position of the 1-dof arm. Hence it was possible to take numerical derivative of this signal to obtain angular velocity of the manipulator. The experimental setup used for closed loop control is shown in Figure 6.16.

Three experimental results in this section are presented. The first one is checking tracking a sine wave with frequency of 0.2 Hz which is shown in Figure 6.17. The aim of this experiment was to evaluate the performance and simulation results of an adaptive PID controller in tracking a desired position similar to the ankle angle. It was assumed that the walking speed is always constant and there is no obstacle or external disturbance to the system which make an uncertainty in the parameters of the system. Also three more experiments ran to check the robustness of the system in the presents of uncertainty or disturbance.

In the second experience shown in Figure 6.17, the mass of the system was increased during the experiments. As it is shown in the Figure 6.18, even by increasing the mass by 15% the control algorithm can still follow the desired trajectory well and there is not a significant change in the performance of the system.

To check the effect of facing an obstacle in the movement, the SMA wire was subjected to an external force which prevented the rotation of the wire. This experiment was planned to see if the SMA wire can follow the desired angle after stopping by an obstacle the amount of time required for the actuator to recovery and continuing the previously designed task. This experiment is shown in Figure 6.18.

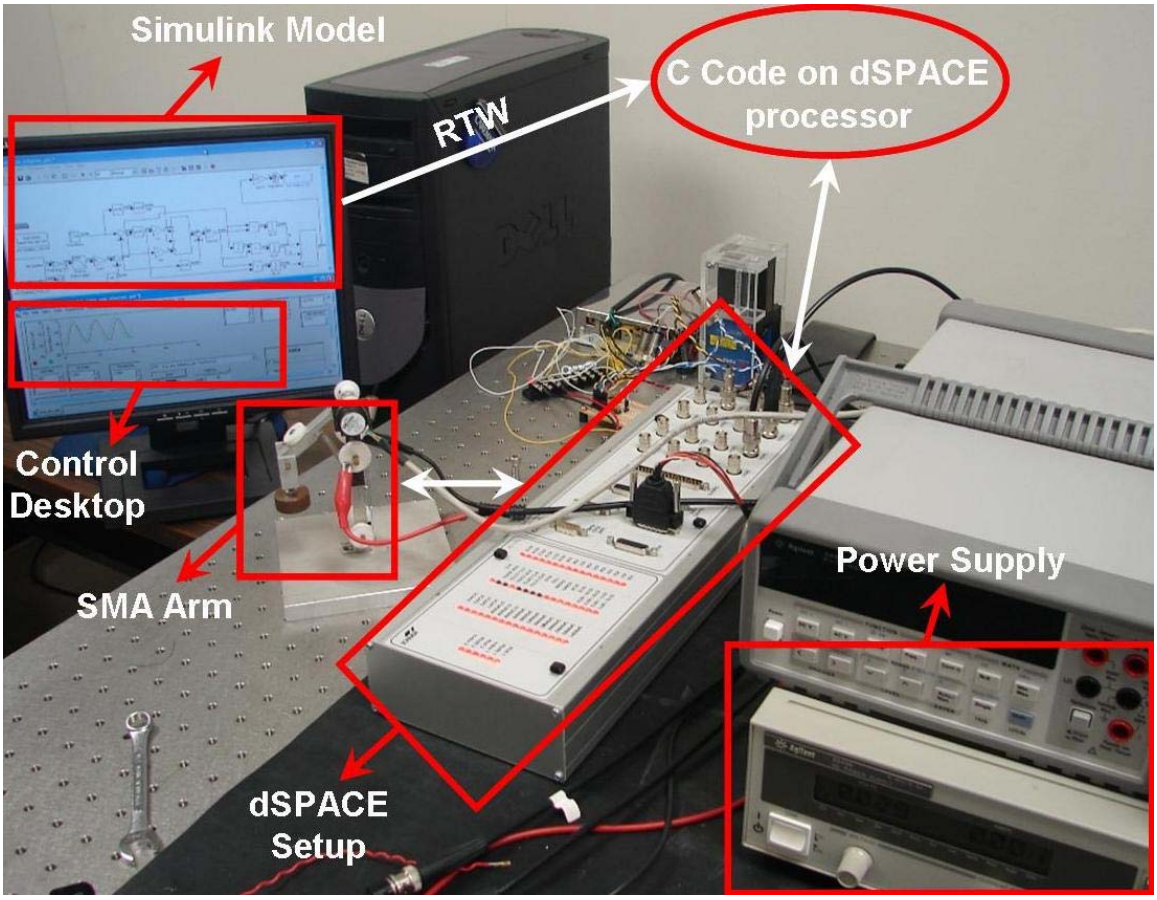

Figure 6-16 dSPACE hardware-in-the-loop solution used for testing the control method experimentally

It should be noted that there is a physical limit in actuating the SMA wires during these experiments which was due to power limits. It was assumed that the controller could not apply a voltage larger than 20 V and the maximum electrical current was allowed to be 0.4 A. To check the effect of voltage limits in the raise time, different voltage limits were check for an Adaptive PID in tracking a sine wave at frequency of 0.2 Hz.

Figure 6.19-21 shows the simulation results in controlling the desired angle with 20, 40 and 60 V as an upper limit for the power supply.

It can be seen that by increasing the voltage limits, the temperature of the wire raise faster and therefore the required time to have the actual actuation decreased. It brings the less delay to the system and results in a smaller tracking error. However by increasing a voltage to 60 V, there is not a significant change in delay time of the system. This delay time is because of the physics of the system and can not be reduces by increasing the voltage limits.

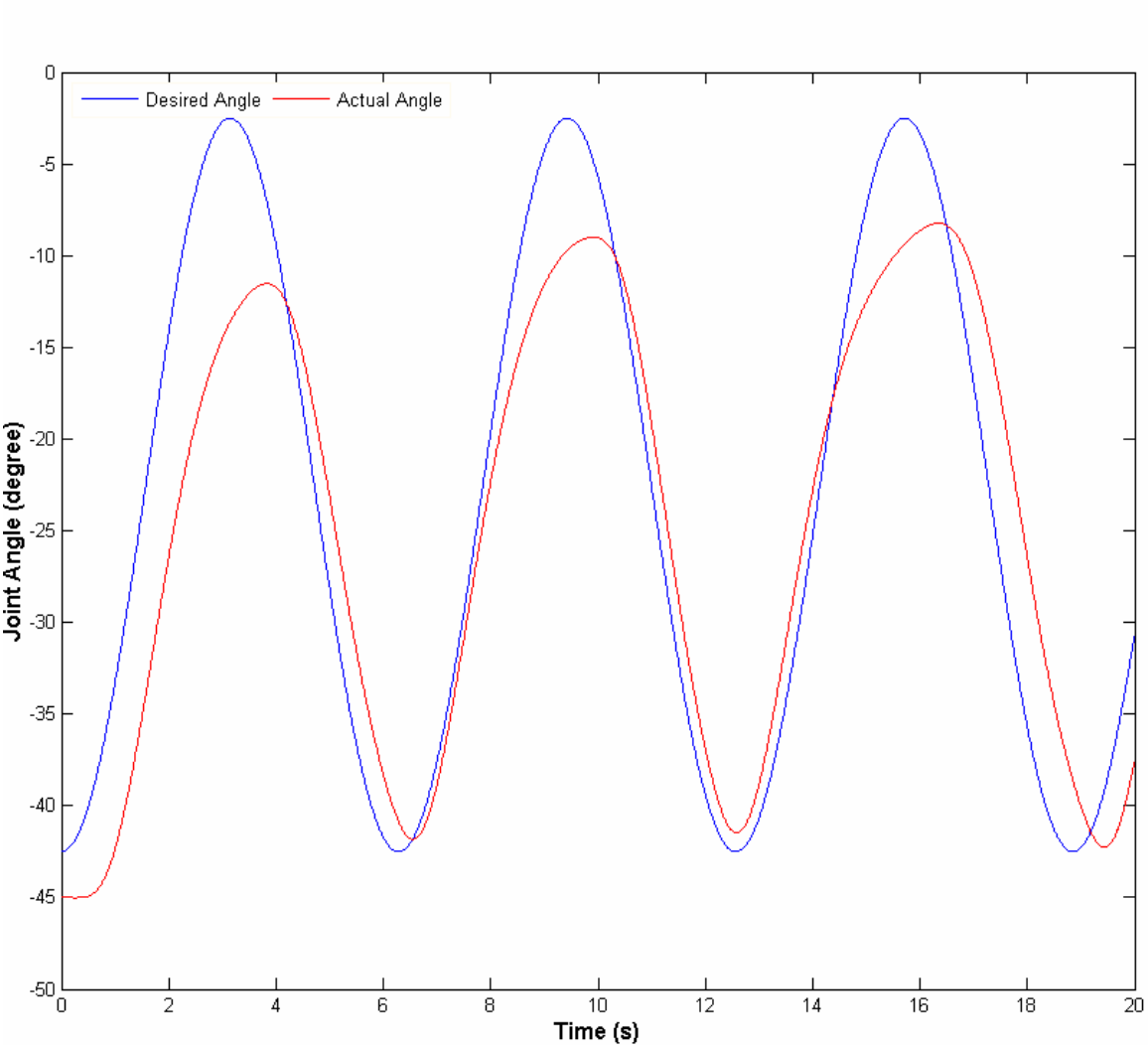

Figure 6-17 Experimental results of tracking a sine wave with an Adaptive PID controller

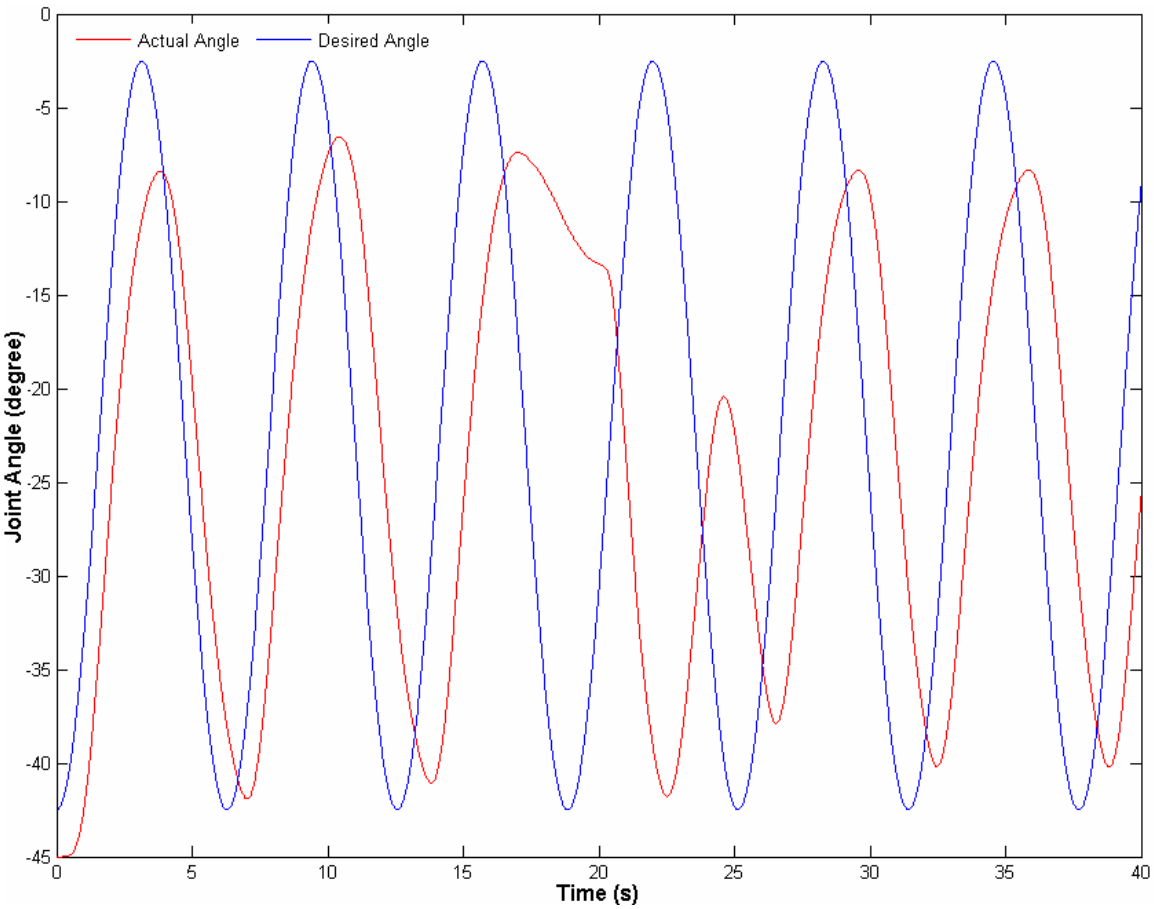

Figure 6-18 Experimental results of tracking a sine wave with an Adaptive PID controller subjected to external force at t=15 to 20

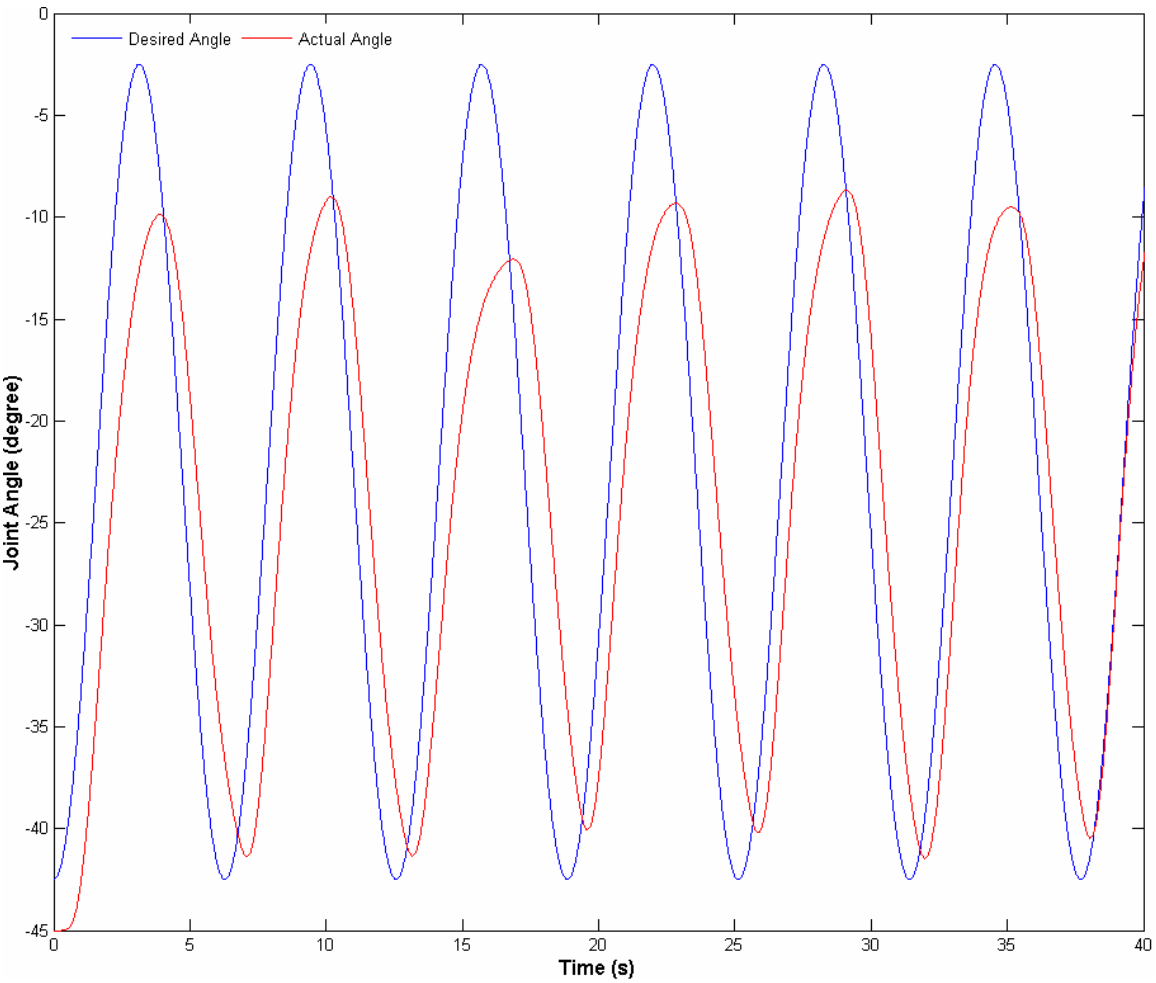

Figure 6-19 Experimental results of tracking a sine wave with an Adaptive PID controller, the mass of the system is increased at t=17 by 15%

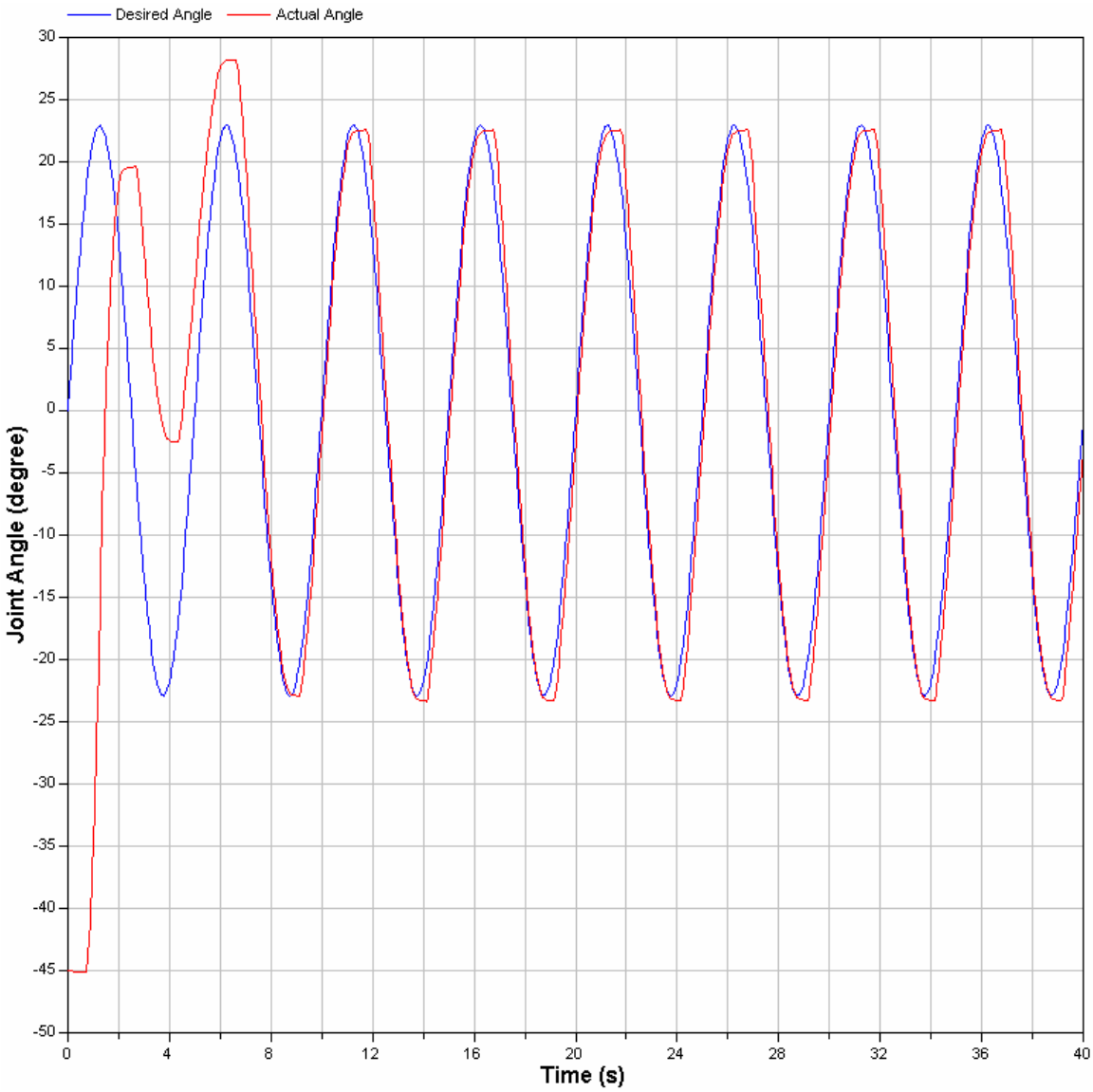

Figure 6-20 Simulation results of Adaptive PID with maximum voltage 20V

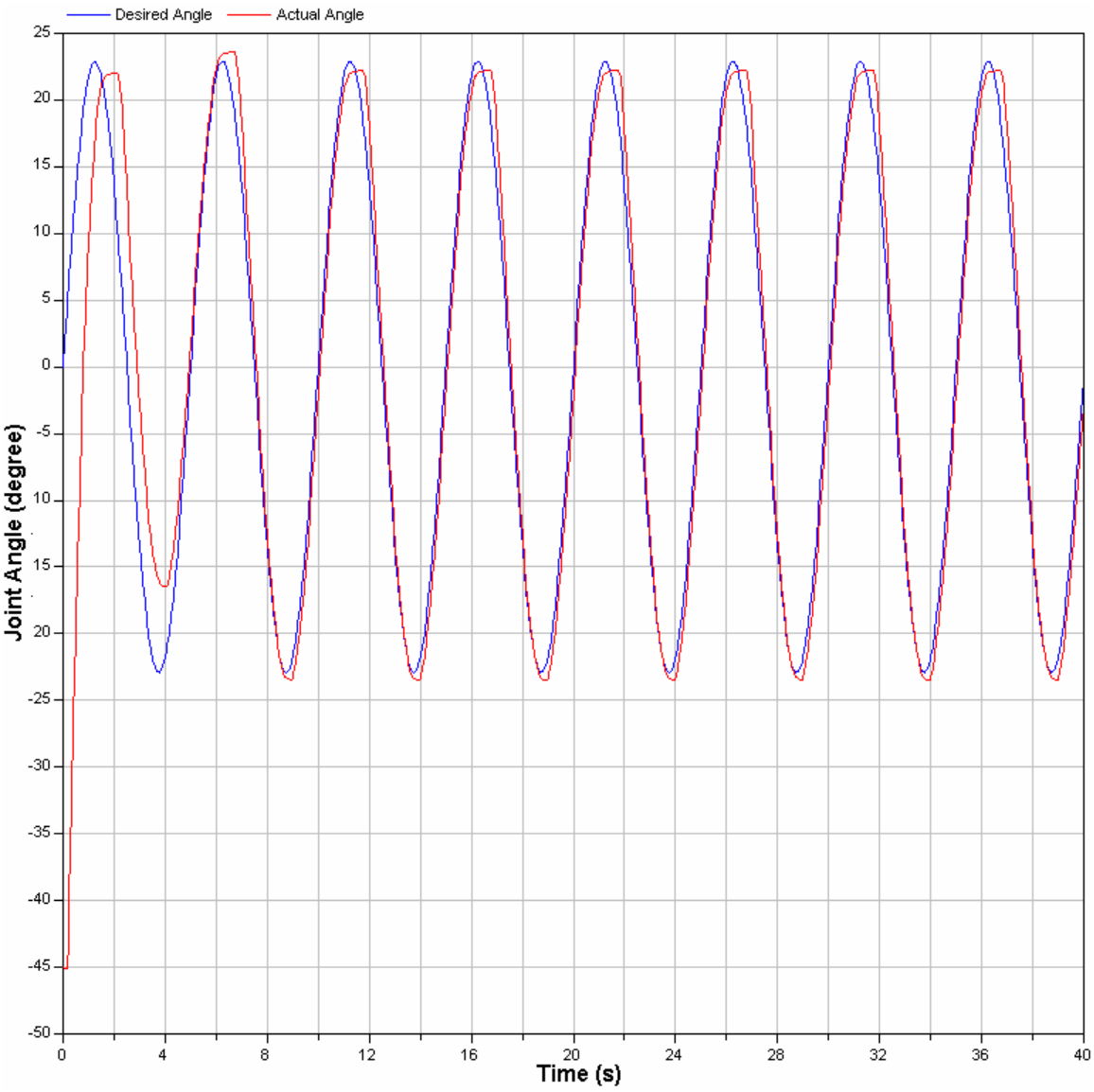

Figure 6-21 Simulation results of Adaptive PID with maximum voltage 40V

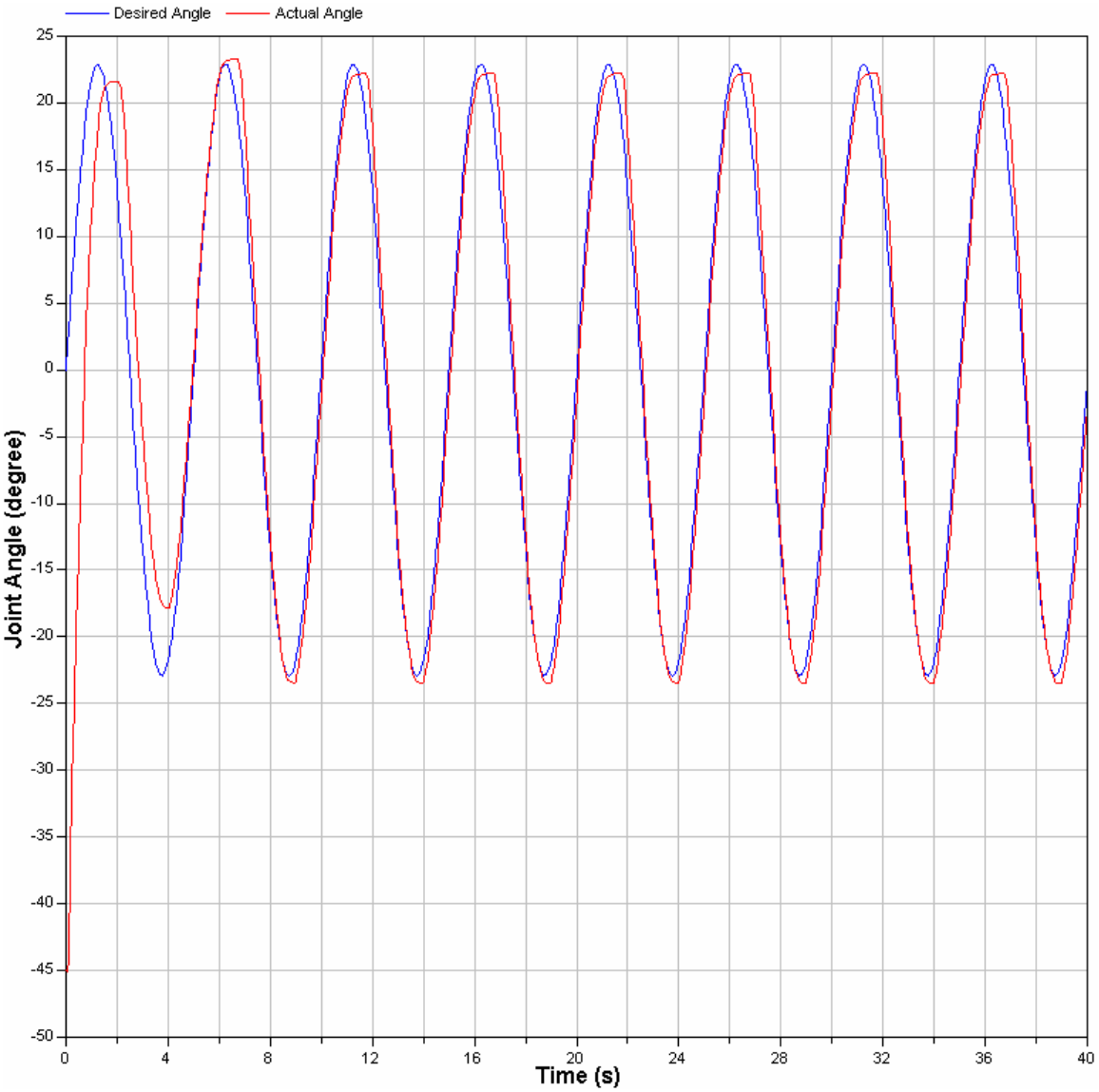

Figure 6-22 Simulation results of Adaptive PID with maximum voltage 60V

6.3. Tracking the Real Ankle Angle

As it was described in the Chapter 3, to test the performance of the active ankle foot orthosis, testing the control performance in tracking the real ankle angle is necessary.

The simulation results show that the tracking error of almost all controllers will increase dramatically for frequencies more than 0.3 Hz. This in turn results in an error up to 20^o at the hill strike while the landing angle is about $20^o - 30^o$, hence this amount of error can not be acceptable.

Therefore the frequency of 0.2 Hz or in the other words the time cycle of 5 seconds is selected to check the stability of walking by using an AAFO. The performance of the controller in tracking the real ankle angle is shown in Figure 6.23.

The tracking error is also shown in Figure 6.24.

As it is shown the system has the largest error between point A and B where no voltage is applied and the wire is cooling down. The passivity of cooling process causes the tracking error and therefore the performance of the system in this part is not related to the type of the controller.

Applying the actual angle of ankle to the stability criterion, it is possible to determine the path way of the ZMP to check the stability. The ZMP of normal walking and walking with AAFO are compared in Figure 6.25. The ZMP path is mostly affected by the trajectory of the hip and therefore the ankle trajectory does not change the stability that much, at a same time a large error in landing or angle may change the stable margins and affect the stability.

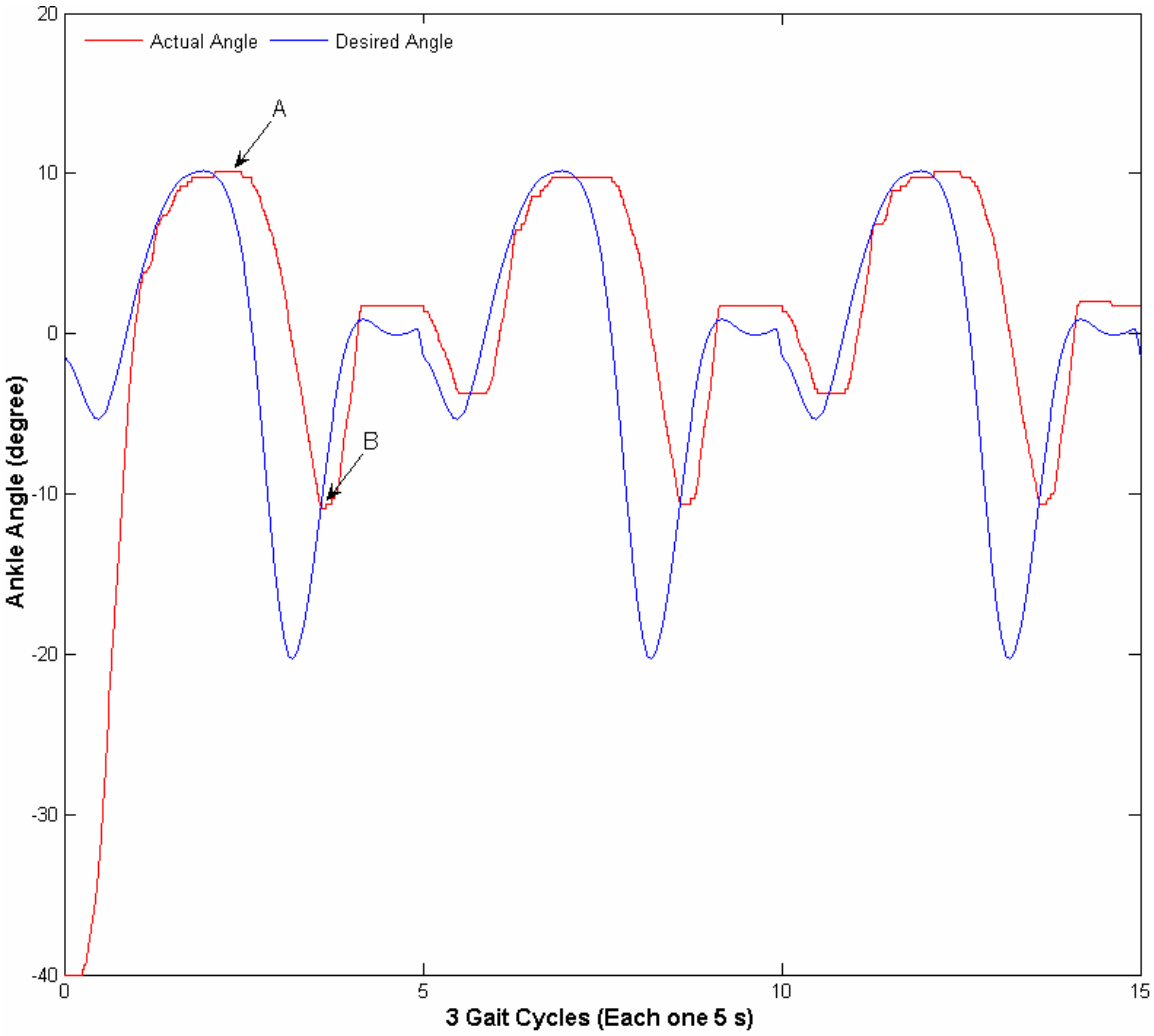

Figure 6-23Experimental results of Adaptive PID controller in tracking a real ankle angle

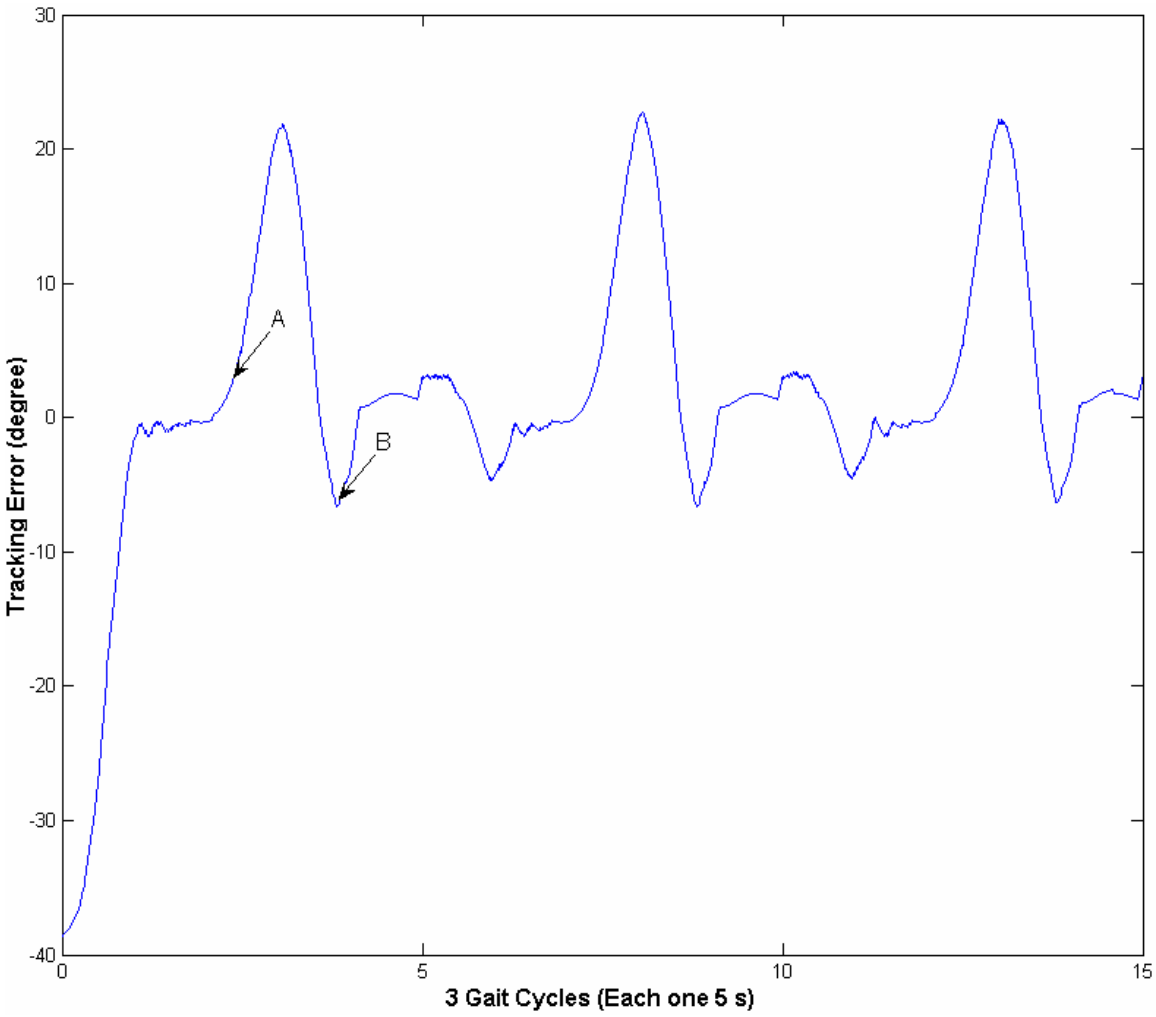

Figure 6-24 Tracking error of Adaptive PID controller experiment in tracking a real ankle angle

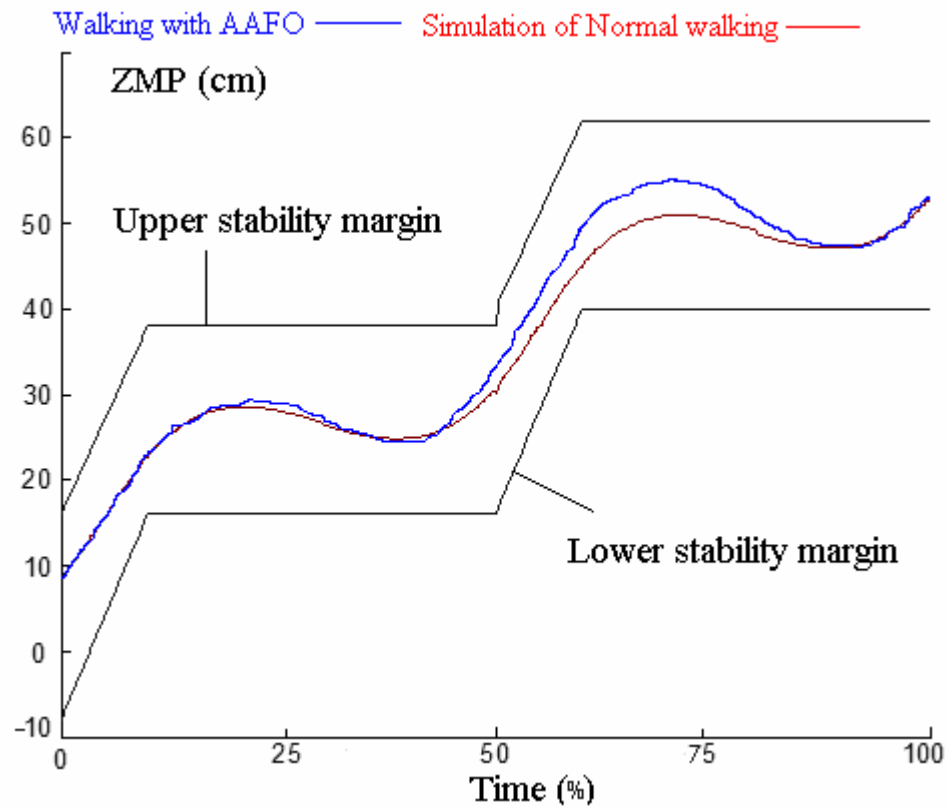

Figure 6-25 The ZMP path of normal walking versus walking with an SMA AAFO

Chapter 7

7. Conclusion and Recommendations

In this thesis it was attempted to develop and control a new active ankle foot orthosis. Shape memory alloys were considered as an alternative to replace the current actuation techniques (pneumatic and DC motors) to provide the motion and the actuation force for drop foot patients.

Studying the dynamic behavior of the ankle joint, a SMA arm manipulator with a similar dynamic model was selected to study the SMA actuation. The model presented for the SMA arm included the nonlinear dynamic of the manipulator and constitutive and heat transfer behavior of the SMA wire. Due to nonlinearity of the system and challenges in controlling the position of the arm, a stress based control sliding mode controller selected which needed a feedback of the stress of the wire. A realistic dynamic model based on the LuGre friction model then used to estimate the stress of the wire.

Comparing the results of the sliding mode controller and a PID controller, it was suggested to use a switching control between sliding mode and PID. The performance of the suggested control techniques was satisfactory. However because of massive calculation in this model, the adaptive PID controller based on the sliding mode suggested which was both robust and practical.

Introducing a trajectory generation technique and a stability criterion, the performance of the AAFO was checked at different speeds. The experimental results of adaptive PID in tracking real ankle angle applied to the ZPM criterion. All other joint were assumed to follow the desired angle. It was observed that by increasing the frequency (more that 0.3 Hz) the error of the angle would reach up to 20 degree at hill strike, which may cause instability. The error of the ankle did not have a large effect on the ZMP path but on the stability margin. Changing the stability margin the tracking error would cause the instability.

It was observed that the adaptive PID can follow the desired trajectory while the wire needs to be heated up. During the cooling process because of the passivity of cooling, the error of the system got larger. The cooling cycle is happening during a linear motion of the ankle where it requires a constant stiffness. Therefore it is recommended to adjust the stiffness of the spring to generate this part of motion.

However different walking speeds may need different stiffness and therefore another approach is to actively cool down the system or isolate the systems.

Finally it should be mentioned that even with using an active cooling system, the whole SMA system will be affected by the environmental changes (such as temperature …) and the current technology allows to use this device in the lab environment and for rehabilitation or muscle memory purposes.

References

[1] Abdel-Aziz, Y.I. and Kara, H. M., (1971) "Direct Linear Transformation from Comparator Co-ordinates Into Object Space Co-Ordinate. Proc.ASP/UI Symposium on Close-range Photogerammery. Am. Soc. of Photogrammetry, Falls Church, VA. pp1-18.

[2] Arai, S., Aramaki, K., Yanagisawa, Y. Cntinuous (1994) "system modeling of shape memory alloy (SMA) for control analysis." IEEE Proceeding of 5th international Symposium on Micr Machine and Human Science, pages 97-99.

[3] Anderson, F. C. and Pandy, M. G. (2001) "Dynamic Optimization of Human Walking" Journal of Biomechanical Engineering, vol 123, pp 381-390.

[4] Ayers, R. A., Simske, S. J., Bateman, T. A., Petkus, A., Sachdeva, R. L. C. and Gyunter, V. E., (1999) "Effect of nitinol implant porosity on cranial bone in growth and apposition after 6 weeks." J Biomed Mater Res, 45:42–7

[5] Azimi, E., Ghobadi, M., Tarkesh, E. **,** Keshmiri, M. and Fadaei A., (2005) "Three-Dimensional Smooth Trajectory Planning Using Realistic Simulation." Lecture Notes in Computer Science, Vol. 3276, Ed by D. Nardi et al, pp. 381-392. Springer-Verlag GmbH.

[6] Bajd, T., Kralj, A., Turk, R., Benko, H., and Sega, J., (1983) “The use of a four-channel electrical stimulator as an ambulatory aid for paraplegic Ptients.” Phys, Ther., 63, 1116, 1983

[7] Bajd, T., Kralj, A., Stefancic, M., and Lavrac, N. (1999). “Use of functional electrical stimulation in the lower extremities of incomplete spinal cord injured patients.” Artificial Organs, 23(5), 403-409.

[8] Banala, S. K., Agrawal, S., (2005) "Gait rehabilitation with an active leg orthosis", In Proceedings ASME Mechanisms and Robotics Conference.

[9] Baz, A., Chen, T. and Ro, J., (1994) “Shape control of NITINOL-reinforced composite beams” Proc. SPIE 2190 436–53

[10] Beckett, R., Chang, K., (1986) “On the evaluation of kinematics of gait by minimum energy,” J. Biomech. 1:147-159.

[11] Belforte, G., Gastaldi, L., Sorli, M., (2001) “Pneumatic active gait orthosis. Mechatronics.” 2001; 11(3):301–323.

[12] Blaya, J. A., Herr, H., (2004) “Adaptive control of a variable-impedance ankle-foot orthosis to assist drop-foot gait.” IEEE Trans Neural Systems Rehab Eng. 2004;12(1):24–31.

[13] Bobbert,M.F., van Soest,A.J., (1994) “Effects of muscle strengthening on vertical jump height: a simulation study.” Medicine and Science in Sports and Medicine 26,1012–1020.

[14] Bowker, J. H., and Hall, C. B., (1975). “Normal human gait.” Atlas of orthotics, C.V. Mosby Co., St. Louis, 133-143.

[15] Cain, S., Gordon, K. E. and Ferris, D. P., (2007) "Human motor adaptation during walking with a powered ankle-foot orthosis depends on control method." Journal of Neuroengineering and Rehabilitation

[16] Chang, W. and Yan, J., (2004) "Adaptive robust PID controller design based on a sliding mode for uncertain chaotic systems" Journal of Chaos, Solitons and Fractals, 26:167-175.

[17] Chao, E. Y. and Rim, K., (1973) "Application of optimization principle in determining the applied moments in human leg joints during gait." J. Biomech. 6:497-510.

[18] Chopra, I., (2002) "Review of state of art of smart structures and integrated systems." AIAA Journal, 40(11):2145-2187

[19] Dario, P., Bergamasco, M., Bernardi, L. and Bicchi, A., (1987) "A shape memory alloy actuation module for fine manipulation." In IEEE Micro Robots and Teleoperactuation Workshop, Hyannis, MA, IEEE Robotics and Automation Council, Nov 9-11

[20] Duerig, T., Stoeckel, D. and Johnson, D., (2002) "SMA: smart materials for medical applications European" Workshop on Smart Structures in Engineering and Technology Proc. SPIE 4763 7–15

[21] Elahinia, M. H. and Ashrafiuon, H., (2002) "Nonlinear control of a shape memory alloy actuated manipulator," Journal of Vibration & Acoustics – Transactions of the ASME, 124(4): 566-575.

[22] Elahinia, M. H. Seigler, T. Michael Leo, D. J. and Ahmadian, M. (2004) "Nonlinear Stress-Based Control of a Rotary SMA-Actuated Manipulator," Journal of Intelligent Material Systems and Structures, 15(6): 495-508

[23] Elahinia, M. H. Ahmadian, M. and Ashrafiuon, H., (2004) "Design of Kalman Filter for Rotary Shape Memory Alloy Actuators," Journal of Smart Materials and Structures, 13(4): 691-697.

[24] Elahinia, M. H., Koo, J., Ahmadian, M., and Woolsey, C. (2005) "Backstepping Control of an SMA-Actuated Robotic Arm," Journal of Vibration and Control, 11(3): 407-429.

[25] Epps, J. J. and Chopra, I., (2001) "In-flight tracking of helicopter rotor blades using shape memory alloy actuators" Smart Mater. Struct.10 104–11

[26] Fattah, A., Agrawal, S., (2005) "On the Design of a Passive Orthosis to Gravity Balance Human Legs", Journal of Mechanical Design, Transactions of the ASME, Vol. 127, No.4., pp.802-808.

[27] Fattah, A., Agrawal, S., Catlin, G., Hamnett, J., (2006) "Design of a Passive Gravity-Balanced Assistive Device for Sit-to-stand Tasks", Journal of Mechanical Design, Transactions of the ASME, Vol. 128, No.5., pp.112-1129.

[28] Feldman, A., (1986) "Once more on the equilibrium-point hypothesis (lambda model) for motor control." Journal of Motor Behavior 18, 17–54.

[29] Ferris, D. P., Czerniecki, J. M. and Hannaford, B., (2005) "An ankle-foot orthosis powered by artificial pneumatic muscles." Journal of Applied Biomechanics, 21:189-197.

[30] Ferris, D. P, Sawicki, G. S. and Domingo A. R (2005) "Powered lower limb orthoses for gait rehabilitation." Topics in Spinal Cord Injury Rehabilitation, 11:34-49.

[31] Gage, J. R., (1991) "An overview of normal walking." Instr Course Lect 1990;39:291-303

[32] Gerritsen, K. G. M., Nachbauer, W. and van den Bogert, A. J., (1996) "Computer simulation of landing movement in downhill skiing:anterior cruciate ligament injuries." Journal of Biomechanics 29, 845–854.

[33] Gilbertson, R. G., (2000) "Muscle Wires Project Book." Mondo-tronics, Inc., PMB-N, 4286 Redwood Hwy San Rafael, CA 94903.

[34] Gilchrist, L. A., and Winter, D. A. (1997) "A Multisegment Computer Simulation of Normal Human Gait," IEEE Trans. Rehab. Eng. 5:290-299

[35] Good, D. G., and Supan, T. J. (1989). "Basic principles of orthotics in neurologic disorders." Orthotics in neurologic rehabilitation, M. L. Aisen, ed., Demos Publications, New York.

[36] Graupe, D., Kohn, K. H., Kralj, A., and Basseas, S., (1983) "Patient controlled electrical stimulation via EMG signature discrimination for providing certain paraplegics with primitive walking functions." J. Biomed. Eng., 5, 220, 1983

[37] Graupe, D., Kohn, K. H., Basseas, S. and Naccarato E., (1984) "Electromyographic control of functional electric stimulation in selected patients." Orthopedcs, 7, 1134.

[38] Gruber, K., Ruder, H., Denoth, J. and Schneider, K. (1998) "A comparative study of impact dynamics: wobbling mass model versus rigid body model." Journal of Biomechanics 31, 439–444.

[39] Guyton, A., and Hall, J. (1996). "Textbook of Medical Physiology." Saunders, Philadelphia, PA.

[40] Hansen, A. H., Childress, D. S., Miff, S. C., Gard, S. A. and Mesplay, K. P., (2004) "The human ankle during walking: implications for design of biomimetic ankle prostheses." J. Biomechanics: 37; 1467-1474.

[41] Harman, B. (2004) "Quality for life" testimony in Department of Veterans' Affairs Prosthetic Rehabilitation and Research Programs, 22 July

[42] Hashimoto, M., Takeda, M., Sagawa, H. and Chiba, I., (1985) "Application of shape memory alloy to robotic actuators." Journal of robotic systems, 2(1):3-25.

[43] Hemami, H., (1980) "A feedback on-off model of biped dynamics." IEEE Trans. On Systems, Man and Dynamics SMC-10:376-383.

[44] Herr, H., Wilkenfeld, A., (2003) "User-adaptive control of a magnetorheological prosthetic knee." Indust Robot. ;30(1):42–55.

[45] Honma, D., Miwa, Y. and Iguchi, N., (1984) "Micro robots and micro mechanisms using shape memory alloy." The 3rd Toyota Conference, Integrated Micro Motion Systems, Micromachining, Control and Applications, Nissan, Aichi, Japan.

[46] Huang, Q., Yokoi, K., Kajita, S., Kaneko, K., Arai, H., Koyachi, N. and Tanie, N., (2001) "Planning Walking Pattern for a Biped Robot", *IEEE International Transition on Robotic and Automation*, Vol. 17, N0. 3, pp 280-289.

[47] Hughes, J., (1972) “Powered lower limb orthotics in paraplegia.” Paraplegia. 9:191–193.

[48] Humbeeck, J. V., (2003) “Damping capacity of thermoelastic Martensite in shape memory alloys “J. Alloys Compounds 355 58–64

[49] Ikuta, K. Tsukamoto, M. and Hirsoe, S. (1991) “Mathematical model and experimental verification of shape memory alloy for designing micro actuator.” Proceesings of the IEEE Micro Electro Mechanical Systems Conference, pages 103-108

[50] Inman, V. T., Ralston, H. J., and Todd, F., (1981) “Human Walking.” Williams & Wilkins, Baltimore.

[51] Isakov, E., Mizrahi, J. and Najenson, T., (1986) “Biomechanical and physiological evaluation of FES-activated paraplegic patients.” J. Rehabil. Res. Dev., 23, 9.

[52] Kang, S. B., Yoon, K. S., Lee, J. H., Kim, J. S., Nam, T. H. and Gjunter, V. E., (2002) “In vivo result of porous TiNi shape memory alloy: bone response and growth.” Jpn Inst Met, 43(5):1045-1048

[53] Kaneoko, S., Yano, H., (1997) “A new concept of dynamic orthosis for paraplegia: the weight bearing control (wbc) orthosis.” Prosthetics and Orthotics International, pages 222–228,

[54] Kasaoka, K., Sankai, Y., (2001) “Predictive control estimating operator's intention for stepping-up motion by exoskeleton type power assist system HAL” IEEE/RSJ International Conference on Intelligent Robots and Systems

[55] Kawamoto, H., Sankai, Y., (2004) "Power assist method based on phase sequence driven by interaction between human and robot suit" 13th IEEE International Workshop on Robot and Human Interactive Communication,

[56] Kazerooni, H., (1996) "The human power amplifier technology at the University of California, Berkeley." Robot Autonom Systems. 19(2):179–187

[57] Kirkup, John, (2007) "A History of limb amputation." Springer 2007

[58] Kobetic, R., Marsolais, E.B., Davy, D., Gaudio, R., Triolo, R., (2003) "Development of a hybrid gait orthosis: a case report." *Journal of Spinal Cord Medicine* 26(3): 254-258.

[59] Koopman, B., Grootenboer, H. J. and de Jongh, H. J., (1995) "An Inverse dynamic model for the analysis, reconstruction and prediction of bipedal walking" Journal of biomechanics, 28 (11)1369-1376.

[60] Kulkarni, R. P. and Bellamy, E. A., (1990) "A new thermo-expandable shape memory nickel-titanium alloy stent for the management of ureteric structures." Br J Urol International, 83:755–9.

[61] Kuribayashi, K. (1986) "A new actuator of a joint mechanism using NiTi alloy wire." The International Journal of Robotic Research, 4(4):103-108.

[62] Liang, C., (1990) "The constitutive modeling of shape memory alloys." PhD thesis, Virginia Tech, Blacksburg, VA.

[63] Liang C. and Rogers, C. A., (1990) "One-dimensional thermomechanical constitutive relations for shape memory materials. Journal of Inteligent material Systems and Structures, 1(2):207-234.

[64] Liberson, W. T., Holmquest, H. J., Scott, D. and Dow, D., (1961) "Functional electrotherapy: stimulation of the personal nerve synchronized with the swing phase of the gait in hemiplegic patients." Arch Phys, Med. Rehabil., 42, 101.

[65] Lipscomb, I. P., Nokes, L. D. M., (1996) "The application of shape memory metals in medicine." Norfolk: Paston Press.

[66] Lombardi, S. and Poncet, P. (2004) "metallurgical principles of Nitinol and its use in interventional devices" C2i2, Fall 2004, 25-28.

[67] Lusardi, M. M., Nielsen, C. C., (2000) "Orthotics and Prosthetics in Rehabilitation." Butterworth-Heinemann press.

[68] Maeda, S., Abe, K., Yamamoto, K., Tohyama, O. and Ito, H., (1996) "Active endoscope with SMA coil springs" Proc. IEEE Micro Electro Mechanical Systems (San Diego, CA) pp 290–5

[69] Marks, L. S., Ettekal, B., Cohen, M. S., Luz Macairan, M. and Vidal, J., (1999) "Use of a shape-memory alloy (nitinol) in a removable prostate stent." Techn Urol, 5:226–30.

[70] Mavroidis, C., Pfeiffer, C. and Mosley, M. (1999) "Conventional actuators, shape memory alloys, and electrorheological fluids." Invited Chapter in Automation, Miniature Robotics and Sensors for Non-Destructive Testing and Evaluation, Y. Bar-Cohen Editor.

[71] Melton, K. N., (1998) "General application of sma's and smart materials." Shape Memory Materials, Edited by K. Otsuka and C. M. Wayman, pages 220–239.

[72] Mesplay, K., (1993) "Mechanical impedance of the human lower limb during walking." Ph.D. thesis, Northwestern University, Evanston.

[73] Miyazaki, S., (1998) “Medical and dental application of shape memory alloy. Shape Memory Materials”, Edited by K. Otsuka and C. M. Wayman, 267–279.

[74] Minetti, A. E., (1998). “The biomechanics of skipping gaits: a third locomotion paradigm” Procedures of the Royal Society of London B, 265, 1227-1235.

[75] Minetti, A. E. and Belli, G., (1994) “A model for the estimation of visceral mass displacement in periodic movements.” Journal of Biomechanics 27,97–101.

[76] Mizrahi, J., Braun, Z., Najenson, T. and Graupe, D., (1985) “Quantitative weight bearing and gait evaluation of paraplegics using functional electric stimulation.” Med. Biol. Eng. Comput., 23, 101.

[77] Mosley, M. J. and Mavroidis, C., (2001) “Experimental Nonlinear Dynamics of a Shape Memory Alloy Wire Bundle Actuator” Journal of Dynamic Systems, Measurement and Control, Vol 123, 103-110

[78] Nakazato, T., Kato, Y. and Masuda, T., (1993) “Position control of SMA actuator by fuzzy reasoning.” Transactions of Japan Society of Mechanical Engineers, Part C, 59(565):141–46

[79] Nattrass, C., Ireland, A. J. and Sherriff, M., (1998) “The effect of environmental factors on elastomeric chain and nickel titanium coil springs.” Eur J Orthodont, 20:169–76

[80] Nigg, B.M., Bobbert, M. F.,(1990.) “On the potential of various approaches in load analysis to reduce the frequency of sports injuries.” Journal of Biomechanics 23 (Suppl. 1), 3–12.

[81] Norkin, C., and Levangie, P., (1983) “Joint structure and function: A comprehensive analysis.” F.A. Davis, Philadelphia.

[82] Novacheck, T. F., (1998). "The biomechanics of running." Gait and Posture, 7, 77-95.

[83] Otsuka, K. and Wayman, C. M., (1999) "Shape Memory Materials." Cambridge University Press, 40 West 20th Street, New York, NY 10011-4211.

[84] Pain, M. T. G. and Challis, J. H. (2006) "The influence of soft tissue movement on ground reaction forces, joint torques and joint reaction forces in drop landings" Journal of Biomechanics, 39:1:119-124.

[85] Perry, J., (1992) "Gait Analysis: Normal and Pathological Function." SLACK Inc., New Jersey.

[86] Perry, J. (1997). "Normal and Pathological Gait." Atlas of Orthoses and Assistive Devices, W. Eversmann, J. Fisk, B. Goldberg, J. Hsu, J. Lonstein, J. Michael, and T. Moore, eds., Mosby, Boston, 67-91.

[87] Roch, I., Bidaud, Ph., Collard, D., and Buchaillot, L. (2003) "Fabrication and characterization of an SU-8 gripper actuated by a shape memory alloy thin film." Journal of Micromechanics and Microengineering. Issue Feb.

[88] Roglin R L and Hanagud S V (1996) "A helicopter with adaptive rotor blades for collective control Smart Mater." Struct. 5 76–88

[89] Rose, J., Gamble J. G., (1994) "Human Walking"2nd Edition

[90] Ruthenberg, B. J., Wasylewski NA, Beard JE., (1997) "An experimental device for investigating the force and power requirements of a powered gait orthosis." J Rehab Res Dev. 34(2):203–213.

[91] Ryhanen, J., Kallioinen, M., Serlo, W., Peramaki, P., Junila, J., Sandvik, P., Niemela, E. and Tuukkanen, J., (1999) "Bone healing and mineralization, implant

corrosion, and trace metals after nickel–titanium shape memory metal intramedullary fixation.” J Biomed Mater Res, 47:472–80.

[92] Schneevoigt, R., Haase, A., Eckardt, V. L., Harzer, W. and Bourauel, C., (1999) “Laboratory analysis of superelastic NiTi compression springs.” Med Eng Phys, 21:119–25.

[93] Seireg, A., Grundman, J. G., (1981) "Design of a multitask exoskeletal walking device for paraplegics.” In: Ghista DN., editor. Biomechanics of Medical Devices. Marcel Dekker, Inc.; New York: pp. 569–639.

[94] Shih, C. C., Lin, S. J., Chung, K. H., Chen, Y. L. and Su, Y. Y., (2000) “Increased corrosion resistance of stent materials by converting surface film of polycrystalline oxide into amorphous oxide.” J Biomed Mater Res, 52:323–32.

[95] Smidt, G. L., (1990). “Rudiments of gait.” Gait in rehabilitation, G. L. Smidt, ed., Churchill Linvingstone, New York, 1-19.

[96] Song, G., Kelly, B. and Agrawal, B. N., (2000a) “Active position control of a shape memory alloy wire actuated composite beam Smart Mater.” Struc. 9(7)11–6

[97] Song, G., Chaudhrt, V. and Bature, C., (2003) “Precision tracking control of shape memory alloy actuators using neural networks and a sliding mode based robust controller” Smart material and structure12:223-231

[98] Song, G., Chaudhry, V. and Batur, C., (2003) “A neural network inverse model for a shape memory alloy wire actuator” J. Intelligent Material Sys and Struc, 14: 371-378

[99] Sturman, D. and Zeltzer, D., (1994) “A survey of glove based input.” IEEE Computer Graphics and Aplications, pages 30–39

[100] Sutherland, D. H., Cooper, L., (1981) “The events of gait.” Bull Prosthet Res1981;10-35:281-282

[101] Sutherland, D. H., (1984) “Gait disorder in childhood and adolescence.” Baltimore: Williams and Wilkins, 1984: 10-13

[102] Tarkesh, E. and Elahinia, M. H., (2007) “Stable Walking Pattern for SMA Actuated Biped ” IEEE/ASME Transaction on Mechatronics, Vol.12, No.5.

[103] Tanaka, Y. (1986) “Athermomechanical sketch of shape memory effect: One-dimiensional tensile behavior.” Res Mechanica, the International Journal of Structural Machines and Materials Science, 18(1):251-63.

[104] Thierry, B., Tabrizian, M., Savadogo, O., Yahia, L., (2000) “Effects of sterilization processes on NiTi alloy: surface characterization.” J Biomed Mater Res, 49:88–98

[105] Townsend, M. A. and Seireg, A., (1972) “The synthesis of bipedal locomotion.” J. Biomech. 5:71-83

[106] Townsend, M. A., Lepofsky, R. J., (1976) “Powered walking machine prosthesis for paraplegics.” Med Biol Eng. 14(4):436–444.

[107] Townsend, M. A. (1981), “Dynamics and coordination of torso motion in human locomotion.” J. Biomech. 14:727-738

[108] U. S. D. O., Commerce, (1994). “Persons using devices and/or features to assist with impairments, by age.” , Table 217 in Statistical Abstract of the United States.

[109] Venugopalan, R., (1999) “Corrosion testing of stents: a novel fixture to hold entire device in deployed form and finish.” J Biomed Mater Res (Appl Biomater), 48:829–32.

[110] Vukobratovic, M., Hristic, D., Stojiljkovic, Z., (1974) "Development of active anthropomorphic exoskeletons." Med Biol Eng. 12(1):66–80.

[111] Vukobratovic, M., Borovac, B., Surla, D., Stokic, D., (1990) "Biped Locomotion: Dynamics, Stability, Control and Application." Vol. 7. Springer-Verlag, Berlin.

[112] M. Vukobratovic and B. Borovac, (2004) "Zero-Moment Point- thirty five years of its life" Int Journal of Humanoid Robotics, Vol. 1, No. 1, pp. 157-173.

[113] Welch, G. and Foxlin, E., (2002) "Motion tracking survey." IEEE Computer Graphics and Applications, pages 24–38.

[114] Whittle, M., (1991) "Gait Analysis: An Introduction." Butterworth-Heinemann Ltd., Boston.

[115] Wilde, K., Gardoni, P. and Fujino, Y., (1999) "Base isolation system with shape memory alloy device for elevated highway bridges" Eng. Struct. 22 222–9

[116] Winter, D. A., (1974) "Sidwall, H. G. and Hobson, D. A. Measurement and reduction of noise in kinematics of locomotion." J. Biomech. 7:157-159

[117] Winter, D. A., (1982) "Camera speeds for normal and pathological gait analysis. Med." Biol. Eng. Comput. 20:408-412

[118] Winter, D. A., (1996) "The biomechanics and motor control of human gait: normal, elderly and pathological." Wiley, New York.

[119] Winter, D., A., (2004) "Biomechanics and motor control of human movement." 3rd Ed Wiley.

[120] Wolfe, T. B., Faulkner, M. G., Wolfaardt, J., (2005) "Development of shape memory alloy actuator for a robotic eye prosthesis." Smart Mater. Struct, 14:759-768

[121] Wright, I. C., Neptune, R. R., van den Bogert, A .J. and Nigg, B.M., (1998) "Passive regulation of impact forces in heel–toe running." Clinical Biomechanics 13,521–531.

[122] Wu, R. H., (1999). "Human readaptation to normal gravity following short-term simulated Martian gravity exposure and the efectiveness of countermeasures," M.S., MIT, Cambridge.

[123] Wu, K. K., (1990) "Foot orthoses: Principles and clinical applications". Wlliams & Wilkins, Baltimore.

[124] Yahia, L., (2000) "Shape memory implants." Berlin: Springer

[125] Zhou, H. and Hu, H., A Survey - Human Movement Tracking and Stroke Rehabilitation, Technical Report, University of Essex, UK, CSM-420, ISSN 17440-8050